A COMPLEX STUDY ON ANTICANCER COPPER CHELATORS

PhD thesis

Gaál Anikó

Doctoral School of Pharmaceutical Sciences

Semmelweis University

Supervisor: Norbert Szoboszlai, Ph.D.

Official reviewers: Tábi Tamás, Ph.D.
                     Laczka Csilla, Ph.D.

Head of the Final Examination Committee: Tamás Török, D.Sc.

Members of the Final Examination Committee: Margit Oltiné Varga, C.Sc.
                                             Gergely Völgyi, Ph.D.

Budapest
2020

Table of Contents

List of abbreviations

5-FU	5-Fluorouracil
AACR	American Association for Cancer Research
ABCB1	ATP Binding Cassette Subfamily B Member 1, P-glycoprotein, P-gp, MDR1
AML	Acute myeloid leukemia
APDTC	Ammonium pyrrolidine dithiocarbamate
ATP7A	copper-transporting ATPase 1
ATP7B	ATPase copper transporting beta
ATR	Attenuated Total Reflectance
BRAF	v-raf murine sarcoma viral oncogene homolog B1
BRCA	Breast cancer gene
BSA	Bovine Serum Albumin
CD	Circular Dichroism
cfDNA	cell-free DNA
chloroquine	(RS)-N'-(7-chloroquinolin-4-yl)-N,N-diethylpentane-1,4-diamine
cisplatin	cis-diamminedichloroplatinum(II), CDDP, Cisplatinum
CMTTdb	Cancer Molecular Targeted Therapy database
COTI-2	1-Piperazinecarbothioic acid, 4-(2-pyridinyl)-, 2-(6,7-dihydro-8(5H)-quinolinylidene)hydrazide
CQ	Clioquinol, 5-chloro-7-iodo-8-hydroxy-quinoline
Cremophor EL	Polyoxyl 35 Hydrogenated Castor Oil
CS	Collateral Sensitivity
CTR1 and CTR2	copper transporter 1 and 2; high affinity copper uptake transporter 1 and 2
D_{avr}	average diameter
DCF	2',7'-dichlorofluorescein
DDS	Drug Delivery Systems
DDTC	diethyldithiocarbamate
disulfiram	N,N-diethyl[(diethylcarbamothioyl)disulfanyl]carbothioamide
dithizone	diphenylthiocarbazone
DLS	Dynamic Light Scattering
DMEM	Dulbecco's Modified Eagle's Medium, cell culture media
DMSO	Dimethyl sulfoxide
DNA	deoxyribonucleic acid
Dp44mT	di-2-pyridyl ketone 4,4-dimethyl-3-thiosemicarbazone
DPBS	Dulbecco's Phosphate Buffered Saline solution
DpC	di-2-pyridylketone-4-cyclohexyl-4-methyl-3-
D-penicillamine	3-Dimethyl-D-cysteine
DPPC	1,2-dipalmitoyl-sn-glycero-3-phosphatidylcholine
DSC	Differential Scanning Calorimetry
DSPE	distearoylphosphatidylethanolamine
DSS	3-(trimethylsilyl)-1-propanesulfonic acid sodium salt

DTPA	diethylenetriaminepentacetic acid
EGFR	Epidermal Growth Factor Receptor
EPR	enhanced permeability and retention effect
ER	endoplasmic reticulum
EVs	extracellular vesicles
FACS	Flow Cytometry
FBS	fetal bovine serum
FDA	US Food and Drug Administration
g	Relative Centrifugal Force (RCF) or G-Force
GLOBOCAN	Global Cancer Incidence, Mortality and Prevalence
$H_2DCF-DA$	2',7'-dichlorodihydrofluorescein diacetate
HEPES	4-(2-hydroxyethyl)-1-piperazineethanesulfonic acid
HER2	human epidermal growth factor receptor 2
HICs	high-income countries
HOR	horizontal
HSPC	hydrogenated soybean phosphatidylcholine
HT	hyperthermia treatment
hZIP1	human ZIP1
IC_{20}	inhibitory concentration corresponding to 20% cell survival
IC_{50}	half maximal inhibitory concentration (50% cell survival)
i.v.	intravenous administration
IR	(Fourier Transform-) Infrared Spectroscopy
LICs	low-income countries
M_2L	metal-ligand complex 2:1 ratio
MDR	multidrug resistance
MEK	Mitogen-activated protein kinase
MICs	middle-income countries
ML	Metal-ligand complex 1:1 ratio
ML_2	Metal-ligand complex 1:2 ratio
MPPC	1-myristoyl-2-palmitoyl-sn-glycero-3-phosphocholine
MPS	mononuclear phagocyte system
MSPC	1-myristoyl-2-stearoyl-sn-glycero-3-phosphocholine
MQ	Milli-Q water
MRI	Magnetic Resonance Imaging
MRPS	Microfluidic Resistive Pulse Sensing
MT	metallothionein
MTT	3-(4,5-dimethylthiazol-2-yl)-2,5-diphenyltetrazolium
n.a.	not available
NAC	N-Acetylcysteine
neocuproine	2,9-dimethyl-1,10-phenantroline, NEO
NIH	National Cancer Institute
NMR	Nuclear Magnetic Resonance
oxine	8-hydroxyquinoline
p	p-value or probability value
p.i.	post injection
p53	Tumor protein p53, tumor suppressor p53

PD-1	programmed death-1
PDI	polydispersity index
PD-L1	programmed death-ligand 1
PDTC	pyrrolidine dithiocarbamate
PEG	polyethylene glycol
PET/CT	Positron Emission Tomography–Computed Tomography
PG	phosphatidylglycerol
PI	propidium iodide
Q4	Q-4, 5-chloro-7-((2-fluorobenzylamino)methyl)quinolin--8-ol
ROS	Reactive Oxygen Species
RPMI	Roswell Park Memorial Institute Medium, cell culture media
RSD	Relative Standard Deviation
RT	Room temperature
SD	Standard Deviation
SDS	sodium dodecyl sulfate
SEC	Size Exclusion Chromatography
SEM	standard error of the mean
SRB	Sulforhodamine B
Tf	transferrin
TfR and TfR1	transferrin receptor and transferrin receptor 1
TPEN	N,N,N',N'-tetrakis(2-pyridylmethyl)ethylenediamine
Triapine	3-AP, 3-aminopyridine-2-carboxaldehyde thiosemicarbazone
TSL	thermosensitive liposome
TTM	Ammonium tetrathiomolybdate
TXRF	Total-Reflection X-ray Fluorescence
US	United States of America
UV/Vis	Ultraviolet–visible spectroscopy
v/v %	percent volume per volume
VER	vertical
VOI	volumes of interest
w/v %	percent weight per volume
w/w %	percent weight per weight
WHO	World Health Organization
ZMC	Zinc metallochaperones

1. Introduction

The research topic of this thesis is related to cancer, which is a major health problem of the population and thus one of the leading causes of mortality worldwide, especially in highly urbanized and industrialized environments. Starting from disease-related statistics, through cancer treatment strategies including platinum-based anticancer drugs, we reach metal-based chemotherapy, highlighting the iron (Fe), copper (Cu) and zinc (Zn) based chelators and complexes, as well as their anticancer activity. In addition, the related drug delivery systems, especially the relevant literature on copper containing liposomes, is briefly summarized.

1.1. Cancer and cancer statistics

Cancer is a major public health problem globally. Based on the data of the World Health Organization (WHO) [1] cancer is, after cardiovascular diseases, the second leading cause of death. In the European Region, the five major non-communicable diseases of diabetes, cardiovascular diseases, cancer, chronic respiratory diseases and mental disorders, when taken together, account for an estimated 86% of the deaths and 77% of the disease burden. Focusing on cancer, the GLOBOCAN database compiled by the International Agency for Research on Cancer provides estimates of incidence and mortality in 185 countries for 36 types of cancer, and for all cancer sites. The GLOBOCAN 2018 database released the latest estimates on the global burden of cancer [2]. Studying the cancer fact sheets, there were an estimated 18.1 million new cases of cancer (17 million excluding non-melanoma skin cancer) and 9.6 million deaths from cancer (9.5 million excluding non-melanoma skin cancer) worldwide in 2018. The incidence statistics for 2018 are projections calculated from cancer registry data collected before 2018. The latest global cancer data shows us that about 1 in 6 deaths is due to cancer; more precisely one in 5 men and one in 6 women develop cancer during their lifetime, and one in 8 men and one in 11 women die from this disease. World incidence and death rates of cancer standardized for age shows that Australia and New Zealand is the lead, followed by North America and Western Europe [3]. According to the WHO, cancer may arise due to interaction between personal genetic factors and 3 categories of external agents, namely physical carcinogens (ultraviolet and ionizing radiation), chemical carcinogens (asbestos, components of tobacco smoke, aflatoxins, and arsenic

compounds) and biological carcinogens (infections from certain viruses, bacteria, or parasites) [1, 4].

The figures for Europe in 2018 show that, excluding non-melanoma skin cancer, there were an estimated 3.91 million new cases and a total of 1.93 million deaths. With regards to the most common cancer locations in the human body, the female breast (523,000 cases) was most common, followed by, in descending order, colorectal (500,000), lung (470,000) and prostate (450,000). These four types accounted for half of the total cancer cases in Europe. The most common types leading to death from cancer were, in descending order, the lung (388,000 deaths), colorectal (243,000), breast (138,000) and pancreas (128,000). In the European Union in 2018, the number of new cases of cancer was estimated to be 1.6 million among males and 1.4 million among females, with death from cancer totaling 790,000 men and 620,000 women [5].

Unfortunately, Hungary recorded the highest age-standardized incidence and mortality rates from cancer among the EU Member States. *Figure 1* represents the age-standardized incidence and mortality rates for all cancers (excluding non-melanoma skin cancers) in Europe 2018. Altogether 1020 cancer cases and 478 deaths from cancer per 100,000 inhabitants were recorded [6].
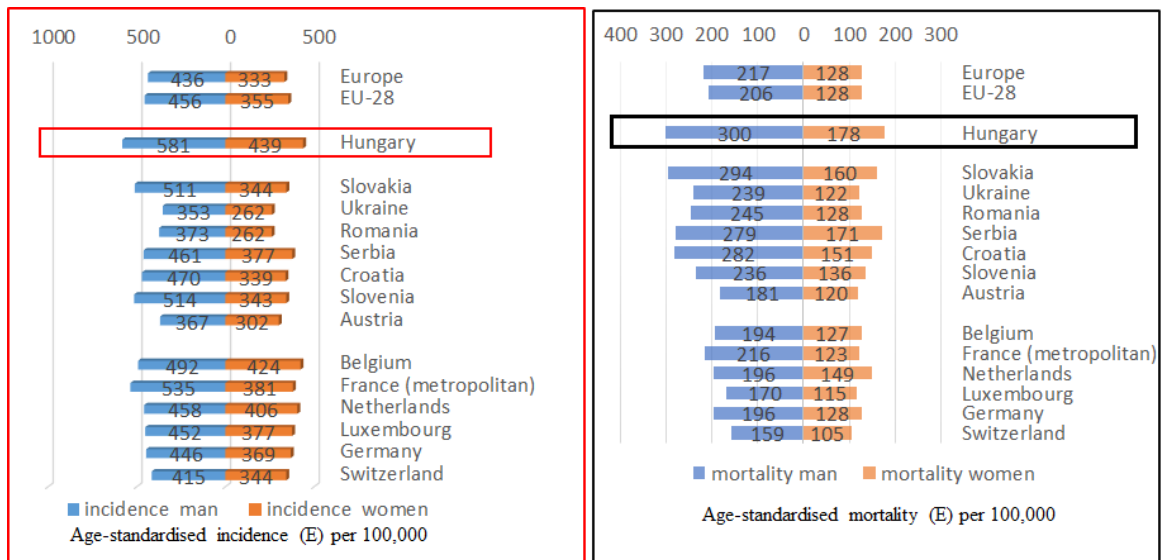
Figure 1. *Age-standardized incidence and age-standardized mortality of cancer (E) per 100,000 inhabitants in Hungary and in neighboring countries compared to the European average, to the European Union (EU-28), and to Western Europe in the year 2018. Hungary recorded the highest age-standardized incidence and death rate from cancer among the EU member states. The figure is based on the review of J. Ferlay et al. [6].*

In Hungary, data collected by the *National Cancer Registry of Hungary* [7] in 2016 (the latest available figures) showed that 51,249 men and 54,358 women were diagnosed with cancer. This represents a figure of around 1080 cancers per 100,000 people. Cancer registry data shows rising cancer statistics year after year, which is similar to the pattern existing in other countries. There are several factors which are responsible for the increase in the burden of cancer. Population growth, or the lack of, and an ageing population are two factors, as are changes in social and economic development, which lead to a change in the prevalence of certain causes of cancer. Developed countries tend to have an ageing population, and ageing increases the risk of contracting cancer. The population of Hungary is ageing significantly due to a low birth rate and emigration, and so the incidence of cancer will increase markedly over previous projections. For men, the lifetime probabilities of developing cancer and of cancer-related death already stand at 56.9% and 27.5%, respectively, and the corresponding figures for women are 51.9% and 21.7%. The total population of Hungary is expected to decrease by 6% between 2016 and 2030 while, for this period, those whose age is 60 and above will increase by 18%. The result of this will be an increase of cancer incidence of 35% and an increase in cancer mortality of 30% for the 65-85 age group. The period 2007-2015 was identified by the Joinpoint Regression Model as the starting point for the increase in new cases. It is estimated that between 2016 and 2030, lung and breast cancer in women will increase yearly by 1.9% and 1.7% respectively, while in men, prostate and colorectal cancer rates will increase yearly by 3.6% and 2.1% respectively [8]. In the last few years, a prospective cohort study comparing mortality in high-income countries (HICs), middle-income countries (MICs), and low-income countries (LICs) with standardized approaches found that in HICs and some upper-MICs, deaths from cancer are now more common than those from cardiovascular disease, marking a shift in the primary causes of deaths for middle-aged (35–70 years) people. As the cases of cardiovascular diseases decrease in many countries, mortality from cancer will probably become the leading cause of death [9, 10]. In addition, we also need to refer to a strikingly disproportionate increase in the prevalence and related mortality in MICs and LICs [11]. Based on projections of cancer mortality shown on Worldometer [12] (based on the latest statistics published by the WHO) cancer deaths will continue to rise, with an estimated 11.4 million dying in 2030. Although a large portion of the most rapidly rising cancers would be avoidable by

implementing public health programs, a substantial portion inevitably remains incurable. This fact also highlights the importance of cancer prevention, therapy and research [13, 14]. Developed countries have placed an emphasis on effective cancer prevention, early detection and treatment strategies [15]. The transformation of cancer from an inevitably fatal disease into a health condition that can be managed over time, has led to the definition of cancer as a chronic disease [16].

1.2. Anticancer strategies

The National Cancer Institute (NIH) [17] defines the disease as follows: *"Cancer is the name given to a collection of related diseases. In all types of cancer, some of the body's cells begin to divide without stopping and spread into surrounding tissues."* In 2011, Hanahan and Weinberg proposed hallmarks of cancer that enable cell growth and metastasis. The proposed hallmarks, which help to understand the biology of cancer, are: (1) sustainment of proliferative signaling; (2) evasion of growth suppressors; (3) activation of invasion and metastasis; (4) enabling of replicative immortality; (5) inducement of angiogenesis; (6) resistance to cell death; (7) avoidance of immune destruction; and (8) deregulation of cellular energetics [18]. In view of these, it is not surprising that firstly, *surgery* for complete tissue incision, secondly *radiotherapy* and thirdly the tumor cells proliferation inhibiting or tumor cell death promoting *chemotherapy* have long been the main pillars of cancer treatment strategies. From the 1990s, the structure symbolizing cancer therapy, has been expanded with two more pillars: molecular targeted therapy and immunotherapy (**Figure 2**) [19].

The oldest method of treatment, which dates back thousands of years, is surgery, and this is the mainstay treatment for those patients who have a solid tumor. Unfortunately, the biological effects that accompany the surgical stress response, together with the pharmacological effects of the anaesthetic may lead to a recurrence of the disease or to its progression. If cancer cells have not been eliminated entirely, either locally or at other undiagnosed sites, the neuroendocrine, immune or metabolic pathways that have been triggered in response to either the surgery or the anesthesia, or both, may enhance the cells' survival and proliferation. Over the past 50 years there has been a change of mindset away from the idea of radical surgery towards multimodal therapy and minimally invasive techniques, so as to avoid the worst effects that such surgery may cause. There is a new focus on preservation of form, function and quality of life without compromising the

possibility of survival [20, 21]. X-rays were discovered in 1895 and, soon after, their usefulness as a clinical treatment for cancer was recognized, so that radiotherapy became the second pillar of cancer treatment as early as 1896. Improvements in technology now mean that radiotherapy can be delivered to tumor lesions with great accuracy and with substantially reduced injury to the neighboring healthy tissues. The importance of radiation therapy remains high, with approximately 50% of cancer patients receiving it at some point during the course of their therapy. This method contributes 40% of the curative treatment for cancer patients [22, 23].

Chemotherapy was first used in an attempt to control cancer in the 1940s through the biological actions and therapeutic applications of the B-chloroethyle amines and sulfides [24]. Since then, cancer patients have been treated with what are broadly toxic chemicals as a matter of course in medical oncology, despite their often severe side effects. The aim in the use of chemotherapeutic agents is to inhibit either directly or indirectly the proliferation of rapidly growing cells. These drugs can be clustered into several different categories, according to their mechanism of action [25]:

(1) *DNA-modifying agents as alkylating* (cyclophosphamide, temozolomide, carmustine etc.) and *alkylating-like agents* (cisplatin, carboplatin, oxaliplatin etc.),

(2) *anti-metabolites* (methotrexate, 6-mercaptopurine, 5-fluorouracil, gemcitabine, etc.),

(3) *spindle poisons* (inhibiting microtubule function like vinblastine, vincristine and paclitaxel, docetaxel etc.),

(4) *topoisomerase inhibitors* (camptothecin, etoposide etc,)

(5) *cytotoxic antibiotics* (doxorubicin, daunorubicin, bleomycin etc.)

(6) *miscellaneous antineoplastics* (L-asparaginase, mitotane, hydroxyurea, procarbazine etc.).

The discovery of cisplatin in the 1960s represented a landmark achievement and set a new era for cancer treatment [26]. Although historically affiliated to alkylating agents, it should rather be referred to as an 'alkylating-like' agent as it is not actually an alkylating agent, but attacks cancer cells in much the same way [27]. The success of cisplatin treatment as a therapy for cancer has led to a great deal of research in the bioinorganic chemistry field. Although cisplatin is of significant clinical benefit in the treatment of

several types of solid tumors, its overall effectiveness is reduced due to its toxic side effects and tumor resistance, which can and does cause the occurrence of secondary malignancies. Hence, researchers have been encouraged to find and develop novel, platinum-free metal complexes which have superior anti-cancer ability and lower side effects compared to cisplatin. Until 2005, about 35 platinum complexes had entered clinical trials in order to find such a superior treatment [28]. The development of platinum (Pt) and other transition metal-based complexes with anticancer activity has had an enormous impact on cancer chemotherapy [29].

A disadvantage of systematic chemotherapy is that the side effects are often severe, and it is not uncommon for resistance to develop (**Section 1.3.**). Anticancer drugs with higher precision of molecular targeting have been developed. These drugs target the molecules that influence cancer cell multiplication and survival. Thus, they are more precise than cytotoxic chemotherapeutics, which target all rapidly dividing cells. Hence the damage to nearby healthy tissues is limited. Genetic alterations are essential for tumor development and survival, and thus targeted therapy focuses on those molecular abnormalities which are specific to cancer. The target is the changes in cancer cells that help them grow, divide and spread. The therapies themselves are composed of dosing monoclonal antibodies and small-molecule drugs to cancer patients [30]. The prospective revolutionary success of targeted cancer therapy was first recognized in 1998, when a monoclonal antibody trastuzumab (Herceptin) against receptor tyrosine kinase HER2 was approved by the US Food and Drug Administration (FDA) for treating patients with HER2-positive metastatic breast cancer [31]. At present, a total of 43 different molecular-targeted anticancer agents have been approved by the FDA [32]. Most targeted therapies are either small-molecule drugs or monoclonal antibodies. Targeted treatment represents a promising therapeutic approach for patients with diverse cancers. Spanning 12 months, from August 1, 2018 to July 31, 2019, the FDA approved 14 new, molecularly targeted anticancer therapeutics. In the meantime, they also approved four previously permitted molecularly targeted anticancer therapeutics for treating further types of cancer [19]. With the rapid progress of molecular targeted therapy research [33] and its clinical application, a large amount of clinical trial data of the targeted agents for treatment of different types of cancer has been published. A new database, called Cancer Molecular Targeted Therapy database (CMTTdb), provides a comprehensive collection of these resources and links

them to clinical use [34]. However, there are still great limitations to these new drugs which aim at a single-target. For example, in numerous studies conducted to explore resistance mechanisms to epidermal growth factor receptor (EGFR) blockade, there are several biomarkers and pathways involved in the development of resistance to anti-EGFR therapy. It is believed that yet more factors regulating and controlling the expression of the targeted drug resistance will soon be found [35].

Certain cancer types are hormone sensitive, including breast, prostatic, and ovarian cancer or endometrial (womb, uterine) cancer, which can be treated with hormone therapy. This kind of treatment uses medicines to block or lower the amount of hormones in the body to stop or slow down the growth of cancer [36, 37].

Immunotherapy has become a powerful clinical strategy for treating cancer. Cancer immunotherapy, including cancer vaccines, immune checkpoint inhibitors, and adoptive cell therapy, represents a scientific breakthrough in the treatment of various malignancies [38]. For many years, oncologists have concentrated on treating the tumor itself, which could result in damage to the tumor's host and immune system. The immune system itself uses a number of innate and adaptive mechanisms. Not only does it guard against pathogens, but it stops malignant transformations ('immune surveillance"). Therefore, any clinically apparent tumor has already selected for those malignant cell clones that can evade immune recognition ("immune evasion"). Recently, the immune systems of patients and their activation via biological therapies have received a lot of attention from researchers. Biological therapies, including immunotherapy and oncolytic virus therapy, are often more physiological and well tolerated [39]. Strategies with a combination of chemotherapy and immunotherapy are also available (chemoimmunotherapy). Certain cytotoxic cancer chemotherapeutic drugs can kill tumor cells by an immunogenic cell death pathway, which activate powerful anti-tumor immune responses and has the potential to significantly increase the efficacy of chemotherapy [40]. Several clinical trials have now been reported that use low, immune-modulating doses of chemotherapy specifically to enhance the activity of cancer vaccines (boost the immune system's ability to recognize and destroy antigen) rather than to subject tumor cells to lysis directly [41].

Metal drugs, besides their well-known cytotoxic anticancer effects, interact considerably with the cancer-immune system and can reverse important aspects of immune evasion [42]. One class of cytotoxic drugs that may become the focus of

combination strategies with checkpoint inhibitor-based immunotherapies are anticancer metal-based compounds. This anticipation is based especially on recent highly promising chemoimmunotherapy data for the combination of platinum drugs and programmed death-1/programmed death-ligand 1 (PD-1/PD-L1) checkpoint inhibitor antibodies in non-small cell lung cancer [43, 44]. According to new literature data, there is a complex interplay between classical metal complex drugs, such as cisplatin or oxaliplatin, together with novel anticancer metal complexes and the anticancer immune response, which both have a direct impact on cancer cell immune recognition [42].

More than half of the global cancer cases are the result of preventable causes, thus great attention must continue to be paid to the most important factors that underpin the pillars: prevention and early diagnosis. Early cancer detection identifies tumors when outcomes are superior and treatment less morbid. A new prospective study evaluated the results of targeted methylation analysis of circulating cell-free DNA (cfDNA) to detect and localize multiple cancer types across all stages at high specificity. The 6689 participants (2482 cancer (>50 cancer types) and 4207 non-cancer patients) were divided into training and validation sets. In validation, specificity was 99.3% [95% confidence interval: 98.3% to 99.8%; 0.7% false-positive rate]: cfDNA sequencing detected more than 50 cancer types across stages [45].
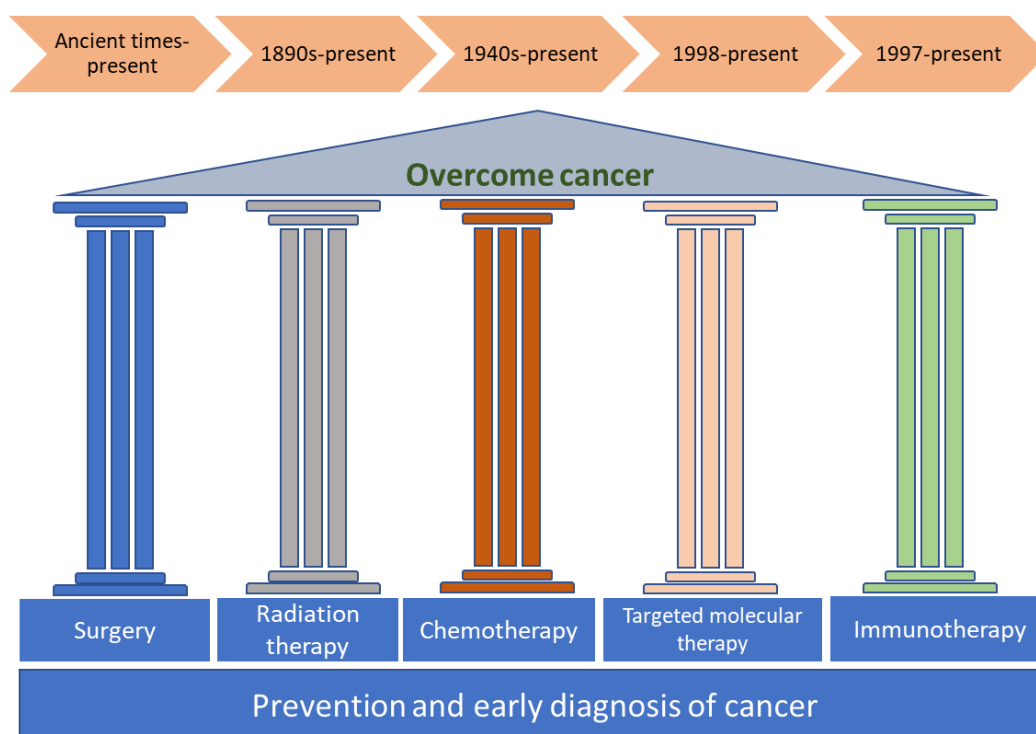
Type of agent
DNA-modifying agents
• Alkylating agents
• Platinum complexes
Anti-metabolites
Spindle poisons
• Vinca alkaloids
• Taxanes
Topoisomerase inhibitors
• Topoisomerase I inhibitors
• Topoisomerase II inhibitors
Antitumor antibiotics
Miscellaneous Antineoplastics

Figure 2. *Five pillars of treatment of cancer. Figure is based on the American Association for Cancer Research (AACR) Cancer Progress Report in 2019 [19]. Chemotherapy plays a vital role in treating free cancer cells and undetectable cancer micro-focuses.*

1.3. Drug resistance

A major problem of chemotherapy is drug resistance, which is an effect where cancer cells that were initially suppressed by an anticancer drug tend to develop resistance to it.

The main reason for this is the increase in the drug efflux and the reduction in drug uptake. If such resistance is efficient against functionally distinct and structurally unrelated drugs, the phenomenon is referred to as "multidrug resistance" (MDR) [46, 47]. Anticancer drug resistance has been especially linked to breast cancer resistance proteins (BCRP, ABCG2), the overexpression of P-glycoprotein (ABCB1), and multidrug resistance-associated proteins 1 and 2 (MRP1/2, ABCC1/2) [46]. A number of MDR-selective compounds with chelating moieties (which include isatin-β-thiosemicarbazones such as NSC73306) have been identified that have an increase in toxicity against MDR cells that express ABCB1 solely in the plasma membrane [48]. A recent review listed several chelator-like compounds that demonstrate preferential hypertoxicity to P-gp positive cell lines [47], showing that the application of drugs which elicit collateral sensitivity (CS) can be effective against MDR cancer cells that have pathological P-gp overexpression [49]. The cytotoxic mechanism is not associated with P-gp. A set of MDR compounds was found to have the capacity for metal chelation, when 42,000 molecules were subject to in silico screening against the NCI-60 cell line panel [50].

Cisplatin and doxorubicin resistance are a major problem generally. The expression of metallothionein (MT) in certain tumor cells has been associated with resistance to anticancer drugs [51]. Anticancer thiosemicarbazones were examined in relation to resistance development [52]. Wehbe et al. supports the potential use of copper-based therapeutics to treat cancer types that are resistant to Pt drugs [53].

1.4. Metal ions and cancer

Biological systems make extensive use of metal ions. Therefore, the idea that metal ions and metal complexes, or chelators, can play an important role in cancer also follows logically. The role of iron, copper and zinc ions in cancers and the related metal contents in tumors have long been studied [54].

1.4.1. Copper and cancer

Copper is an essential element/ion in several important processes of various biological systems, including the human body. However, an excess of copper can lead to oxidative damage. Copper has been found to be involved in the development and progression of cancer, and can facilitate cancer growth, metastasis and angiogenesis. Recent research

into the involvement of copper in cancer has shown that it could possibly be used as a novel selective target for cancer therapies. Many types of cancer show an increase in intratumoral copper and/or altered systematic copper distribution in many cancer types. Elevated levels of copper were found in malignant tissues for several types of cancer, including breast, ovarian, cervical, lung, colon, and stomach, and in leukemia by Gupte and Mumper (2009) [55]. Surprisingly, leukemic and breast cancer cells can have up to four-fold the copper content of healthy ones [56, 57]. Strikingly, elevated serum copper correlated with the stage of the disease and its progression in colorectal and breast cancers [58, 59]. In patients with advanced breast, lung or colon cancer treated with various chemotherapeutics, serum copper levels were clearly linked to drug resistance [60]. Cases unresponsive to treatment had approximately 130–160% more copper in their serum. Ratios of Cu/Zn, Cu/Fe and Cu/Se appear to be better diagnostic markers of the presence of cancer than Cu, Zn, Fe or Se levels alone [57]. The high-affinity copper transporter CTR1 and CTR2, copper efflux transporters, ATP7A and ATP7B, together with the organic cation transporter 2 (OCT2) heighten acquired resistance against chemotherapeutics. The expression of CTR1 in cultured cells is inversely proportional to cisplatin accumulation and resistance, suggesting that CTR1 is responsible for cisplatin uptake across the plasma membrane [61]. Conversely, ATP7A abundance is positively correlated with increased resistance to cisplatin. Over-expression of ATP7A and ATP7B is observed in multiple cancers [62]. Furthermore, their expressions are associated with cancer prognosis and treatment results of cisplatin chemotherapy. Low expression of ATP7A and ATP7B suppresses tumorigenesis and increases the sensitivity to platinum drugs. Copper chelators reverse platinum drug resistance by decreasing ATP7A/7B levels [63].

1.4.2. Iron and cancer

The malignant cancer phenotype is often found in association with a deregulated iron homeostasis, particularly in the expression of iron-regulated genes that fuel their higher metabolic iron demands, which are needed for growth and survival [64]. Both the beneficial and deleterious effects of iron have a role in cancer. As early as 1940, exposure to iron oxide dust was shown to triple the incidence of pulmonary tumors in mice [65]; in the 1950s, intramuscular injection of iron–dextran was shown to induce sarcoma in rats

[66]. However, mice fed a low-iron diet, prior to implanting tumor cells, showed considerably delayed tumor growth [67].

Iron uptake by transferrin receptor is the most important way for cancer cells to absorb iron, and accumulating evidence has proven that transferrin receptor (TfR) 1 (TfR1) participated in tumor onset and progression, and its expression was dysregulated considerably in many cancer types [68]. Some relationship may exist between ferritin and cancer. In fact, despite no increase in Fe stores, serum ferritin is increased in patients suffering a number of neoplasms. In general, tumor cells contain low quantities of ferritin when compared to their normal counterparts. This is difficult to explain considering the high Fe uptake rate by tumors via the TfR1 [64].

Several population-based studies have examined the relationship between iron and cancer risk. Stevens et al. studied 14,000 participants in the first US National Health and Nutrition Examination Survey in order to study the relationship between biochemical markers and cancer. They showed a significantly higher level of saturation of the iron-binding transporter transferrin (Tf) enrolment of men, who then went on to develop cancer, compared to those men who did not [69, 70]. Further studies found similar results [71, 72]. A relationship has also been found between the risk of cancer and dietary iron intake. From a meta-analysis of 33 studies that examined a connection between iron intake and colorectal cancer it was revealed that approximately three-quarters of the studies associated higher iron intake with an increase in the risk of contracting colorectal cancer [73]. However, there are limitations to both of the analyses described above. The first analysis did not include measures such as serum levels of ferritin, which are thought to more closely mirror levels of iron in the body. The second analysis had inherent difficulties, such as the inferential assessment of iron intake, the variability in iron absorption post-intake, and the sample size [74].

1.4.3. Zinc and cancer

The role of zinc in cancer has received increasing attention [75, 76]. It has been found that the imbalance of zinc ions and compounds and dysfunction of zinc transporters may result in many chronic diseases, including cancer, especially prostatic cancer. Zinc deficiency causes oxidative DNA damage and chromosome breaks in animals fed a zinc-deficient diet. In rats, dietary zinc deficiency causes an increased susceptibility to tumor development when exposed to carcinogenic compounds [77].

Inutsuka et al. [78] found that the plasma copper level increased and the plasma zinc level decreased significantly in the group with carcinoma of the digestive organs. The Cu/Zn ratio was not only significantly higher than in the normal group, but also was high in cases with advanced carcinoma, especially when liver metastasis was present.

The prostate secretes high amounts of zinc in prostatic fluid and contains the highest concentration of zinc in any soft tissue of the body. Mawson et al. found that carcinomatous prostate tissues contained less zinc than normal prostate [79]. Zinc concentrations in malignant prostate tissues are about 10-25% of that in healthy prostates, suggesting that high zinc concentrations may be essential for the maintenance of prostate health [80]. Nevertheless, despite modest discrepancies, the available research data supported a reduced zinc content in the sera of prostate cancer patients [81].

The studies of Franklin et al. clearly establish that human ZIP1 (hZIP1) gene expression is down-regulated and zinc is depleted in adenocarcinomatous glands. This observation, together with the numerous reports of loss of zinc accumulation in prostate cancer, leads to the proposal that down-regulation of hZIP1 is a crucial early event in the development of prostate cancer [82].

Chakravarty et al. [83] hypothesized that supplementing zinc to malignant patients prior to and following chemotherapy could help in improving their immune response against tumor and, consequently, regulate tumor growth and delay the ability to form metastasis [84].

Despite the lower intake of zinc by prostate cancer patients, a meta-analysis by Mahmoud et al. indicated that there is no evidence for an association between zinc intake and prostate cancer when examining data of histologically confirmed prostate cancer patients (n = 127) and a control group (n = 81) [85]. Li et al. [81], after accumulating research data, strongly suggested mobile zinc as an excellent candidate biomarker for the clinical diagnosis of prostate cancer.

The p53 tumor suppressor is a transcription factor which contains a single zinc center near the DNA binding domain. Zn^{2+} is required for adequate transcriptional activation. Excessive, or insufficient amounts of zinc cause misfolding of p53 by several mechanisms, which results in functional loss of DNA. Zinc supplementation reactivates p53 and suppresses tumor growth. The p53 activity can be restored by zinc

supplementation. The cell permeable chelator 1,10-phenanthroline has been shown to activate p53 in mouse cells [86].

A correlation has been suggested between metallothionein (MT) protein levels and the growth and invasiveness of certain tumors. MT is a cysteine-rich, low molecular weight (6 to 7 kDa) protein that binds zinc, copper and cadmium. The role of MTs and zinc in cancer development is closely connected, and the structure and function of MTs are dependent on Zn^{2+} status [87]. Moreover, MT overexpressing cells and tissues show significant resistance to antitumor agents, like cisplatin or doxorubicin [88, 89].

1.5. Therapeutic strategies in cancer related to metal ions

There are several clinical applications of chelators and chelator metal complexes [90]. Metal-based antitumor drugs play an important role in medical bioinorganic chemistry. The main goal is to develop novel, metal related technologies for more advanced cancer detection, diagnosis and treatment.

1.5.1. Metal-based chemotherapy

Platinum compounds are at the heart of metal-based chemotherapy. Their history began with the discovery by Rosenberg of the anti-cancer action of cisplatin [26] in the twentieth century. Since the therapeutic activity of metal complexes was first discovered, the search has been on to find further complexes, which have similar or better activity, with fewer negative side-effects.

In 1978, the US FDA approved Platinol®, a brand of cisplatin, as a combination therapy in the management of metastatic testicular, ovarian and bladder cancers. One noteworthy mark of the success of platinum drugs is that, since the introduction of cisplatin into the treatment regimen of testicular cancer patients, the cure rates have exceeded 95% [91]. To treat metastatic testicular cancer, three to four cycles of cisplatin in combination with etoposide and bleomycin are used. However, for testicular cancer survivors an increased risk of developing metabolic syndrome is observed. Johannessen et al. [81] suggest that the cisplatin-based chemotherapy has long-term effects on the epigenome. They hypothesize that epigenomic changes may also play a role in the development of metabolic syndrome in the survivors [92]. Cisplatin is currently used primarily to treat testicular, gynaecological, lung, bladder, and head and neck cancer, so the "penicillin of cancer" is widely used in clinics [93]. The four steps of the mechanism

of cisplatin is quite clear now: (1) cellular uptake, (2) aquation/activation, (3) DNA-binding, and (4) cellular processing of DNA lesions leading to apoptosis [94]. However, cisplatin plays a role in other alternative, interesting mechanisms, such as endoplasmic reticulum (ER) stress, disruption of RNA transcription, inhibition of oncogenic proteins, acidification of the cytoplasm and change metabolism of cancer cells. Moreover, cisplatin has a pleiotropic effect on cellular proteins, affecting their conformation and function. Cisplatin may also exert antitumor immunomodulation [93]. Modern studies reveal that high affinity copper transporter protein CTR1 is also responsible for cisplatin uptake, e.g. Ref. [61]. Despite cisplatin being the first-line therapy for several cancers, the response curve for dosage is very steep for both antitumor and adverse health effects. Attempts to reduce toxicity through the administration in hypertonic saline and with pharmacokinetically based dosing schedules, thus allowing for an increase in the dose of intravenous cisplatin, have led to a partial success in the reduction of nephrotoxicity and bone marrow suppression. However, this has led to the emergence of new dose-limiting toxicities, namely peripheral neuropathy and ototoxicity, which thus continue to restrict the use of high dose cisplatin therapy. Proposed chemoprotective, chelator-like agents, including sodium thiosulfate, WR2721, and diethyldithiocarbamate (DDTC) are being extensively investigated as "rescue agents" for either regional or systemic administration of cisplatin along with the potential clinical benefits [95].

In 1989, the FDA approved Paraplatin® (carboplatin) as a combination therapy in the management of ovarian cancer. Eloxatin® (oxaliplatin) was initially launched in France in 1996 and became formally available in European countries in 1999 and in the US in 2002. This is a platinum-based drug with oxalate and diaminocyclohexane ligands. Diaminocyclohexane ligands play a major role in cytotoxicity and protect it against cross-resistance with cisplatin and oxaliplatin [29].

The platinum-based drugs of cisplatin, carboplatin and oxaliplatin dominate in the treatment of cancer globally, whilst three other platinum derivatives have been synthesized with established clinical success and different scopes of approval: Aqupla® (nedaplatin) approved for use in Japan in 1995, heptaplatin for use in Korea in 1999, and lobaplatin for use in China in 2010. Other than these six drugs, new platinum agents have been slow to enter clinical use. In addition to the next generation of cisplatin-like platinum(II) complexes, different steroid, folate and peptide targeting of platinum(II)

structures were synthetized and examined. These were followed by platinum(IV) prodrugs that release classical platinum(II) anticancer agents [29, 94]. Lipoplatin is a liposomal form of cisplatin designed to enhance the pharmacokinetic safety profile and allow dosage manipulation, while targeting cancer cells [96, 97]. Platinum complexes, being synthesized following the model of cisplatin, have been shown to have several mechanisms of action, as have synthesized complexes with different metal ions. Mechanisms include not only interactions with DNA, but other actions including topoisomerase inhibition, hydrolytic cleavage, groove binding, oxidative cleavage, inducing reactive oxygen species (ROS) and proteasome inhibition [98].

The nature of metal ion functions in biology has stimulated the development of new non-Pt metal-based drugs with the aim of obtaining compounds acting via alternative mechanisms of action. Many other compounds, other than Pt complexes, are potentially attractive as anticancer agents (**Table 1**).

Table 1. *Non-Pt metal-based drugs in metal-based chemotherapy.*

Metal	Statement about its supposed suitability for cancer therapy	References
Sc	• Radio-scandium (^{47}Sc) was produced and purified, a potential radioisotope for cancer theranostics.	[99]
	• Scandium metallocene complexes show antiproliferative activity *in vitro* against a breast (MDA-MB-231) and prostate (DU145) cancer cell line.	[100]
Ga	• Gallium(III) shares certain chemical characteristics with iron(III), which enables it to interact with iron-binding proteins and disrupt iron-dependent tumor cell growth.	[101]
	• Gallium-nitrate, tris(8-quinolinolato)gallium(III) (KP46) and gallium maltolate compounds that have been evaluated in the clinic for cancer treatment.	[102] [103]
Sn	• The therapeutic properties of triphenyltin acetate in mice tumors were observed in the early 1970s.	[103]
	• Organotin complex derived from propyl gallate and 1,10-phenanthroline indicates antitumor activity by interacting with the biological target DNA at molecular levels.	[104]
	• Due to the high cytotoxicity that they present *in vitro*, they exhibit the possibility of overcoming multidrug resistance.	[105] [106]
Sb	• Trivalent and pentavalent antimony compounds have been synthetized with *in vitro* cytotoxic effect.	[107, 108]
	• An antimony(III) complex with the heterocyclic thioamide was synthetized with anti-metastatic capability study.	[109]
	• Antimony(III) complexes with hydroxyquinoline derivatives: anti-trypanosomal activity and cytotoxicity against human leukemia cell lines.	[110]

Table 1. (continued) Non-Pt metal-based drugs in metal-based chemotherapy.

As	• Arsenic compounds have been epidemiologically associated with various types of cancer.	[111, 112]
	• Arsenic trioxide (As_2O_3, ATO) has been used as a therapeutic agent for over 2000 years, the recipe originated in China.	[113, 114]
	• As_2O_3 has been for years a front-line drug for treatment of acute promyelocytic leukemia and is in clinical trials for treatment of other malignancies, including multiple myeloma.	[113, 115, 116]
	• All-trans retinoic acid (ATRA) and arsenic trioxide have been suggested as frontline therapy for newly diagnosed acute promyelocytic leukemia.	[115, 117]
	• Targeting the Warburg effect (in over 90% of all tumor forms) with dichloroacetate and the increased mitochondrial activity of glutaminolysis with ATO in breast cancer cells was more effective at inhibiting cell proliferation and inducing cell death than either drug alone.	[118]
	• Coencapsulation of arsenic- and platinum-based drugs: arsenic loading into a liposome in response to a transmembrane gradient of aqua-cis-Pt acetate resulted in cellular uptake and thus anti-cancer efficacy against folate receptor overexpressing tumor cells.	[119]
Bi	• First anti-tumor trials for bismuth compounds were those containing the anion derived from 6-mercaptopurine with anti-leukemic activity.	[108]
	• Antitumor activity was demonstrable for lipophilic bismuth nanoparticles (BisBAL NPs) on breast cancer cells.	[120]
Ti	• Titanocene dichloride metallocene reached the clinical trial for cancer treatment, although the results of phase II clinical trials were not satisfactory.	[121, 122]
	• Series of other Ti(IV)-compounds has been synthesized and shown *in vitro* cytotoxicity.	[123]
	• Incorporation of Ti(IV)-compounds using nanostructured silica, a higher Ti-uptake by the treated cancer cells (from 4% to 23% of the initial amount of Ti) was observed when compared with the "free" titanocene compounds.	[103]
V	• Vanadium(IV)-complex is a suitable candidate for cancer treatment. It appears that V(IV) has lower side effects than platinum metal ions.	[124]
	• Vanadium complexes could induce a p53 dependent apoptotic mechanism in high risk HPV16-positive cervical cancers.	[125]
	• A synthetized complex might be considered as a safe new drug for treatment of hepatocellular carcinoma with low side effects on control liver cells.	[126]
	• V(V)-peroxide complexes have been designed and synthesized as potential antitumor compounds.	[124]
Pd	• Several Pd(II)-complexes (121 tested complexes) showed promising cancer selectivity and activity against triple-negative breast carcinoma cell line.	[127]
	• Palladium complexes are shown to have lower kidney toxicity than cisplatin due to the inability of proteins in the kidney tubules to replace the tightly bound chelate ligands of Pd(II) with sulfhydryl group.	[128]
	• A novel palladium(II) complex significantly reduces the growth of tumor cells *in vivo* model.	[129]

Table 1. (continued) *Non-Pt metal-based drugs in metal-based chemotherapy.*

Ru	• Coordination and organometallic ruthenium derivatives are available with various oxidation states, such as Ru(II), Ru(III), Ru(IV).	[124, 130]
	• Tumor cells represent overexpression of transferrin receptor, formation of transferrin-Ru adduct directs the complex to the tumor cells.	[124]
	• Ru(II) complex showed less cytotoxicity in normal MRC-5 cells and more cytotoxic effects in cisplatin-resistant A2780/CP70 cells than cisplatin.	[131]
	• The antitumor activity of a ruthenium(II) polypyridyl complex was comparable with cisplatin *in vivo*.	[132]
	• Ru(III)-complexes can be readily reduced to Ru(II)-complexes.	[133, 134]
	• One ruthenium compound successfully entered phase I clinical trials and has significant efficacy in inhibiting tumor metastasis.	[135–137]
	• Another Ru-compound entered clinical trial: KP1019/1339, but the toxic potential of KP1019 is enhanced in the presence of various metal ions.	[137]
	• Ru-complexes and photodynamic therapy could be a good combination.	[138]
	• Encapsulating Ru-complexes into nanomaterials can improve their targeting capability through EPR effect.	[139]
Rh	• 2(1H)-quinolinone derivatives and their rhodium (III) complexes were synthesized. One compound effectively inhibited tumor growth in the NCI-H460 xenograft mouse model with less adverse effect than cisplatin.	[140]
	• *In vitro* cellular uptake has been assessed of N-protected phenylalanine dinuclear Rh(II) complexes.	[141]
	• Brachytherapy with radioactive isotopes of rhodium 106-Ru/106-Rh plaques can be recommended for small (T1a,b) and medium-sized (T2) choroidal melanomas.	[142]
	• Rhodium(III) isoquinoline derivatives Rh1 and Rh2 generated anticancer activity. Rh1 exhibited a more favorable *in vivo* safety profile than cisplatin, and the tumor inhibition ratios were comparable.	[143]
Au	• Two gold(III) complexes: $AuCl_3$ and $AuCl_2$ compounds demonstrated a good cytotoxic activity compared to cisplatin. They were shown to interact closely with proteins such as albumin and transferrin, but only weakly and reversibly with DNA.	[144]
	• Bioconjugation of Au(III)-complexes has emerged as a promising strategy for improving the selectivity of this class of compounds for cancer cells over healthy tissues.	[145]
	• Gold nanoparticles (Au-NPs) as drug carriers or Au-NPs combined with hyperthermia might be good perspectives: Au-NP–cetuximab–gemcitabine nanocomplex was superior to any of the agents alone or in combination *in vitro* and *in vivo*. In addition, citrate-coated Au-NPs bound with thiolated PEG and tumor necrosis factor-α (TNF-α) and AuroShell® particles for photothermal therapy have reached early-phase clinical trials.	[146]
Ag	• Several Ag(I) complexes containing a mixed ligand system of phosphine and thiazolidine were successfully synthesized with *in vitro* cytotoxic efficacy.	[29, 147, 148]
	• Antitumor activity is one of the promising properties of silver nanoparticles.	[149]

Table 1. (continued) Non-Pt metal-based drugs in metal-based chemotherapy.

Fe	• The anticancer activity of iron complexes was first reported for ferrocenium picrate and ferrocenium trichloroacetate salts, and was attributed to their ability to form reactive oxygen species ROS, leading to oxidative DNA damage.	[150]
	• An Fe(III)-marimastat complex has been evaluated as a hypoxia-activated drug carrier.	[151]
	• The success with ferrocene-tamoxifen complex prompted the next research in this field.	[152, 153]
Zn	• Potential prostate cancer therapy: membrane-penetrating peptide Novicidin connected to zinc-Schiff base (complex formation) as a carrier vehicle for the delivery of zinc to prostate cells.	[154]
	• Quercetin–zinc (II) complex was evaluated and both cell migration ability and invasiveness were markedly reduced.	[155]

In addition to the approved platinum-based anticancer drugs, arsenic (As_2O_3), bismuth (Bi(III)-compound, anion derived from 6-mercaptopurine), titanium (titanocene dichloride), ruthenium (NAMI-A, KP1019, NKP-1339), molybdenum (ammonium tetrathiomolybdate, hereinafter TTM), and copper (Casiopeinas®) containing compounds have entered clinical trials (**Table 1** and Ref. [156]).

According to the Swiss physician and chemist, Paracelsus (1493-1541), "All substances are poisons; there is none that is not a poison. The right dose differentiates a poison from a remedy." [157]. This is true for ionic forms of metals, such as iron, copper and zinc. They are essential for life. In a healthy body, their deficiency and excess can manifest themselves in various symptoms. In relation to cancer, therapies can be based on the absence and toxicity of different metal ions.

1.5.2.   Iron depletion

It has long been known that neoplastic cells express high levels of TfR1 and internalize iron from Tf at a very high rate. As neoplastic cells require a very large amount of Fe, it is extremely important to understand its metabolism in order to devise potential new therapies [64]. A number of strategies for antitumor therapies have been designed that target intracellular iron, including utilization of TfR1-mediated cytotoxic drug conjugates and iron chelators. The Achilles' heel of cancer cells is that they have a high demand for iron in order to sustain their proliferative capacity. Several pre-clinical studies and clinical trials show targets related to tumor iron metabolism: TfR antibody (monoclonal antibody against TfR), deferoxamine (desferrioxamine, DFO), Triapine (3-AP, 3-aminopyridine-2-carboxaldehyde thiosemicarbazone), deferasirox (EXJADE®), VLX600 (6-methyl-3-

((2E)-2-(1-(pyridin-2yl)ethylidene)hydrazinyl)-5H-(1,2,4)triazino(5,6-B)indole) and DpC (di-2-pyridylketone 4-cyclohexyl-4-methyl-3-thiosemicarbazone) [158].

The role of iron chelators in the context of resistance has been investigated. The mechanism of action of an 8-hydroxiquinoline derivate, NSC297366, shows exceptionally strong P-gp-potentiated toxicity. The toxicity of NSC297366 is linked to cellular iron depletion, which is exacerbated by P-gp. Treatment of cells with NSC297366 resulted in changes associated with the activity of potent anticancer iron chelators [159].

1.5.3.   Mechanisms related to zinc homeostasis of the cancer cells

Changing the cellular and tissue zinc levels provides the basis of a treatment regimen that restores elevated zinc levels in the malignant cells and induces the cytotoxic/tumor suppressor effects of zinc. [160].

Several studies examine the biological mechanisms and significance of the depletion of labile endogenous Zn^{2+} stores in the cell related to anticancer strategy. Hashemi et al. demonstrate that the modulation of intra and extracellular zinc alone is sufficient to induce apoptosis in two breast cancer cell lines MCF-7 and MDA-MB-468. Treatment of breast cancer cells with a cell membrane permeable zinc chelator, N,N,N',N'-tetrakis(2-pyridylmethyl)ethylenediamine (TPEN) and the membrane impermeable zinc chelator, diethylenetriaminepentaacetic acid (DTPA) resulted in a significant increase in cell death. N-Acetylcysteine (NAC) inhibited the cytotoxic effect of DTPA and TPEN, indicating that oxidative stress is the mediator of Zn-deficiency-related cytotoxicity [161].

One ionophore which successfully acts as a zinc delivery agent is clioquinol (CQ; 5-chloro-7-iodo-8-hydroxyquinoline). CQ has a moderate zinc binding affinity. Costello et al. shows that CQ treatment of ZIP1-deficient cells in the presence of physiological levels of zinc results in 80% inhibition of proliferation [160].

Xue et al. [162] studied the interaction of zinc ions with another ionophore, chloroquine ((RS)-N'-(7-chloroquinolin-4-yl)-N,N-diethylpentane-1,4-diamine), in a human ovarian cancer cell line (A2780). It was found that zinc uptake was enhanced by A2780 cells in a concentration-dependent manner, measured using a fluorescent zinc probe. Chloroquine and hydroxychloroquine compounds were widely mentioned in connection with the COVID-19 pandemic [163].

Zinc metallochaperones (ZMC) have been identified as potential anticancer agents in cases where there is a zinc deficiency due to cancer. They are a new class of mutant p53

reactivators that restore wild-type structure and function to zinc-deficient p53 mutants. They were identified by a screen of the National Cancer Institute (NCI) database looking for compounds that inhibited growth of cell lines expressing the TP53 mutations at codons 175, 248 and 273 compared to cells expressing wild-type p53. The supplementation of $ZnCl_2$ within a narrow concentration range (5–15 µmol/L) succeeded in increasing the cell growth inhibition activity of ZMC1 (NSC319726) two-fold [164].

Two thiosemicarbazones were investigated as possible ZMCs: Triapine and COTI-2 (4-(2-pyridinyl)-2-(6,7-dihydro-8(5H)-quinolinylidene)hydrazide-1-piperazinecarbothioic acid). Triapine was not found to exhibit zinc metallochaperone activity. However, it has been theorized that COTI-2 might exhibit mutant p53 reactivating activity. It is unlikely to be a mutant-p53-specific therapy, as both wild-type and mutant p53-expressing cells exhibited sensitivity to the agent [165, 166]. Zaman et al. [167] showed that thiosemicarbazone ZMC1 has affinity for copper that is approximately 10^8 greater than Zn^{2+}. They identified an alternative zinc scaffold (nitrilotriacetic acid) and synthesized derivatives to improve cell permeability. In summary, it is difficult to find an anti-cancer chelator-like structure which forms a stable complex with zinc, and in which copper-mediated toxicity does not play a role.

1.5.4. *Anticancer mechanism related to copper*

The use of copper-binding ligands to target tumor copper could provide a novel strategy for cancer selective treatment (**Figure 3**). The number of studies in this area has multiplied in recent decades. Copper has been found to be a limiting factor in several aspects of tumor progression, including growth, metastasis and angiogenesis. As a result, copper-specific chelators are being developed as therapies to inhibit the aforementioned processes. A further approach is to use specific ionophores, which can increase intracellular copper levels. In addition, studies were conducted to look for replacement of platinum with copper in coordination complexes, only platinum currently being used in mainstream chemotherapies [168].

1.5.4.1 *Copper depletion*

Copper is essential to metastatic cancer progression, and may have a role in tumor growth, epithelial-mesenchymal transition, and the formation of tumor metastasis and microenvironment. In addition, higher copper levels were found in serum and tumor tissues of breast cancer patients as compared to healthy controls. As a result, copper

depletion has emerged as a novel therapeutic strategy in the treatment of metastatic cancer (**Figure 3**).

Preclinical data are available concerning copper chelation agents, including D-penicillamine, Trientine®, disulfiram, clioquinol and TTM, across a variety of tumor types [169].

The targeting of the elevated copper (both in serum and tumor) and oxidative stress levels was examined by Gupte et al. [55] with the aid of a copper chelator D-penicillamine for potential cancer treatment. They have discussed the application of D-penicillamine as an anticancer agent as it causes oxidative stress in cancer cells through the ROS production in the presence of copper through metal catalysed oxidation, resulting in cell death.

The Cu chelator TTM is efficient in BRAFV600E-driven melanoma models, and of all BRAF mutations, V600E mutation makes up 90%. Kim et al. showed that copper is required for MEK1 and MEK2 activity through a direct Cu-MEK1/2 interaction [170].

Ishida et al. presented a strategy to mitigate the limitations for the anticancer drug cisplatin, whose uptake is mediated by the copper transporter CTR1. They show that therapeutic preconditioning with a copper chelator (TTM) enhances cisplatin uptake and the killing of cancer cells without affecting normal organs in a mouse model of cervical cancer [171]. D-penicillamine and cisplatin acts synergistically to inhibit tumor growth. Moreover, investigators conducted a trial with combination agents, including LipoDox®, carboplatin and Trientine® (the latter being a chelator similar to TTM or D-penicillamine), in order to develop the clinical application of copper chelators in conjunction with cytotoxic agents to conquer platinum-resistance [169].

1.5.4.2 *Copper accumulation*

When considering non-Pt compounds, copper complexes are potentially attractive as anticancer agents. Much research has been conducted on copper compounds based on the assumption that endogenous metals may be less toxic to the host. Besides the elemental form, copper can be stabilized in four oxidation states: Cu(I), Cu(II), Cu(III), and Cu(IV), though very few examples of Cu(III) and Cu(IV) compounds are reported [172]. The majority of the coordination chemistry of copper has been concentrated on Cu(II) derivatives with few, but nevertheless important, examples of Cu(I) compounds. In terms of anticancer activity, only Cu(I) and Cu(II) complexes can be mentioned. The variety of

available arrays allows for a substantial choice of ligands (from mono- to hexa-dentate chelates), and of donor atoms (N, O, S and halides). The redox potential of Cu(I)/Cu(II) alters dramatically depending upon the ligand environment due to the geometry of the complex, the substituent electronic effect, and the substituent steric effect [173, 174].

Over the past decade, the number of copper complexes studied with anticancer activity has increased, and a number of reviews have detailed their synthesis, development and *in vitro* and *in vivo* efficacy [173, 175].

The synthetized complexes can be classified into the following structural groups: thiosemicarbazone complexes, conjugates Schiff Base complexes, imidazole-, benzimidazole-, pyrazole- and triazole-complexes, phenanthroline and bipyridine complexes, phosphine complexes and miscellaneous complexes. There are several mechanisms of action related to the different structures: DNA interaction, groove binding, oxidative cleavage, hydrolytic cleavage, topoisomerase and proteasome inhibition. Most of the investigated compounds belong to the family of Cu(II) complexes showing either five-coordinate environments, comprising distorted square pyramidal and trigonal bipyramidal geometries or distorted six-coordinate octahedral arrays. It is thought that due to the coordination chemistry of copper and the flexible Cu(I)/Cu(II) redox behavior, there is a good chance of designing more potent and less toxic copper based antiproliferative drugs [173, 176, 177]. There is a correlation between the anticancer activity of Cu(II) complexes and their ability to induce ROS accumulation [178]. Different mechanisms may also be related to their ability to accumulate copper [179, 180]. Chelator-like structures capable of binding copper are more cytotoxic than the chelator alone. Moreover, in the presence of free copper, these chelators can be more cytotoxic than the preformed copper complexes [179, 181–183]. Hence, a further strategy exploits the high cytotoxicity of intracellular Cu accumulation via Cu ionophores (**Figure 3**) [175].

It is useful to divide the copper related chelator-like structures into two categories: copper–ligand complexes and copper–drug complexes. In general, copper-drug complexes typically may not require Cu for activity, whereas copper-ligand complexes are significantly more active in the presence of copper [184].

To date, a great variety of copper complexes have been tested and found to be effective *in vitro.* However, only a few *in vivo* experiments have been published, due to the critical

property of many of these copper complexes in that they have poor water-solubility and a relatively high *in vivo* toxicity [173].

The published *in vivo* studies, which have reported varying degrees of success in terms of antitumor effects related to neocuproine (2,9-dimethyl-1,10-phenantroline) [179], to phosphine complexes [185], Casiopeínas® [186, 187], to a 1,2-propylenediaminetetraacetic acid-copper(II) complex [188], a Cu(II) compound derived from tridentate Schiff base ligand [189], to a ternary Cu(II) complex [190] and copper bis(thiosemicarbazone) complexes [191], or tridentate thiosemicarbazone copper complexes [192]. From the family of Cu(II) compounds known as Casiopeínas®, one named CasIII-ia has been selected as the most suitable to go into clinical trial Phase I [186]. In addition, a metal ionophore, clioquinol, entered into phase I study [193].

Although copper-drug complexes appear to offer great promise in the search for efficacious cancer treatments, they have as yet not been approved for use with patients. The problem lies in their extremely low water-solubility, necessitating the need for a solubilizing agent. To date, most of the data showing promising results for copper-complexes has been obtained from compounds solubilized in dimethyl sulfoxide (DMSO), and this has made *in vivo* testing very challenging as DMSO and Cremophor EL are not suitable for clinical testing, due to their high toxicity. In a further study of a Cu(II)-thiosemicarbazone complex used in *in vivo* experiments, a vehicle solution of 20% (v/v) Cremophor EL, 30% (v/v) PEG400 and 50% (v/v) saline solution was used. The result was a 75% reduction of the tumor mass [192]. Different methods using liposomal formulations of poorly water-soluble compounds may be a solution to this problem, resulting in an injectable, less toxic formulation [184]. Over the past decades, various delivery systems have been developed including prodrug, ligand design and nanocarriers, aimed at enhancing the performance profile of these novel metallodrugs. Better solubility properties, thus simplification of *in vivo* applicability and lower toxicity are expected from these nanosystems. These drug delivery systems (DDS) may open a new path in metal-based chemotherapy by re-examining a number of promising complexes and chelator-like structures [194].

Moreover, various Cu(II)-complexes have been shown to exert potent antiangiogenic and antimetastatic properties [195, 196].

Concerning the effects of Cu on the immune system, early experiments showed that Cu depletion suppressed anticancer immunization. Also, several anticancer Cu compounds that might support an active immune answer against cancer have been described [42].
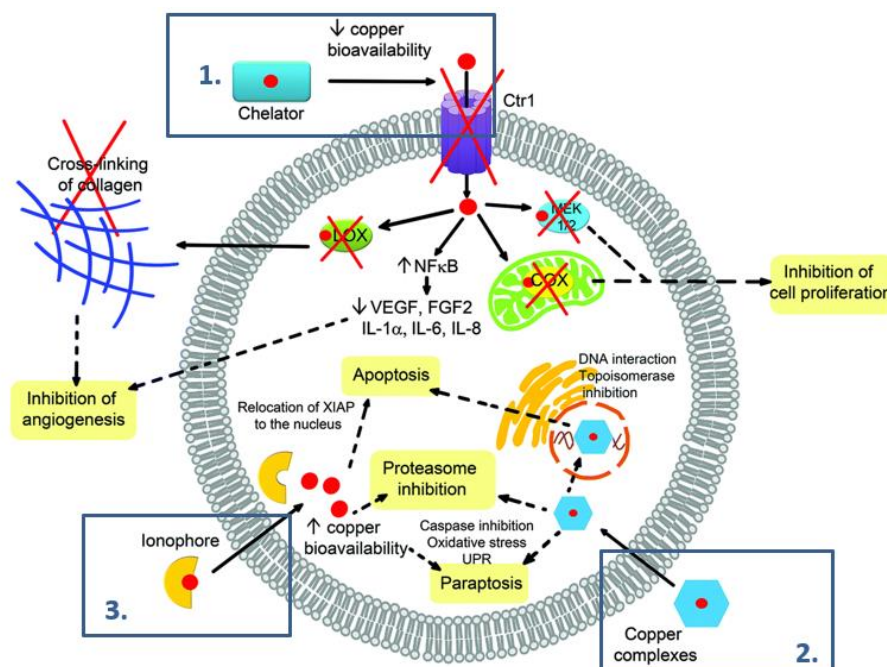
Figure 3. *Copper coordination compounds targeting cancer cells. The figure is based on Denoyer et al. [168]. Copper-associated therapy can be based on copper depletion using extracellular chelators (1.) or on copper accumulation using copper complexes or ionophores (2. and 3.). In each case, several mechanisms of action leading to apoptosis have been described.* Abbrevations: COX = cytochrome c oxidase, Ctr1 = copper transporter 1, FGF2 = fibroblast growth factor 2, IL-1a, -6, -8 = interleukin-1a, -6, -8, LOX = lysyl oxidase, MEK1/2 = mitogen-activated protein kinase/ERK (extracellular-signal-regulated-kinase) kinase 1/2, NF-kB = nuclear factor-kappa B, UPR = unfolded protein response, VEGF = vascular endothelial growth factor, XIAP =X-linked inhibitor of apoptosis.*

1.6. Anticancer chelating agents related to this thesis

Several studies have shown that tumor cells are more sensitive to Fe deprivation than normal cells [197]. A series of synthesized aroylhydrazone and thiosemicarbazone iron chelators with potent antitumor activity, the di-2-pyridyl ketone 4,4-dimethyl-3-thiosemicarbazone (Dp44mT) was found to be the most active *in vitro* and *in vivo* [198, 199]. This chelator shows increased doxorubicin-induced toxicity and selective poisoning of DNA topoisomerase IIα [200]. Yuan et al. indicated that Dp44mT induced the mitochondrial pathway of apoptosis and accounted, at least in part, for the activation of caspases [199]. Not only does Dp44mT bind Fe, but Cu as well. Both complexes are redox active, thus contributing to their marked cytotoxicity [201]. A novel generalized

strategy related to the copper complex is thought to selectively target lysosome function for chemotherapeutic intervention against cancer [180].

Other thiosemicarbazones were intensively developed in multiple clinical phase I/II trials, namely, Triapine, COTI-2 and DpC. Based on the strong metal-binding properties of thiosemicarbazones, interference with the cellular Fe and Cu homeostasis is assumed to play an important role in their biological activity [202].

It is a well-known that the cytotoxic effects of phenanthroline structures can be increased considerably in the presence of copper [179, 181]. The 1,10-phenantrolines are typical copper ionofores, and their copper complexes show antineoplastic properties. Both the Cu(I) and Cu(II) complexes of neocuproine have been shown to be potent cytotoxic agents against different cell lines, and their activity was potentiated by adding Cu(II) ions to cell culture medium [203, 204]. The neocuproine is frequently used as an inhibitor of Cu-mediated damage in biological systems [205].

The antioxidant potential of the pyrrolidine dithiocarbamate (PDTC) against protein damage induced by hypochlorous acid was investigated. The effects of PDTC were compared to those of reduced glutathione and NAC [206]. PDTC can spontaneously bind with tumor cellular copper and form a proteasome inhibitor and an apoptosis inducer. The results showed that only PDTC-copper mixture could inhibit proliferation of LNCaP cells in a dose dependent manner [207].

Several quinoline-based compounds show anticancer activity. Quinoline and its analogs have recently been examined for their modes of function in the inhibition of tyrosine kinases, proteasome, tubulin polymerization and DNA repair. *In vitro* and *in vivo* anticancer activities of quinoline analogs is being studied by several research groups [208–210]. The Cu(II) complexes of 8-hydroxyquinoline and quinoline have shown markedly higher *in vitro* cytotoxicity than quinolines alone [211–215]. Three related Mannich bases of 8-hydroxyquinoline (Q-1) also showed copper binding. The studied derivatives harbor a CH_2-N moiety at position 7 linked to morpholine (Q-2), piperidine (Q-3), and chlorine and fluorobenzylamino (Q-4) substituents. Pape et al. identify Q-4 (hereinafter Q4) as a potent and selective anticancer candidate with significant toxicity in drug resistant cells [216].

The first study to recognize the usefulness of 2,2'-biquinoline as a specific chromogenic reagent for copper was published in 1939. The common name "cuproin"

was assigned to the compound by Hoste [217]. Based on the work of the group Starosta et al., a novel water and air stable Cu(I) complex, containing 2,2'-biquinoline, has been synthesized with antimicrobial activity. Cuproin seems to be a good candidate for further investigations in light of the photodynamic therapy of cancer [218]. The structure is involved in a number of synthesized complexes, containing ruthenium(II), palladium(II), or iridium(III), with detectable *in vitro* antitumor activity [219–221].

Intensely dark-green diphenylthiocarbazone (*aka* dithizone) originally earned its place in analytical chemistry because of the colorful complexes it forms with numerous metals [222]. Dithizone is used to assess the purity of human pancreatic islet preparations used for transplantation into patients with Type 1 diabetes [223–225]. However, dithizone induced the symptoms of diabetes in several animals [104, 105]. The chelator is also related to cancer therapy. The high zinc content of human prostate was first reported in 1921. Later reports have suggested some beneficial effects of dithizone administration in patients with prostatic cancer [226]. Reduction in size and consistency of the prostate was achieved in most cases, but these were small case studies mentioning several side effects. Later, no objective benefit from using dithizone in prostate cancer was found [227]. Kohroki et al. found a potent ability of dithizone to induce both the differentiation and apoptosis of two human myeloid leukemia cell lines. Dithizone with Mn^{2+}, Pb^{2+}, Zn^{2+} and Cu^{2+} ions, but not Fe^{3+} and Mg^{2+} ions, efficiently inhibited dithizone-induced differentiation in HL-60 and ML-1 cells [228].

1.7. Drug delivery systems (DDS)

Modern drug delivery systems have undergone continuous progress since the 1950s, when the first sustained release formulation, Dexedrine, was introduced [229]. The fast advancement of nanotechnology has profoundly influenced clinical therapeutics in general in the past two decades. The development of new drug molecules is expensive and time-consuming, so attempts are being made concurrently to improve the safety efficacy ratio of "old" drugs. Nonspecific distribution and uncontrollable release of drugs in conventional drug delivery systems have led to the development of smart nanocarrier-based drug delivery systems. Their usual purpose is to improve the pharmacological activities of therapeutic drugs and to overcome problems such as limited solubility or chemical stability, drug aggregation, low bioavailability, poor biodistribution, lack of selectivity, or to reduce the side effects of therapeutic drugs [230]. The purpose of a drug

delivery system is to provide and maintain therapeutic concentrations of the drug at the target biological site. In the last few years, the increased availability of versatile materials, including polymers [231–234], lipids [235], inorganic carriers [236–238], polymeric hydrogels [239–241], and biomacromolecular scaffolds [242–244] has led to the development of systems that can deliver drugs to a target with enhanced therapeutic efficacy.

The main chemotherapeutic treatment for most types of cancer remains the use of cytotoxic agents. While there has been some success through the use of conventional chemotherapy, there are a substantial number of drawbacks. For example, there are adverse side effects, such as a requirement for high dosage, poor bioavailability, low therapeutic indices and the possibility of the development of multiple drug resistance. In addition, the agents themselves are non-selective, with the potential to damage healthy cells, which sometimes results in treatment failure. The DDS became of interest as an alternative to chemotherapy due to the possibility of site-specific drug delivery. Among the many DDS that have been developed and found to be able to deliver chemotherapeutics to tumor sites with greater therapeutic efficacy are liposomes, dendrimers, micelles, gold nanoparticles, carbon nanotubes, mesoporous silica nanoparticles, super paramagnetic iron-oxide nanoparticles, and quantum dots [245]. Nanoscale drug carriers have shown the potential to overcome some of the challenges posed by conventional chemotherapy by improving treatment efficacy while at the same time avoiding toxicity in normal cells. Their enhanced efficacy is due to highly selective accumulation within tumors through the enhanced permeability and retention effect (EPR), and through active cellular uptake [246]. Utilization of the EPR effect is, therefore, an effective strategy for delivering nanoparticles to the site of a tumor, and has been widely documented using various tumor types and animal models since its discovery in the 1980s [247, 248].

The development of several anticancer drugs has also produced new pharmaceutical technologies, which have been termed controlled-release technology [249]. The controlled release of a drug at the target site is essential if the required therapeutic effect is to occur. Controlled release technologies are excellent tools for improving both the safety and performance of drugs. The most favored strategy for drug delivery currently is stimuli-response delivery. This strategy allows the tumor-specific delivery and controlled

release of cargo with both exogenous and endogenous triggers. Exogenous triggers include temperature-triggered and light-triggered strategies that are induced using exogenous methods. Endogenous triggers include ROS-sensitive, pH-sensitive, redox-sensitive, enzyme-sensitive and temperature-sensitive delivery strategies. Other strategies used in the design of stimuli-response systems are magnetic-triggered, X-Ray triggered and ultrasound-triggered [230]. Efforts to design liposomes that are pH sensitive, temperature sensitive, antibody targeted, or fusogenic have all been pursued with various degrees of success [250].

The delivery of DDS can be enhanced by functionalizing them utilizing a variety of targeting molecules which are commonly over-expressed on malignant cells, such as antibodies, carbohydrates and ligands [251]. The DDS agents seem to have less toxicity than conventional chemotherapeutic drugs. However, there are sometimes DDS-specific side effects, such as hypersensitivity reactions, peripheral neuropathy and various skin reactions. Therefore, clinicians need to fully understand the agents and their possible side effects to achieve the required positive clinical outcomes [252].

1.7.1. *Liposomal formulations*

Lipid-based drug delivery systems have emerged as biocompatible candidates that overcome many biological obstacles [253]. Liposomes have been shown to have better drug loading and encapsulation efficiency. They have the ability to enhance the bioavailability and solubility of poorly water-soluble and/or lipophilic drugs. They can minimize the expulsion of drugs, accommodate more drug molecules, as well as being able to modify the drug release profile through varying the lipid matrix [254, 255].

Liposomes are bilayer spherical vesicles composed of different lipids that in water form at least one lipid bilayer surrounding an aqueous core, which may encapsulate both hydrophilic drugs (e.g., Doxil®, encapsulated doxorubicin) and hydrophobic compounds (e.g., AmBisome®, trapped amphotericin B) [256]. The various fabrication techniques of drug-loaded lipid nanocarriers and the selection of components and techniques based on the drug and lipid characteristics are to improve the oral bioavailability of poorly water-soluble drugs [257]. Liposomes are pharmaceutical carriers for numerous medical applications, such as for the controlled and targeted delivery of drugs or diagnostic materials.

The targeted liposomes are of the third generation of liposomes and are prepared through the modification of their surface using appropriate ligands. These liposomal systems can be used for both active and passive targeting. In the case of passive targeting, the liposomal systems display increased accumulation of the drug inside the tumor cells, due to the EPR effect. In addition to their passive targeting ability, the third generation of liposomes has physicochemical and active targeting potential. Liposome functionalization can be done by peptides and antibodies, which can deliver the drug to a specific site due to selective affinity for a particular receptor [238].

Functionalization of liposomes enables the accumulation of anti-cancer drugs at target organs, which means that they are more effective at controlled drug release in the tumor microenvironment. There are around 1,200 clinical trials containing the terms "liposome" and "cancer" according to NIH's 'ClinicalTrials.gov' and the EU Clinical Trial Register 'clinicaltrialsregister.eu' websites [258, 259]. In some clinical trials, the synergistic cytotoxicity of a combination of two agents, such as irinotecan-floxuridine and cytarabine-daunorubicin in liposomal forms were evaluated.

The advantages of conventional liposomes are their ability to encapsulate amphiphilic, hydrophobic and hydrophilic compounds, together with their biodegradability and biocompatibility. However, a major drawback is that they are rapidly cleared from the bloodstream, which shortens their blood circulation time [246, 260]. Several approaches have been undertaken to counter this drawback. One such approach is to use liposomes with "stealth" properties. To obtain these types of stealth, or sterically stabilized liposomes, the bilayer surface is modified with inert polymers, and this controls semi-phase processes and prevents the interaction of liposomes and blood components. Small fractions of hydrophilic polymers, for example, polyethylene glycol (PEG), are used as surface coatings. This has the effect of extending the blood circulation half-life from a few minutes (in respect of conventional liposomes) to several hours (stealth liposomes). The PEGylated liposomes with a mean diameter of 100–150 nm have been found to reduce the interaction of liposomes with plasma proteins such as opsonins [246, 254, 261, 262]. Thus, PEG prevents liposome opsonization and consumption by the reticuloendothelial system, as it entangles 2–3 molecules of water per oxyethylene unit. This can increase the apparent molecular weight by 5-10 times. The solubility is thus improved and there is a decrease in both the aggregation and the immunogenicity of the

drug, causing a circulation time 10 times longer and an increase of liposome accumulation in damaged tissues [254, 263, 264]. The PEG can be incorporated onto the liposomal surface by a number of methods. However, anchoring the polymer in the liposomal membrane via a cross-linked lipid, PEG-distearoylphosphatidylethanolamine (DSPE) is reported to be the most widely accepted method [265, 266]. The PEGylation can be performed by two means: the addition of PEG lipids to lipid composition before liposome formation (pre-insertion method), or the mixing of PEG-lipids and liposomal dispersion (post-insertion method). Both the length and coverage density of the PEG influence the liposomal PEGylation efficiency. Usually PEG molecules with medium length are used for liposome modification, as very short PEG molecules cannot prevent protein absorption or increase the blood circulation time, while very long PEG chains lead to a significant decline in transfection activity. The higher the molar PEG-lipid/lipid composition ratio, the higher the coverage density: (1) <5% PEG gives less than 100% coverage, with a mushroom-like shape; (2) 5–15% PEG gives around 100% coverage, with a mushroom- or brush-like shape; (3) >15% PEG gives around 100% coverage, with a brush-like shape. In general, liposomes that have a brush-like coverage have a more stable steric barrier and a longer circulation time in blood.

In addition, pre-clinical studies with PEGylated liposomes have demonstrated that cytotoxic agents entrapped in PEGylated liposomes tend to accumulate in tumor foci [267, 268]. Liposome PEGylation increases the circulation time by inhibiting the mononuclear phagocyte system uptake, i.e. preventing liposome–macrophage interactions. However, recent preclinical studies on anti-cancer drugs enclosed in PEGylated liposomes in rodents and dogs have shown a rapid blood clearance of the PEGylated drug carrier system, due to the increased anti-PEG-IgM production [269, 270].

An example of a PEGylated liposomal formulation which has been extensively studied is PEGylated liposomal doxorubicin (Doxil, Caelyx) [271, 272]. On the market, there are various clinically approved stealth and non-stealth liposomal formulations [273], with or without cholesterol.

Cholesterol is an important strategic component of liposomes. It affects the properties of the lipid bilayer of the liposomes. By incorporating cholesterol into the liposomes, the fluidity of the liposomal membrane bilayer is decreased, the permeability of water-soluble molecules through the liposomal membrane is reduced, and the stability of the liposomal

membrane in such biologic fluids as blood and plasma is improved. Without cholesterol, liposomes can often interact with blood proteins, such as transferrin, albumin, macroglobulin and high density lipoproteins [254, 274]. However, the quantity used to achieve appropriate formulation has not yet been clarified. Each composition requires special consideration for cholesterol content [275].

The general structure of liposomes and the properties of the membrane depend on five factors: first, on the nature of the lipid itself, whether it is synthetic or natural; secondly, on the phospholipid polar headgroup and its charge; thirdly, on the length and degree of unsaturation of the fatty acids; fourthly, on the temperature before and after the liposome synthesis; and finally on the addition of other compounds such as PEG, proteins, cholesterol, ligands and antibodies to the surface of the liposome or the membrane.

The liposomal co-delivery system has become a promising technology for successful cancer treatment. Recently, liposomal systems that are now being evaluated in phase II clinical trials, including CPX-351 (cytarabine:daunorubicin) and CPX-1 (irinotecan: floxuridine), have been developed [276]. Moreover, MRI imaging is possible when using specific co-delivery systems, for example, manganese ions with chemotherapeutics [277–279].

One method of improving drug retention is to load drugs into liposomes using different techniques resulting in high intra-liposomal concentrations that are greater than their solubility limits, for example which enhance precipitation in the liposomes. Another method is to encapsulate polyanions, such as dextran sulfate. It is possible also to convert non-weak base drugs, such as docetaxel, to weak base prodrugs, which allows encapsulation and liposomal retention [280, 281].

The nature of liposomes means that they can act as an immunological adjuvant, thus triggering the immune response. Elements of the immune response, such as activation of macrophages, production of antibodies, induction of cytotoxic cells and the resultant antitumor activity can be enhanced by incorporation of antigens into the interior water core of the liposome, or their reconstitution into liposomal membranes.

Using liposomes as immunological adjuvants makes use of their characteristics of being biodegradable, having low toxicity and low antigenicity, and being able to target specific cells *in vivo* [235].

However, it remains a priority to synthesize non-toxic liposomes, which have the attributes of being able to circulate for a long time, to evade the immune system of the host, and to have high stability. Recent reports have concluded that there are advantages in using extracellular vesicles (EVs) for drug delivery. Five advantages have been pinpointed: (1) they are small and thus can penetrate into deep tissues; (2) they are able to evade the immune system; (3) they have a membrane structure that is similar to that of cells; (4) they possess negative zeta potential, which allows long circulation; and (5) they have the ability to escape degradation. There have been a few clinical trials performed that used EVs from cells in cancer therapy, and the results have been positive in respect of their safety and feasibility. Recently there has been much interest in the possibility of using EVs as drug delivery vehicles [282, 283].

1.7.1.1 *Copper containing liposomal formulations*

The ability of lipids to bind copper has been investigated in several studies. Phosphatidylserine embedded within supported lipid bilayers was found to bind Cu^{2+} from solution with extraordinarily high affinity [284]. The equilibrium dissociation constant was in the femtomolar range. Detailed investigation of Cu(II) binding with natural lipid phosphatidylglycerol (PG) in aqueous solution was examined by Mlakar et al. The Cu-PG interaction was enabled by the formation of Cu-phenanthroline complex [285]. Varga [273] found a relatively fast ion binding to the lipid headgroups during the analysis of the DPPC/CuCl$_2$ system by means of Molecular Dynamics simulations. The Cu(II), initially placed randomly in the water region, migrate towards the headgroup region of the bilayer, according to the increment in the number of the carbonyl oxygens around the metal ions. A 3:1 ratio lipid-copper complex was obtained from the simulation [286].

Several copper complexes containing liposomal formulation were achieved in *in vitro* and *in vivo* studies (**Table 2**). Although Cu complexes have been investigated as anticancer agents, there has not been any report published on Cu(II) as an anticancer agent. A stealth liposomal Cu formulation (LpCu) was studied *in vitro* and *in vivo* [287].

Table 2. *Short overview of the copper(II) ions containing liposomal formulations in the literature.*

Liposomal formulation	Statement/main finding	Ref.
Anticancer properties of liposomal copper alone	• LpCu (stealth liposomes) injected as a therapeutic in tumor-bearing mice was effective at reducing overall tumor burden but had little effect on the tumor growth rate.	[288]
Copper diethyldithiocarbamate ($Cu(DDC)_2$)	• Convection-enhanced delivery of a $Cu(DDC)_2$ formulation prepared using 1,2-distearoyl-sn-glycero-3-phosphocholine (DSPC)/cholesterol liposomes into a rat model of F98 glioma engendered a 25% increase in median survival time relative to vehicle-treated animals.	[289]
Liposomal formulation of Cu-clioquinol	• Formulation did not exhibit interesting therapeutic effects *in vivo*.	[290]
Liposomes rely on the complex formation between CX-5461 and copper	• CX-5461 is currently in Phase I/II clinical trials • Low pH is necessary to enhance solubility of CX-5461. • Cu(CX-5461) was more active than CX-5461 in AML models *in vivo*. • Cu(CX-5461) formulation may serve as an alternative formulation for CX-5461 in BRCA-deficient cancers.	[291]
Liposomal Cu(II)-quercetin formulation	• There is a need to improve quercetin's solubility. • Liposome has been shown to work well in combination with irinotecan *in vitro*.	[292]
Cu−doxorubicin complex liposomal formulation	• The 1:2 complex of copper and doxorubicin with a stability constant of 10^{16} forms when a neutral pH is created within liposomes. • The antitumor activity of copper−doxorubicin liposomes alone was similar to that of the ammonium sulfate-loaded doxorubicin liposomes, although with reduced toxicity.	[293]
Cu-doxorubicin thermosensitive liposome	• Formation of a pH-sensitive complex (CuDox) between doxorubicin (Dox) and copper in the core of lysolipid-containing temperature-sensitive liposomes. • Complete regression of local cancer of a murine breast cancer model.	[294]
5-Fluorouracil (5-FU) delivered by thermosensitive stealth liposomes in the presence of Cu(II)	• 5-FU complexation with copper-polyethylenimine improved 5-FU retention into liposomes • Heat-triggered release (using focused ultrasound) of the drug within 10 min at 42°C.	[295]
Intrabilayer ^{64}Cu labeling of photoactivatable, doxorubicin-loaded stealth liposomes	• Doxorubicin (Dox)-loaded stealth liposomes with incorporation of small amounts of porphyrin-phospholipid (PoP). • PoP is also an intrinsic and intrabilayer ^{64}Cu chelator. • Formulation enables chemophototherapy and strongly inhibited primary tumor growth.	[296]

Table 2. (continued) *Short overview of the copper(II) ions containing liposomal formulations in the literature.*

Co-encapsulation of cytarabine and daunorubicin inside liposomes (CPX-351, Vyxeos)	• Copper gluconate containing liposomal formulation, loading cytarabine drug was dissolved into the copper gluconate buffer used to hydrate the lipid film, further daunorubicin was incubated with the liposome. • The efficacy observed for CPX-351 was far greater than predicted when the two individual liposomal drug components contributed additively to the overall therapeutic effect, consistent with *in vivo* synergistic activity.	[297]
Nanoformulations of a potent copper-aquaporin (1,10-phenantroline) complex	• Neutral phospholipids – ePC, DMPC and DPPC, PEGylated, addition of positively charged surfactant-Stearylamine, Cu-phen aqueous solution. • Cu-phen has a cytotoxic effect against melanoma and colon cancer cell lines, show *in vivo* targeting and accumulation in tumor sites.	[298]
Topophore C: a liposomal nanoparticle formulation of topotecan for treatment of ovarian cancer	• Topotecan was encapsulated into preformed liposomes containing copper sulfate and the divalent metal ionophore A23187. • Markedly increased survival using ES-2 ovarian tumor bearing mice.	[299]
Irinotecan (CPT-11) liposomal formulation with CuSO$_4$	• Irinotecan is stably entrapped in the active lactone conformation within preformed copper-containing liposomes as a result of metal-drug complexation. • DSPC/cholesterol (55:45 mol%) preparations have relied on pH gradients.	[300]
Irinotecan formulation using divalent cation ionophore A23187 and Cu(II) ions	• Formulation with ionophore A23187 (exchanges internal metal^{2+} with external $2H^+$ to establish and maintain a transmembrane pH gradient). • Cu^{2+}/A23187 liposomal formulation of irinotecan is significantly more active than the free drug.	[301]

Overcoming the pharmaceutical challenge of developing copper-based therapeutics (mostly insoluble in aqueous solutions under physiological conditions) can be addressed via two main methods: by the modification of chemical structures, or by using Metaplex technology by which the poorly soluble copper complex (precipitate) can be delivered inside the liposome [184].

1.7.2. *Hyperthermia and thermosensitive liposomes*

One of the important factors in determining the effectiveness of a therapeutic agent is achieving local delivery to the tumor site. Controlled release of anti-cancer drugs can occur by mild hyperthermia treatment. The delivery strategy of liposomes (stealth liposome, e.g., Doxil) was based on the passive accumulation in tumor intestinal space, followed by slow release within the interstitium. Thermosensitive liposomes (TSL) are liposomes used for the external targeting of drugs at solid tumors, when used in combination with local hyperthermia. The TSL facilitate targeted drug delivery, when combined with localized hyperthermia, which can be mediated by microwave energy, focused ultrasound, or radiofrequency ablation mediated heating [302, 303]. The drug uptake directly correlates with duration of heating [304]. The TSL release is actively triggered and can be extravascular or intravascular release depending on where the release occurs. For extravascular triggered release, the targeting is passive and generally based on the EPR effect. The key requirements, which must be fulfilled by TSLs to be effective, are the encapsulation of the drug payload with minimum leakage, prolonged circulation and the release of the encapsulated drug at the target location [305].

At temperatures of 41–43°C, hyperthermia treatment (HT) has been shown to increase blood flow [306] and oxygenation [307]. The HT has also been demonstrated to increase the permeability of tumor vessels to antibodies [308–311], ferritin [312], and Evans Blue dye [313]. Hyperthermia treatment has been shown to increase permeability of tumor vessels to liposomes [314]. Triggered release occurs because of a lipid membrane phase transition that results in increased permeability across the liposome membrane [315]. A peak in the membrane permeability occurs coincident with the midpoint of the gel-liquid crystalline transition

ThermoDox® (doxorubicin), a thermal-sensitive liposome being developed by Celsion Corporation is being taken through human clinical trials and is setting the stage for the formulation and testing of other temperature-sensitive chemotherapeutic drugs, including cisplatin, as well as imaging agents. ThermoDox in combination with mild hyperthermia was found to be considerably more effective than free drug or current liposome formulations for reducing tumor growth in a human squamous cell carcinoma xenograft line [316, 317]. The HT-triggered liposomal drug release can contribute to more

effective therapy and demonstrates the importance of rapid drug release from the drug carriers at the tumor site [318].

Doxorubicin and 5-fluorouracil containing liposomes are examples of copper-containing thermosensitive liposomes (**Table 2**).

TSL were actively loaded with doxorubicin using manganese(II) (Mn(II)) gradient. Doxorubicin and Mn(II) form a stable complex [277], with the paramagnetic Mn(II) serving as an MRI contrast agent. Using this strategy, it was possible to show that release of doxorubicin was heterogeneously distributed in the tumor model, and the lysolipid-containing thermosensitive liposomes administered during hyperthermia had the highest antitumor effect when compared with other administration strategies [319].

2. Objectives

With the increasing incidence of cancer, its clinical management continues to be a challenge in the 21st century. The discovery of cisplatin (cis-diammine-dichloroplatinum(II) complex) laid the foundation for the use of metal-based compounds in the treatment of several cancer types. The development of further Pt-based compounds has been the subject of intensive research. Simultaneously, alternative metal-based complexes are also being investigated. Copper (Cu) chelating compounds are primary candidates for development, given the strong *in vitro* toxicity of the complexes, in addition to their persistent toxicity even in multidrug resistant cell lines.

Common examples of copper chelating ligands include derivatives of dithiocarbamate, 8-hydroxyquinoline, thiosemicarbazone and phenantroline structures. These ligands form stable and cytotoxic copper complexes. Cells efficiently protect their intracellular milieu by hiding copper from cellular constituents, thereby preventing the accumulation of free ionic copper. These defensive processes can be circumvented by special copper chelator structures. The exact mechanism through which copper increases the toxicity of certain chelator compounds is not known. The toxicity of copper chelating ionophores is usually accompanied by higher cellular accumulation of copper.

The aim of this thesis is to investigate the copper accumulation ability of different chelating structures, and their role in cytotoxic effect. Due to their poor *in vivo* selectivity and high toxicity, a drug delivery system, namely, the liposomal delivery of these drugs, appears to be at the forefront of overcoming the pharmaceutical challenge of developing metal-based therapeutics. One of the main aims of the present research is to show the applicability of copper chelating compounds *in vivo* using liposomal formulations. The goal of this PhD was to formulate liposomes that will achieve acceptable loading of an ionophore structure in the presence of Cu(II) ions, while the formulation allows drug targeting using mild hyperthermia.

3. Materials and methods

3.1. Chemicals
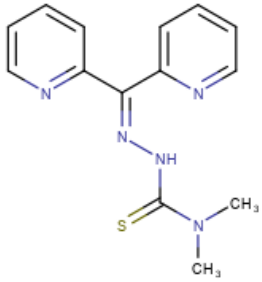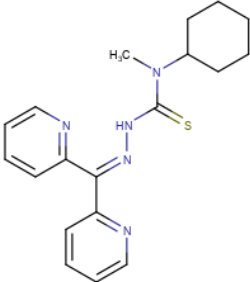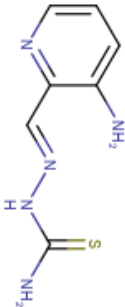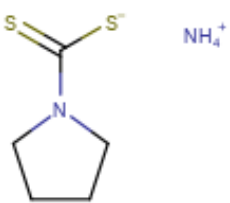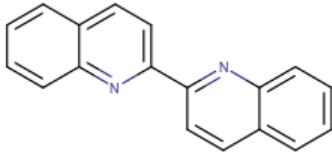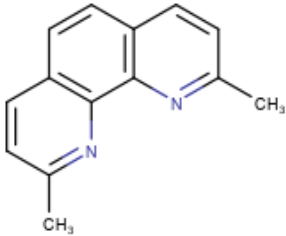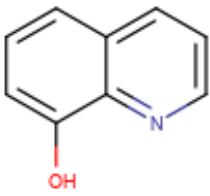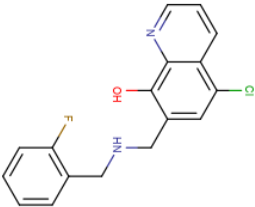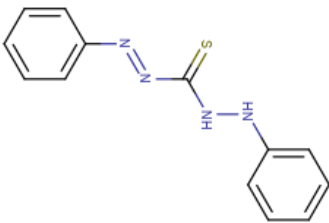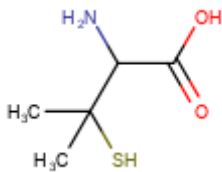
Throughout the experiments, deionized Milli-Q (MQ, Millipore, Molsheim, France) water with a relative resistivity of 18.2 MΩ·cm was used. All the chemicals were of analytical grade, if not stated otherwise. Copper(II) sulfate anhydrous, iron(II) sulfate heptahydrate, iron(III) chloride, zinc(II) sulfate heptahydrate, cobalt(II) chloride hexahydrate, nickel(II) chloride hexahydrate, lead(II) chloride, cadmium(II) chloride and mercury(II) chloride were purchased from Sigma Aldrich Ltd (Budapest, Hungary). The structural formulae and chemical nomenclature of the investigated chelators (purchased from Sigma Aldrich) can be seen in **Table 3**. Q4 chelator was a kind gift from Dr. Gergely Szakács. Metal salts were dissolved and applied in aqueous solutions, while the chelators were dissolved in DMSO, except neocuproine hydrochloric salt for the preparation of liposomes, which was taken up in Milli-Q water.

Other chemicals required for the experiments: hydrochloric acid, acetic acid, sodium hydroxide, 2-amino-2-(hydroxymethyl)-1,3-propanediol (Tris base), 4-(2-hydroxyethyl)piperazine-1-ethanesulfonic acid sodium salt (HEPES sodium salt), ascorbic acid, bovine serum albumin (BSA), sodium dodecyl sulfate (SDS), potassium nitrate, potassium chloride, formaldehyde, 3-(trimethylsilyl)-1-propanesulfonic acid sodium salt (DSS, NMR standard) and deuterium oxide (Heavy water, D_2O) were purchased from Sigma Aldrich; the NaCl 0.9% from B. Braun (Melsungen, Germany); and the solvents n-octanol, dimethyl sulfoxide (DMSO) were obtained from Sigma Aldrich; chloroform and methanol from Reanal (Budapest, Hungary).

Synthetic high-purity 1,2-dipalmitoyl-sn-glycero-3-phosphatidylcholine (DPPC), hydrogenated soybean phosphatidylcholine (HSPC) and 1,2-distearoyl-sn-glycero-3-phosphoethanolamine-N-[amino(polyethylene glycol)-2000] (ammonium salt) (DSPE-PEG 2000) were obtained from Avanti Polar Lipids (Alabaster, AL, US) or from Sigma Aldrich. Disposable PD-10 and PD MidiTrap G-25 desalting columns for purification of liposomes were provided by GE Healthcare Bio-Sciences AB (Uppsala, Sweden).

Concentrated nitric acid (65% w/w) and H_2O_2 (30% w/w) of Suprapur quality (Merck, Darmstadt, Germany) were applied for sample preparation of cell lines for the Total Reflection X-ray Fluorescence (TXRF) determination of trace elements.

Table 3. *Investigated chelator-like structures and their chemical nomenclature. Tested compounds include thiosemicarbazone, phenanthroline, 8-hydroxyquinoline, thiocarbazone, dithiocarbamate, biquinoline derivatives. D-penicillamine is used in chelation therapy to remove toxic metals from the body, not because of cytotoxicity, so it was achieved as control chelator.*

Dp44mT	DpC	Triapine	APDTC	2,2'-biquinoline
2-(Di-2-pyridinylmethylene)-N,N-dimethyl-hydrazinecarbothioamide, Di-2-pyridylketone-4,4,-dimethyl-3-thiosemicarbazone	Di-2-pyridylketone-4-cyclohexyl-4-methyl-3-thiosemicarbazone	3-Aminopyridine-2-carboxaldehyde thiosemicarbazone, 3-AP, PAN-811	Ammonium pyrrolidinedithiocarbamate, 1-Pyrrolidinecarbodithioic acid ammonium salt, Ammonium pyrrolidinecarbodithioate, PDC, PDTC	2,2′-Diquinolyl, Cuproin
neocuproine	oxine	Q4	dithizone	D-Penicillamine
2,9-Dimethyl-1,10-phenanthroline, DMPHEN	8-Hydroxyquinoline, 8-Oxychinolin, 8-Quinolinol	5-Chloro-7-((2-fluorobenzylamino)methyl)quinolin-8-ol	Diphenylthiocarbazone	3,3-Dimethyl-D-cysteine, 3-Mercapto-D-valine, D-(−)-2-Amino-3-mercapto-3-methylbutanoic acid

3.2. Determinations of protonation constants of Dp44mT by UV/Vis-pH titration

All the pH-titration measurements were carried out on a Jasco (Easton, MD, US) Model V-550 spectrophotometer at room temperature in the 250-500 nm spectral range. Acidic and alkaline stock solutions were made with the following composition: 50 μM Dp44mT, 0.01 M HCl, or 0.01 M NaOH and 0.14 M KCl to adjust the ionic strength. These solutions were dispensed and mixed in proper aliquots to obtain samples of various, accurate pHs. The pH was determined by a Metrohm 6.0234.110 combined glass electrode (Methrohm, Herisau, Switzerland) calibrated against four standard buffers of the National Institute of Standards and Technology (Gaithersburg, Maryland, US) [320]. Each titration was evaluated by the method of Szakács and Noszál [321]. Briefly, the whole absorbance matrix was evaluated by the OPIUM software [322] to obtain protonation constants and individual UV-Vis spectra of each species.

3.3. Determination of complex stability constants

The stability constant of the zinc complex was determined by NMR titrations. A solution of 2 mM Dp44mT in 0.01 M HCl and 5 % (v/v) D_2O was titrated with accurate (calculated) volumes of 50 mM $ZnSO_4$ solution. Spectra of ^{1}H NMR were recorded after the addition of zinc sulfate solution in known amounts. Typically, 64 transient spectra were recorded. The water signal was suppressed by excitation sculpting [323]. The chemical shifts were referred to internal DSS. The stability constants of Fe(II)-, Fe(III)-, Cu(II-), Co(II)- and Ni(II)-Dp44mT complexes were measured by UV/Vis-spectroscopy. The conditional stability constants complexes of Cu(I) and Cu(II) with 2,2'-biquinoline, oxine, APDTC, Dp44mT and neocuproine were determined by the same method. A solution with a concentration of 50 μM of each chelator in 0.15 M KNO_3 was titrated with calculated volumes of 3 mM of each metal salt solution. In order to prevent the oxidation of Fe(II), 10 mM of ascorbic acid was also dissolved in the titrant solution. This solution was stable over 24 hours. The chemical shift or absorbance versus metal ion concentration datasets were also evaluated by the OPIUM software [322].

3.4. Determination of octanol-water partition coefficients (log $P_{octanol/water}$)

Partition coefficients were determined using the standard shake-flash method [324]. The chelators were dissolved in 0.05 M acetic acid buffer (pH=5.0, previously saturated with n-octanol), and two phases were saturated by shaking in a thermostatic water bath

for 3 hours at 25 °C. The phases were allowed to separate on 18-h standing. Concentration of the solute was determined by UV/Vis spectrophotometry at λ_{max} for each chelator. Each log $P_{octanol/water}$ value is an average of three replicates. For the complex species, the aqueous solutions contained stoichiometric amount of Cu(II) sulfate.

3.5. Circular dichroism (CD) spectroscopy

The CD spectra of isolated compounds were recorded in methanol on a Jasco J720 Spectropolarimeter (Jasco Inc., Tokyo, Japan). The spectra were acquired three times from 350 nm to 200 nm with a bandwidth of 1 nm and a scanning step of 0.2 nm at a scan speed of 50 nm/min. The following experiments were carried out: *(i)* analysis of 0.02% w/v erythrocyte of lyophilized chicken DNA (Supelco, Sigma Aldrich) incubated with appropriate amounts of chelating agent solutions diluted from methanolic stock solutions of approximately 0.2% w/v for each; *(ii)* analysis of DNA solution incubated with 2–10 µL of 0.75% w/v Cu(II) sulfate stock solution [~0.05 M]; *(iii)* chelating agent solutions were incubated with one third dilution of 1 mL of DNA stock solution and 2.5 µL, 5 µL, 7.5 µL and 10 µL of Cu(II) stock solution. In the resulting solutions, the Cu-to-chelating agent molar ratio corresponded to 1:1, 2:1, 3:1 and 4:1, respectively. The DNA quality was controlled by the UV 260/280 ratio.

3.6. *In vitro* studies

3.6.1. *Cell lines*

The following cancer cell lines were used: HT-29 (No.: HTB-38), HCT-15 (No.: CCL-225), HCT-116 (No.: CCL-247) colon adenocarcinoma were obtained from ATCC (LGC Standards GmbH, Wesel, Germany) [325] and C-26 (also referred to as Colon-26) mouse colon carcinoma cell lines from CLS (Cell Lines Service GmbH, Germany). The A-375 (No.: CRL-1619) malignant melanoma; MCF-7 (No.: HTB-22), MDA-MB-231 (No.: HTB-26) and ZR-75-1 (No.: CRL-1500) breast adenocarcinomas; Caov-3 (No.: HTB-75) and NIH:OVCAR-3 (OVCAR-3, No.: HTB-161) human ovarian carcinoma cell lines; PANC-1 (No.: CRL-1469) pancreatic cancer cell line; H358 (NCI-H358, No.: CRL-5807) lung (bronchioalveolar) carcinoma; and HT-1080 (No.: CCL-121) fibrosarcoma cell were also purchased from ATCC. The MES-SA (No.: CRL-1976) uterine sarcoma cell line and its doxorubicin selected derivative MES-SA/Dx5 (No.: CRL-1977) were

purchased from ATCC. The ABCB1-overexpressing subline MES-SA/B1 was produced by lentiviral transduction of pRRL-EF1-ABCB1 [159].

The mouse leukemic P388 and its doxorubicin selected subline P388/ADR were obtained from the NIH's Developmental Therapeutics Program (Bethesda, MD, US). The P388/ADR and MES-SA/Dx5 cells were maintained in 800 and 500 nM doxorubicin (Adriamycin), respectively. Doxorubicin was purchased from TEVA (Petach Tikva, Israel). The KB-3-1 cervix carcinoma cell line and its vinblastine selected derivative KB-V1 was a gift from Dr. Michael M. Gottesman (NIH, Bethesda, MD, US). The phenotype of the resistant cell line pairs was verified using cytotoxicity assays (data available in the related 'Results' Section). As healthy controls, peripheral blood mononuclear cells (PBMC) were obtained from healthy human subjects and were isolated by density gradient centrifugation using Ficoll-Hypaque (Amersham Pharmacia Biotech AB, Uppsala, Sweden).

3.6.2. Cell culture conditions

Cell lines were cultured in RPMI-1640 (developed by Moore et al. at Roswell Park Memorial Institute, hence its acronym RPMI) or in Dulbecco's Modified Eagle's Medium (DMEM) media according to manufacturer's instructions. The RPMI and DMEM (Sigma Aldrich) were supplemented with 10% FBS (fetal bovine serum, Gibco, purchased from Thermo Fisher Scientific, Waltham, Massachusetts, US), 5 mM glutamine, and 50 unit/mL penicillin and streptomycin (Life Technologies, Waltham, Massachusetts, US). Cell cultures were kept in a humidified incubator at 37 °C, and in 5% CO_2 atmosphere. Washing steps were executed by Dulbecco's Phosphate Buffered Saline solution (DPBS, without Ca^{2+} and Mg^{2+}, Gibco, purchased from Thermo Fisher Scientific); cells were trypsinized by the required concentration of 10x Trypsin–EDTA solution (5.0 g/L porcine trypsin and 2.0 g/L EDTA·4 Na in 0.9% v/v sodium chloride solution purchased from Sigma Aldrich). The cell number was counted with either a Bürker counting chamber (Marienfeld Superior - Paul Marienfeld GmbH & Co. KG, Lauda-Königshofen, Germany) or TC20 Automated Cell Counter (Bio-Rad Laboratories, Budapest, Hungary) using Trypan Blue (Gibco, purchased from Thermo Fisher Scientific).

3.6.3.   Evaluation of in vitro toxicity of investigated chelators, complexes and liposomes

Three types of viability assay were used to evaluate the results of this thesis. The initial seeded cell number of a 4-, 24-, and 72-hour-long experiment was generally at a density of 30,000; 20,000 and 5,000 cells/well, respectively. The dissertation shows the results of experiments with several kinds of cell lines, and in certain exceptional cases we may deviate from the given cell numbers (extreme doubling time compared to the average). A known fact is the influence of the increase in passage number on several cell line-specific characteristics, thus we tried to keep the passage number as small as possible for the different experiments. Cells within 20 passages were used in the current study. Briefly, cells were seeded in the inner 60 wells of 96-well tissue culture plates (Sarstedt, Newton, NC, US or Orange Scientific, Braine-l'Alleud, Belgium) in 100 µL completed media and allowed to attach for 12 hours. After cell attachment, serially diluted compounds were added to the wells in a final volume of 200 µL, thereafter, the plates were incubated until analysis.

Chelators were added in 100 µL volume in different concentration ranges (depending on the time of the experiment and on the toxicity of the compounds). If the different metal salts were used for *in vitro* studies, the metal ions were added in 50 µL volume before pipetting the chelators in other 50 µL volume. The liposomes were dispensed into the culture media to obtain a 10-fold dilution, and 100 µL was added for the highest concentration of treatment to the cells plated in 100 µL media, resulting in 1:1 dilution.

Curve fit statistics (Section 3.10.) were used to determine the concentration of test compound that resulted in 50% toxicity (IC_{50}). Data were normalized to untreated cells. The IC_{50} value (given in µM) is the average of at least three independent determinations. Every IC_{50} value represents the corresponding GI_{50} value (the average growth inhibition of 50%). The IC_{20} (inhibitory concentration corresponding to 20% cell survival) values required in some experiments were determined with the same method.

3.6.3.1   *MTT viability assays*

The   MTT   (3-(4,5-dimethyl-2-thiazolyl)-2,5-diphenyl-2H-tetrazolium   bromide) viability assays were performed as described earlier with some modifications [326–328]. After the incubation period at 37 °C in 5% CO_2 atmosphere, the viability of cells was determined by MTT staining process using a final concentration of 367 mg/L fresh medium containing MTT reagent (purchased from Sigma Aldrich) in each well. After a

three-hour-long incubation with MTT, cells were centrifuged at 300 *g* for 5 min, the supernatant was removed carefully, and the crystals were dissolved in DMSO. The absorbance was determined using an ELISA-reader (Labsystems MS Reader, Vantaa, Finland) at 540 nm and at 620 nm as reference wavelengths.

3.6.3.2 *Sulforhodamine B (SRB) assay*

Minor modifications were achieved during the SRB-assay related to further references [329–331]. After the different treatments with metal salts and chelating agents, cell monolayers were fixed with 10% (v/v) trichloroacetic acid (powder from Sigma Aldrich) in 70 µL volume for 1 hour at 4 °C and stained for 20 min with 0.4 w/v% SRB (dissolved in 1 v/v % acetic acid, powder purchased from Sigma Aldrich) dissolved in 1% acetic acid at room temperature (RT). Cells were repeatedly washed with 1 v/v % acetic acid to remove the excess dye. The protein-bound dye was dissolved in 10 mM Tris buffer (pH 7.4) and optical density (OD) determined at 570 nm using a microplate reader (EL800, BioTec Instruments, Winooski, VT, US).

3.6.3.3 *PrestoBlue assay*

After incubation, lasting for 4-h, 24-h, or 72-h, the supernatant was removed, washed once with DPBS and the viability was assessed by means of the PrestoBlue assay (Invitrogen; purchased from Thermo Fisher Scientific) [332], according to the manufacturer's instructions. Viability of the cells was measured spectrophotometrically (measuring fluorescence, excitation at 560 nm and emission at 590 nm) using an EnSpire microplate reader (Perkin Elmer, Waltham, Massachusetts, US).

3.6.4. *Clonogenic assay*

Long time antiproliferative effect of chelating agents was assessed by performing clonogenic assay. The assay was performed as described earlier with minor modifications [331, 333]. Briefly, 1,000 cells were seeded in 6 well plates (Corning Costar, Sigma Aldrich) and upon adhesion, the medium was replaced with fresh medium supplied with 2 µM Cu(II) and each chelating agent at a concentration corresponding to their IC_{20} (inhibitory concentration corresponding to 20% cell survival) overnight. Fresh medium was supplied after the treatment and on every third day. On the 10th day, cells were fixed with a 3:1 mixture of methanol-acetic acid and stained with crystal violet dye (0.5 w/v%, Sigma Aldrich). Excess dye was removed by distilled water. The ImageJ open-source software (NIH) [334, 335] was used for quantifying the number of colonies. After staining

with crystal violet, the attached dye was dissolved in 2% SDS solution and measured as in the SRB assay by spectrophotometry. For comparison, both methods were used in the evaluation. Data were normalized to untreated colony formation in percentage.

3.6.5. *Spheroid generation and treatment*

Spheroids of uniform size were generated for HCT-116 cell line using the hanging-drop method. Using single cell suspension, hanging drops with a volume of 6 μL were made, each drop containing approximately 400 cells. After 4 days, 30 spheroids were formed and transferred, each to a 96-well Ultra Low Attachment plate (Corning Costar, Sigma Aldrich). Spheroids were further grown for an additional four days. Then fresh medium was given and they were treated with the chelating agents in a IC_{20} concentration for each and 2 μM Cu(II). Control groups with and without the addition of Cu(II) were also subjected to this experiment.

Pictures were taken of each spheroid on the third and sixth day upon treatment, using a phase-contrast microscope (Nikon Eclipse TS100, Melville, NY, US). Pictures were analyzed with ImageJ [334] to measure the area from which the spheroid volume was calculated. Measured area (A) of the spheroids was used to calculate the radius (r) and volume of the spheroids (V) of an equivalent sphere using $r = (A/\pi)^{1/2}$ and $V = 4/3 \times \pi \times r^3$ formulae, respectively, according to Ref. [336].

3.6.6. *Determination of the in vitro apoptotic effect by flow cytometry (FACS)*

The HT-29 cells were cultured as described before. To study the apoptotic effect of the investigated chelating agents, a number of 1×10^5 cells per well were plated on 24-well plates (Corning Costar, Sigma Aldrich). After 24-h incubation at 37°C, cells were treated for 20 min with 5 μM chelating agents dissolved in serum-free medium and applying Cu(II) in increasing concentrations (0.5 μM, 5 μM and 50 μM). Control cells were also treated with serum-free medium for 20 min. After incubation, treatment solutions were removed, and cells were washed with serum-free medium twice. After centrifugation (216 *g*, 5 min, 4 °C), the supernatant was removed, and 100 μL of trypsin (Trypsin 1x, diluted by Ca^{2+} and Mg^{2+}-free solution from Trypsin 10x, product of Sigma Aldrich) was added to the cells. The effect of trypsin was stopped with 900 μL of HPMI (100 mM NaCl, 5.4 mM KCl, 0.4 mM $MgCl_2$, 0.04 mM $CaCl_2$, 10 mM HEPES, 20 mM glucose, 24 mM $NaHCO_3$ and 5 mM Na_2HPO_4 at pH 7.4, products of Sigma Aldrich)

[337] containing 10% v/v FBS, and the cells were transferred from the plate to FACS-tubes (In vitro Technologies, Victoria, Australia). Cells were centrifuged at 216 g for 5 min at 4 °C and the supernatant was removed.

After this procedure, the nonspecific cell death and apoptosis were determined by staining with allophycocyanin labeled Annexin-V (APC-Annexin-V, Invitrogen, Thermo Fisher Scientific). Cells were washed once with ice cold phosphate-buffered saline (DPBS) and then resuspended in 100 µL binding buffer, containing 10 mM HEPES of pH 7.4, 140 mM NaCl, 2.5 mM $CaCl_2$, 0.1 % bovine serum albumin. Then, 3 µL of APC-Annexin-V was added to the cell suspension and they were incubated for 15 min on ice, protected from light. Additionally, 1 µL of propidium iodide (PI) of 1 mg/mL stock solution (Sigma Aldrich) was added to the tubes. After 15 min labeling, further 380 µL of cold binding buffer was added to each tube and immediately analyze by flow cytometer LSR II (BD Bioscience, San Jose, CA, US), at 635 nm (JDS Uniphase Helium Neon, Laser 2000 GmbH, Wessling, Germany; 20 mW laser, channel APC BP660/20) using the FACSDiVa 5.0 analysis software (BD Biosciences). Viable cells are both Annexin V-FITC and PI negative (Annexin-V-/PI-), while cells that are in early apoptosis are Annexin V-FITC positive and PI negative, membrane integrity is present (Annexin-V+/PI-). The PI-positive cells (Annexin-V+/PI+ and Annexin-V-/PI+) were classified as late apoptotic or already dead. This assay does not distinguish cells that have undergone apoptosis vs. those that have died of necrotic pathway. Usually apoptosis is measured over time; these three stages suggest apoptotic events. All measurements were performed in triplicates.

3.6.7. Analysis of ROS by flow cytometry

To assess ROS production of investigated chelators in the presence of Cu(II) ions, an oxidation-sensitive marker, 2',7'-dichlorodihydrofluorescein diacetate (H_2DCF-DA, SantaCruz Biotechnology, Dallas, Texas, US) was used [338]. The HT-29 cells were seeded in 24-well plates at a concentration of 1×10^5 cells/well and treated with all investigated chelating agents in a concentration of 5 µM each and Cu(II) in increasing concentration (0.5 µM, 5 µM and 50 µM). After 1 hour of treatment, cells were harvested by trypsinization, then washed with DPBS. Cells were transferred from the plate to FACS-tubes and after centrifugation (216 g, 5 min) resuspended in labeling media containing 0.1 µM of H_2DCF-DA, following incubated for 30 min at 37 ºC, in air of 5%

CO_2 content, protected from light. After removing H2DCF-DA by centrifugation and washing twice with DPBS, the intracellular fluorescence intensity of 2',7'-dichlorofluorescein (DCF) was measured by flow cytometry (LSRII, BD Bioscience) using the 488 nm laser for excitation and detected at 535 nm.

For negative and positive control, cells were incubated with 5 mM N-Acetylcysteine (NAC, ROS scavenger, Sigma Aldrich) in culture medium and 0.1 mM H_2O_2 (strong oxidizing agent; grade for ultratrace analysis, Supelco, purchased from Sigma Aldrich) in DPBS, respectively. Treatment with 5 µM D-penicillamine was also performed as a negative control (extracellular chelator, toxicity does not depend on the Cu(II) concentration).

3.7. Multi-element analysis

3.7.1. TXRF analysis for the determination of intracellular Cu, Fe and Zn

For the determination of the intracellular Cu, Fe and Zn content of cells, a total-reflection X-ray fluorescence (TXRF) method was used as reported elsewhere [339]. Briefly, all determinations were performed on an Atomika 8030C TXRF spectrometer (Atomika Instruments GmbH, Oberschleissheim, Germany). Gallium (Ga) was used as an internal standard. The stock solution of 1000 mg/L Ga was purchased from Merck (Darmstadt, Germany). The Kα lines were used for Cu, Fe, and Zn determinations at 8.047 keV, 6.403 keV, 8.638 keV, respectively. Applicability of TXRF for the elemental analysis of human cells has been demonstrated earlier [340, 341].

3.7.1.1 Sample preparation for determination of intracellular Cu levels

Cells were seeded into 6-well culture plates (10^6 cells/well) in 2 mL completed media. Cells were incubated overnight and the medium was changed to 2 mL FBS-free medium before the treatment (or to fresh completed media in some experiments). Cells were treated with the different chelators with or without varied metal ions. After a 4-hour-long incubation, cells were harvested with a trypsin–EDTA solution. After 5 minutes incubation the trypsinization was stopped using the usual media completed by 10% FBS and was transferred to 1.5 mL Eppendorf tubes (VWR International Ltd., Debrecen, Hungary). After centrifugation (300 *g*, 5 min), cells were washed twice with 1 mL of DPBS. The cell number was counted with either a Bürker counting chamber or a TC20 Automated Cell Counter using Trypan Blue. After the last centrifugation, the DPBS was removed completely and 20 µL of 30% H_2O_2, 80 µL of 65% HNO_3 and 15 µL of 10

µg/mL Ga were added to the cells and digested for 24hours at room temperature. From the resulting solutions, 2-10 µL was pipetted on the quartz reflectors used for TXRF analysis. Data normalized to counted cell numbers was in good agreement with the determined sulfur content.

3.7.1.2 *Cu determination in the liposomes*

Liposomes in 100 µL volume were dissolved in 100 µL methanol and diluted 100-fold with Milli-Q water. Samples were measured by TXRF method using 1500 ng Ga as an internal standard.

3.7.2. X-ray imaging

3.7.3. Sample preparation for X-ray imaging

Cells were grown on 7.5 mm × 7.5 mm low stress silicon nitride windows with a thickness of 500 nm supplied by Norcada (Edmonton, AB, Canada). Copper treatments were performed with Cu(II) and chelators for 1 hour for each. Then the samples were fixed with 2% (v/v) formaldehyde and transported to the Diamond Light Source facilities.

3.7.4. Micro-XRF imaging

Scanning X-ray micro-fluorescence (XRF) was performed on beamline B16 of the Diamond Light Source (Harwell Science and Innovation Campus, Oxfordshire, UK) [342, 343]. A double multilayer monochromator was used to select 17 keV X-rays which were focused down to a 460 nm vertical (VER) × 640 nm horizontal (HOR) spot with Kirkpatrick-Baez focusing optics and projected at 45 degrees horizontally onto the sample. This yielded a focal spot of 460 nm VER × 900 nm HOR on the sample, which was used to excite the K-lines of elements from Cl to Zn. The step size was set to 500 nm. Initially, in order to localize the cells on the membranes, a coarse resolution sample raster scan with steps of 5 µm was performed. The XRF spectra from the specimen were acquired with a four-element energy dispersive silicon drift detector (Vortex, Hitachi, Tokyo, Japan). Spectral analysis of the fluorescence spectrum of each pixel provided images of the spatial distribution of each element. Spectral deconvolution was performed using PyMca [344]. The sample was mounted on silicon nitride (SiN) foils (thickness of 500 nm, American Elements, Los Angeles, CA, US). The reading time was 5 s/pixel.

3.8. Preparation of Drug-loaded Liposomes

3.8.1. *Cu-containing liposomes loaded with the chelator neocuproine*

Thermo-sensitive and thermo-resistant liposomes were prepared by the lipid film hydration and extrusion method. Lipid mixtures containing DPPC, HSPC and DSPE-PEG2000 in the weight ratios summarized in **Table 4** were dissolved in chloroform, and dried to receive a thin lipid film under a stream of N_2 gas, followed by incubation overnight under vacuum to remove the residue of the solvent. As a next step, 100 mM (or 10 mM, 300 mM for LIPO1) of $CuSO_4$ solution was applied to hydrate the lipid films to gain a total lipid concentration of 35 mg per 3 mL, when mixing with a magnetic stirrer in a 60°C water bath for 30 minutes. The resulting multi-lamellar vesicle (MLV) suspension was subjected to five cycles of freeze-and-thaw (5 min each, freezing in liquid nitrogen and thawing at 60°C), before being extruded 13 times at 60°C through a 100 nm polycarbonate membrane filter (Whatman, Springfield Mill, UK) via a LIPEX® Extruder (LIPEX Biomembranes, Vancouver, B.C., Canada) to produce large unilamellar vesicles (LUVs), which encapsulate the Cu salt. Residual un-encapsulated Cu was removed by means of size-exclusion chromatography via passing 2.5 mL liposome suspension through a desalting PD-10 column and eluting with 3.5 mL 100 mM HEPES buffer (pH=7.8±0.1), prepared from HEPES-Na salt and setting the pH by hydrochloric acid. The pH of the buffer was adjusted manually by using S20 SevenEasy pH-meter (Mettler Toledo, Columbus, Ohio, US). The resulting liposomal formulations contained the indicated copper ion solution (typically an unbuffered solution that was at pH 4.5) inside and the HEPES buffer pH 7.8 outside [300]. After separation, 0.1 M neocuproine hydrochloric acid (dissolved in MQ water) was added in 0.2:1 mol drug-to-mol phospholipid ratio (or more: 0.4:1 and 0.8:1 ratios during the optimization process) and incubated overnight at room temperature for loading of the drug into the liposome. The unencapsulated neocuproine or copper-neocuproine complex was removed by loading 2.5 mL sample on a PD-10 column and eluting the purified liposome fraction with 3.5 mL sterile 0.9% NaCl solution.

Table 4. Lipid composition of the prepared liposomes.

Sample name	DPPC (mg)	HSPC (mg)	DSPE-PEG2000 (mg)	w/w% of DPPC and HSPC
LIPO1 *hereinafter* **HEAT RES LIPO**	0	30	5	100%HSPC:PEG
LIPO2	15	15	5	50%DPPC:50%HSPC:PEG
LIPO3 *hereinafter* **HEAT SENS LIPO**	21	9	5	70%DPPC:30%HSPC:PEG
LIPO4	24	6	5	80%DPPC:20%HSPC:PEG
LIPO5	27	3	5	90%DPPC:10%HSPC:PEG
LIPO6	30	0	5	100%DPPC:PEG

3.8.2. Cu(II) containing liposomes loaded with the chelator Q4

Lipid composition of LIPO3 (**Table 4**) was prepared as before for formulation of liposomes with 100 mM CuSO$_4$. A solution of 10 mM Q4 dissolved in Milli-Q water was achieved for loading using a 5:1 lipid-to-drug molar ratio, resulting yellow liposomes related to the colors of the Cu(II)-Q4 complexes. The further sample preparation steps are the same, as described in **Section 3.8.1**.

3.8.3. Methods for characterization of the liposomes

To characterize the prepared liposomes, dynamic light scattering (DLS), microfluidic resistive pulse sensing (MRPS), differential scanning calorimetry (DSC), infrared (IR) spectroscopy, ultraviolet–visible (UV-Vis) spectrophotometry and TXRF were used.

3.8.3.1 *Dynamic light scattering (DLS)*

The mean particle diameter and size distribution function of the samples during the preparation procedure were determined by means of DLS at 20 °C, performed on a W130i DLS apparatus (Avid Nano Ltd, High Wycombe, UK), applying low-volume, disposable cuvettes (UVette, Eppendorf Austria GmbH, purchased from Sigma Aldrich). The DLS instrument is equipped with a diode laser ($\lambda = 660$ nm) of 30 mW power and a side scatter detector fixed at an angle of 90°. For DLS experiments, to check the monodispersity of liposomes during preparation procedure, samples were diluted 10-fold with the liposome containing solvent (MQ, HEPES buffer or final liposomes diluted by 0.9% NaCl solution). The data evaluation was performed with iSIZE 3.0 software (Avid Nano), utilizing the CONTIN algorithm.

3.8.3.2 *Microfluidic resistive pulse sensing (MRPS)*

Microfluidic resistive pulse sensing (MRPS) is the nanoscale implementation of the coulter principle in a microfluidic cartridge [345–348]. The MRPS measurements were performed with a nCS1 instrument (Spectradyne LLC, Torrance, CA, US). Samples were diluted 100-500-fold with BSA solution at 1 mg/mL concentration in 0.9% NaCl, filtered through an Amicon Ultra-0.5 mL (100K, Merck), 100 kDa MWCO membrane filter, according to the manufacturer's instructions. All measurements were performed using factory calibrated TS-300 cartridges in the measurement range of 50-300 nm.

3.8.3.3 *IR spectroscopy*

The IR measurements were carried out using a Varian FTS-2000 (Scimitar Series) FTIR spectrometer (Varian Medical Systems Inc., Palo Alto, CA, US) equipped with a 'Golden Gate' single reflection diamond attenuated total reflection (ATR) accessory (Specac Ltd, Orpington, Kent, UK). A 3 µl aliquot of each measured sample was spread on the surface of the diamond ATR element and a thin dry film was obtained by applying slow evaporation of the buffer solvent under ambient conditions. Spectral resolution of 2 cm^{-1} and co-addition of 64 individual spectra were adjusted. The ATR correction and buffer background subtraction were applied for each recorded spectrum. Spectral manipulations, including curve-fitting procedures, were performed by utilization of the GRAMS/32 software package. For curve-fitting, band positions were estimated using the second derivative, and the band shapes were approximated by Gauss functions until the minimum of χ^2 was reached.

3.8.3.4 *Determination of the concentration of active ingredients*

Neocuproine content and encapsulation efficacy of the neocuproine were measured by the spectrophotometric method. A 20 µL aliquot of the sample was dissolved in 50 µL methanol and diluted with Milli-Q water to 100 µL to release encapsulated Cu and neocuproine from liposomes. The complex was reduced with ascorbic acid (10x excess) and the absorption of the sample was recorded at 450 nm. Calibration solutions were prepared with a Cu-neocuproine ratio of 1:1 (stock solution 1 mM). Encapsulation efficacy was calculated as a proportion of the neocuproine administered and received after column filtration.

3.8.3.5 *Differential scanning calorimetry (DSC)*

The DSC method was used to characterize thermotropic phase transitions of liposome samples. Measurements were performed on a µDSC 3 EVO (Setaram, France) instrument in the temperature range of 20-60 ºC with 0.2 ºC/min. heating rate using 300-400 mg of the liposome samples.

3.8.3.6 *Stability of the liposomes*

To test the stability of the liposomes, 200 µL aliquot of each sample was centrifuged through Zeba Spin Desalting Columns, 40K MWCO, 0.5 mL (cut off or exclusion limit: 40 kDa, Thermo Fisher Scientific) after previous washing procedures according to the instructions of the manufacturer, combined with UV-Vis spectrophotometry using an EnSpire microplate reader (Perkin Elmer).

The release of the copper-neocuproine complex from the HEAT SENS LIPO and HEAT RES LIPO was tested at different temperatures (temperature dependence release) and at different time points after preparation (time dependence of the stability). The absorbance was measured spectrophotometrically at 450 nm (maximal absorbance of Cu(I)-neocuproine complex). Data were normalized to unheated or to the freshly prepared liposome.

3.8.3.7 *Size exclusion chromatography (SEC)*

A 100 µL aliquot of liposome sample (HEAT SENS LIPO and HEAT RES LIPO) was incubated with 900 µl of completed DMEM medium (containing 10% FBS) for 4 hours at 37 °C, 5% CO_2 modeling cell culture conditions. A 10 µL aliquot of each incubated sample was injected into a Jasco HPLC system (Jasco, Tokyo, Japan), consisting of a PU-2089 pump with an UV-2075 UV/Vis detector and using Tricorn 5/100 glass columns (GE Healthcare Bio-Sciences AB), filled with Sepharose CL-2B (Sigma Aldrich). The eluent was DPBS with a flow rate of 0.5 mL/min. The UV-Vis chromatograms were collected at 450 nm, corresponding to the absorption maximum of the Cu(I)-neocuproine complex.

3.9. *In vivo* studies

3.9.1. *In vivo anti-tumor efficacy of copper and neocuproine-containing liposomes*

The $2x10^6$ mouse colon carcinoma (C-26) cells were injected into the left flank of 6-to-9-week-old male BALB/c mice from our specific pathogen-free colony subcutaneously (s.c.) in a volume of 0.2 mL serum-free media. Two weeks after injection

(when tumors were detectable), the mice were randomly and evenly divided into groups (10 mice/group). Treatment groups received 10 µL liposome / 1g body weight intravenously (i.v.) on the first and eighth day of the treatment. The concentration of the complex (Cu:neocuproine) was taken as 1 mM, resulting in an amount of 2.8 mg/kg of "active ingredient" calculated for the thermosensitive formulation. The dose of the encapsulated drug for the "thermoresitant" formulation was 2.6 mg/kg. Controls received equivalent volumes of sterile NaCl 0.9%. All animals were included in the analysis. Changes in their body weight were also determined throughout the study. No adverse events were observed during the experiment. The antitumor effects were registered twice a week by measuring the tumor size with a caliper. The absolute tumor volume was calculated with the formula for an ellipsoid shape (L (length)$\times$ W (width)$^2 \times (\pi/6)$) [349]. Eighteen days after the first treatment, the mice were euthanized, and the tumors were extracted and dried in an oven to obtain a constant weight. The samples were weighed on an analytical balance (Mettler Toledo XS105, Greifensee, Switzerland). Statistical analysis was performed using Graph Pad Prism 8 software using One-Way ANOVA analyses. Animal experiments were carried out at the Department of Experimental Pharmacology, National Institute of Oncology, Budapest, Hungary and the animal-model experiments were conducted following the standards and procedures approved by the Animal Care and Use Committee of the National Institute of Oncology, Budapest (license number: PEI/001/2574–6/2015). All animal protocols were approved by the Hungarian Animal Health and Animal Welfare Directorate, according to the directives of the European Commission.

Tumors were heated to test the temperature dependent release of liposomes in two treated animal groups. Animals were treated under anesthesia with desflurane (9% desflurane in 30% oxygen/air). Local mild hyperthermia (41-42ºC $\pm$ 0.5°C) was performed under anesthesia with a custom-made contact heating device based on direct heat conduction using a metal rod connected to a temperature-controlled water bath. Intratumoral temperature was measured with optical sensors (Luxtron FOT Lab Kit, LumaSense Technologies, Inc., Milpitas, CA, US) and kept between 41-42°C ($\pm$ 0.5°C) for 20 min. The applied temperature for mild hyperthermia is above the phase transition temperature of the thermosensitive liposome (HEAT SENS LIPO). The permeability of

the lipid bilayer is known to be enhanced above this temperature, so using hyperthermic treatment causes pronounced drug release.

3.9.2. *In vivo antitumor efficacy of Q4-containing liposomes*

Two animal models were evaluated to test the antitumor effect of the liposome containing Cu(II)-Q4 complex. The C-26 mouse colon adenocarcinoma in BALB/c male mice model was used first, details as described above with the dosage (10 µL liposome / 1g body weight i.v.). For other models, to test the MDR-selective toxicity of the liposomal formulation related to doxorubicin resistance, a doxorubicin sensitive-resistant cell line pair was selected, P388 and P388/ADR, respectively. Cells (1×10^6 cells/animal) were injected into the intraperitoneal cavity of 6-8-week-old male BALB/c mice and after 48 hours the liposomes were given a daily dose of 10 µL per 1 g body weight intraperitoneally. The animals were weighed 3 times per week and monitored/observed frequently each day for any sign of pain.

3.9.3. *In vivo PET imaging*

3.9.3.1 *Radiolabeling of liposomes with Cu-64*

A 1 mL aliquot of extruded liposome sample containing HSPC (9 mg/3 mL), DPPC (21 mg/3 mL) and DSPE-PEG2000 (5 mg/3 mL) hydrated with 100 mM non-radioactive $CuSO_4$ solution was first purified on a G-25 Midi-Trap column to remove the non-entrapped Cu^{2+}. The purified liposome fraction was eluted with 1.5 mL sterile 0.9% NaCl solution and it was subsequently mixed with 200 µL (400 to 450 MBq) no carrier added [^{64}Cu]$CuCl_2$ labeling agent (produced on the cyclotron TR-FLEX (Advanced Cyclotron Systems, Inc., Richmond, BC, Canada), at the Helmholtz-Zentrum Dresden-Rossendorf). After incubation at room temperature for 60 minutes, 0.425 mL 100 mM HEPES buffer and 24 µL 0.1 M neocuproine hydrochloric acid (dissolved in Milli-Q water) stock solution was added to the liposome sample (thermosensitive formulation) and incubated overnight at room temperature for loading of the neocuproine into the liposomes. Finally, the sample was purified on a PD-10 column with sterile 0.9% NaCl solution resulting in 120 to 150 MBq radiolabeled liposomes in 2 mL volume with approximately 95 to 97% radiochemical purity (based on the desalting efficiency of the PD-10 column according to the manufacturer).

3.9.3.2 *Small animal imaging*

Copper-64 ($T_{1/2}$ = 12.7 hours; β+, 0.653 MeV [17.8 %]; β−, 0.579 MeV [38.4 %]) has decay characteristics that allow positron emission tomography (PET) imaging. The NMRI-Foxn1$^{nu/nu}$ (NMRI-nu immundeficient mouse, Janvier Labs, Le Genest Saint Isle, France) mice (n = 3) with U251-HRE (ECACC, purchased from Sigma Aldrich) xenografts were used for the *in vivo* imaging experiments. The [^{64}Cu]Cu-neocuproine liposome suspensions (8.2 ± 0.8 MBq) were injected via the tail vein. One of the mice received local mild heat treatment following the liposome (thermosensitive formulation) injection, while the remaining 2 mice served as controls. The PET/CT measurements were performed with a nanoScan® PET/CT (Mediso Ltd., Budapest, Hungary) with a system PET resolution of 0.9 mm and the detection limit of a focal signal of 0.073 mm^3. All animals were anaesthetized with 1.5% inhaled isoflurane during imaging. The PET data acquisition started 1 and 4 hours post-injection for the control animals, and 3 hours post-injection for the animal that received mild hyperthermic treatment, and performed for 60 min in list mode. A 5 ns coincidence window and a 400-600 keV energy window was applied in a scan range of 94.7 mm. A 3D expectation maximization (3D EM) PET reconstruction algorithm (Mediso Tera-TomoTM) was applied to produce PET images including corrections for decay, attenuation and scatter, dead time and random coincidences. The helical CT scans were acquired with 35 kV tube voltage, 300 ms exposure time, 1 mA tube current, 1:4 binning and 360 projections. The images were reconstructed with 0.12 mm isovoxel sizes. The PET attenuation correction was based on the CT images. After 4 iterations the reconstruction resulted in images with 0.4 mm isovoxel size. The results of PET measurements were quantified in units of radioactivity measured per unit volume (MBq/mL). Image analysis was performed with VivoQuant software (inviCRO, Boston, MA, US). Following registration of the PET and CT data, tumor and muscle volumes of interest (VOI) were selected by hand. The radioactivity concentrations of tumor VOI's are presented as a ratio to the image-based whole-body radioactivity concentration. Animal whole-body volumes were determined in mm^3 using a semi-automatic image thresholding algorithm in VivoQuant based on CT densities and corrected with the PET volumes.

3.10. Statistical data analysis

Statistical data analysis was performed by Student's t-test at the 95% confidence level, using Origin software (OriginLab Corporation) [350]. Analysis and graphing solutions were performed by various versions of Origin and GraphPad Prism [351] software. The IC_{20} and IC_{50} values were determined from the dose-response curves. Curves were fitted by using the sigmoidal function (Origin) or sigmoidal dose–response (comparing variable and fixed slopes) model (GrapPad Prism) and they were expressed as the mean of three independent experiments (each one performed with three replicates). Data shown as average of six independent experiments and effect of treatment are expressed relative to the control. Statistical analysis for the differences in metal contents and IC_{50} values was performed using a Student's t-test or ANOVA, with $p < 0.05$ considered to be statistically significant. The P values are shown in the 'Results' Section as follows below. For *in vivo* studies, statistical analysis was performed using Graph Pad Prism 8 software using One-Way ANOVA analyses.

4. Results

4.1. Results related to the chelator Dp44mT

4.1.1. Physicochemical properties of Dp44mT

4.1.1.1 The neutral ligand is the sole species at physiological pH.

The decadic logarithm values of the protonation constants of Dp44mT determined by UV titrations at 0.15 M ionic strength are: $\lg K_1 = 10.48 \pm 0.04$ and $\lg K_2 = 3.49 \pm 0.03$ [352]. The third protonation constant corresponding to the second dissociable proton of the pyridyl group could not be determined at 0.15 M ionic strength. It can be determined in strong acidic solutions only. According to our estimation, $\lg K_3$ is around 0.5.

4.1.1.2 Complex formation takes place with different transition metal ions (Cu^{2+}, Fe^{2+}, Fe^{3+}, Co^{2+}, Ni^{2+}, Zn^{2+})

The decadic logarithm values for the conditional stability constants for Dp44mT (L) with Co(II), Cu(II), Fe(II), Fe(III) and Zn(II) as metal ions (M) according to the ML, ML_2 and M_2L stoichiometry are listed in **Table 5.** Although pH buffering cannot be applied to this type of experiment, the pH was continuously monitored, and it did not decrease below 5. Except for Cu, the most stable metal ion − Dp44mT complex composition is ML_2 as can be seen in the UV-Vis titration curves [352]. In the case of Cu, complexes with 1:1 Cu-to-L ratios are characterized by higher stability. Among the ML_2 complexes, the difference between their stability constants is about one or two orders of magnitude for Fe(II), Fe(III), Ni(II) and Co(II). Only in the case of Zn(II) is the stability constant for the ML_2 complex approximately between five and six orders of magnitude lower than for the above-mentioned transitional metal ions. The stability order among the highly essential metal ions (Cu(II), Fe(II) and Zn(II)) is the following: $CuL > Fe(II)L_2 > ZnL_2$. Theoretical speciation curves were simulated with the following input data: 10 μM of total Cu(II) and 10 μM of total Dp44mT concentration in the presence of Fe(II), Ni(II) and Co(II) separately at increasing concentrations comprising five orders of magnitude from 10^{-6} M to 10^{-1} M [352]. According to the calculation, Co(II), Ni(II) and Fe(II) would displace 50% of Cu at concentrations of 13-, 80- and 2,000-times higher than the initial Cu(II) concentration, respectively.

Table 5. *Conditional complex stability constants for Dp44mT (L) with Co(II), Cu(II), Fe(II), Fe(III) and Zn(II) as metal ions (M) according to the ML, ML$_2$ and M$_2$L stoichiometry at pH 5 and 0.15 M KNO$_3$ solution.*

Metal ion	lg β ± SD		
	ML	ML$_2$	M$_2$L
Cu(II)	7.08 ± 0.05	n.a.	9.80 ± 0.08
Fe(II)	n.a.	10.25 ± 0.06	n.a.
Fe(III)	7.06 ± 0.04	12.67 ± 0.06	n.a.
Co(II)	n.a.	12.47 ± 0.07	n.a.
Ni(II)	n.a.	11.68 ± 0.06	n.a.
Zn(II)	n.a.	5.56 ± 0.06	n.a.

Abbreviations: L - ligand; M - metal ion; n.a. - not available; SD - standard deviation.

4.1.2. Effect of Dp44mT on cancer cell lines and PBMC regarding different metal ions, with special reference to copper(II)

4.1.2.1 Dp44mT increases intracellular Cu content, while a decrease in Zn content is observed

The percentage of the intracellular Fe, Cu and Zn concentration of cancer cell lines and PBMC, used as control, incubated with growth medium and 50 μM Dp44mT compared to that of the sole growth medium can be seen in **Figure 4A**. In this case, Fe, Cu and Zn originated only from the culture medium. The elemental composition of the culture medium [353] and that of HT-29 cell lines [341] as well as the Fe uptake [339] was determined earlier. The intracellular concentration of Cu significantly ($p < 0.05$) increased for all investigated cancer lines compared to the growth medium, whereas the intracellular Zn concentration decreased in each case. On the other hand, the intracellular concentration of Fe varied between 78% and 163% compared to the intracellular Fe level registered in untreated cells. In spite of this random variation, the Fe level did not decrease markedly in the studied cancer cells. The Cu incorporation was much higher when the concentration of Cu, Fe and Zn of the pool was increased to 2 μM (**Figure 4B**). In the case of five different cancer cell lines, – colon (HT-29), melanoma (A-375), lung (H358) and ovarian (OVCAR-3 and Caov-3) – the intracellular Cu content increased more than

30-times compared to the control, when Dp44mT was added to the culture solution. The increase observed for Cu was at least 10-fold compared to the control growth cell culture for all cancer cell lines investigated. However, it should be mentioned that the intracellular Cu concentration of the PBMC cells also increased approximately 30-fold. Nevertheless, competition between Cu, Fe and Zn was not observed. For some cell lines, the Fe concentration was between two and four times higher upon increasing the Fe, Cu and Zn concentration of the growth medium. When the concentration of Dp44mT was further increased ten times, the intracellular element concentration did not markedly increase.
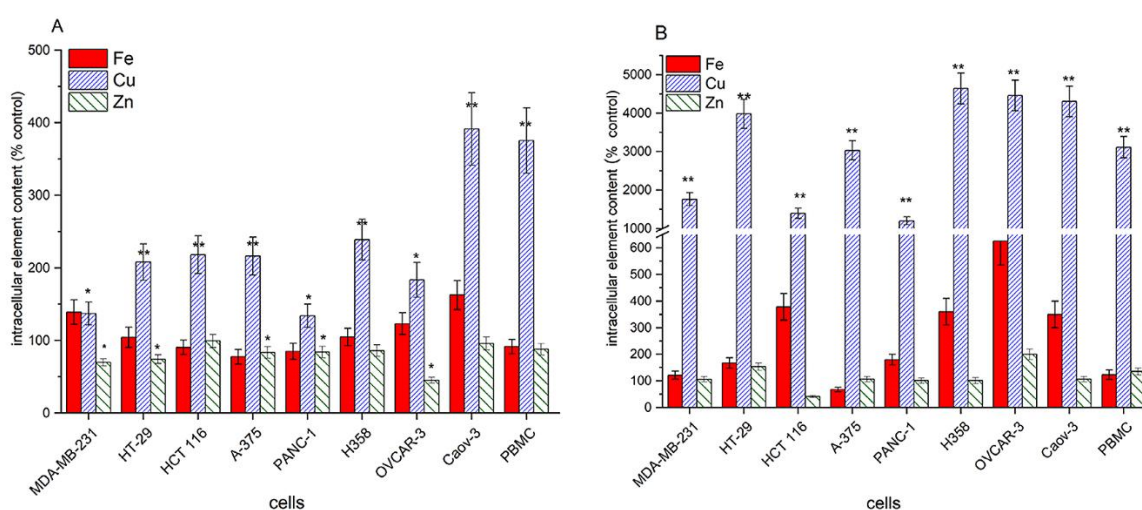
Figure 4. *Intracellular Fe, Cu and Zn content related to the untreated cells (% control) of different cancer cell lines and PBMC after 4 h. (**A**) Cells treated with 50 µM Dp44mT. (**B**) Cells treated with 5 µM Dp44mT in the presence of 2 µM of Fe(II), Cu(II) or Zn(II). Dp44mT was added after one-hour incubation with metal ions. *, versus control, p < 0.05; **, versus control, p < 0.01; ***, versus control, p < 0.001.*

4.1.2.2 *A rise in the concentration of copper(II) in the presence of Dp44mT appears to derive a saturation-like curve in terms of intracellular Cu content.*

The Cu content of cells as a function of increasing treatment with Cu(II) from 0.1 µM to 100 µM and 5 µM chelator concentration after 4 hours can be seen in **Figure 5A**. The Cu content of cells showed an increase up to 20 µM on treatment with solutions of increasing Cu(II) concentration. Above this concentration, the Cu content of the cells increased negligibly, and it seemed to reach a saturation plateau. The same was observed at 0.1 µM Dp44mT concentration. The Cu content in the control sample was 4.5 ng/10^6 cells. Therefore, an extremely high increase of 20,000% was observed as compared to the control in the case of the treatment with 20-100 µM Cu(II) (**Figure 5A**).
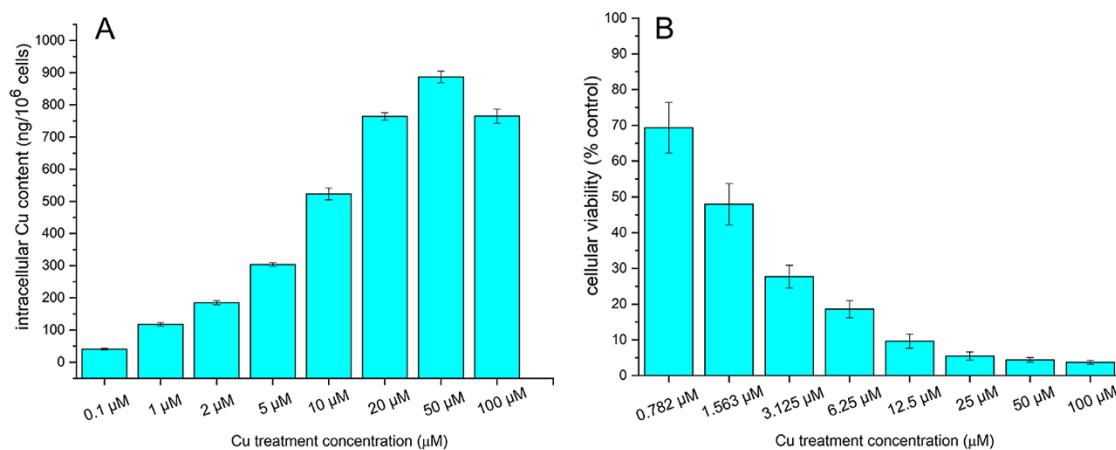
***Figure 5.** (A) Intracellular Cu content (ng/10^6 cells) with increasing concentrations of Cu(II) and in the presence 5 µM Dp44mT after 4 h. Dp44mT was added after one-hour incubation with metal ions. (**B**) Cellular viability of HT-29 cells related to untreated cells (% control) by MTT assay with increasing concentrations of Cu(II) and in the presence 0.0625 µM of Dp44mT after 24 h. Dp44mT was added after one-hour incubation with Cu(II).*

4.1.2.3   *Increasing the Cu(II) concentration in the presence of Dp44mT increases the in vitro cytotoxicity markedly*

According to MTT assays of the current study, the IC$_{50}$ of Dp44mT for 24 hours in the case of the HT-29 cell lines was 0.13 ± 0.05 µM. The presence of metal ions was investigated to see whether they were responsible for the unusually high standard deviation (SD). The Ni(II) and Fe(II) hardly influenced the toxicity, Co(II) decreased it, while Cu(II) increased it. Therefore, it can be stated that Cu(II) is the determining factor for the toxicity of Dp44mT. As can be seen in Figure 5, increasing the Cu(II) concentration from 0.78 µM to 100 µM resulted in cell viability drastically decreasing from about 70% to 5% when Dp44mT was applied at a concentration of 0.0625 µM (**Figure 5B**).

4.1.2.4   *Intracellular Cu content decreases markedly in the presence of Co(II)*

Competition studies were conducted considering formation constants for Fe(II), Co(II) and Ni(II) and Dp44mT, determined previously in this study. The Cu(II) concentration in the culture cell was fixed at 2 µM, and the concentration of Fe(II), Co(II) or Ni(II) was increased to 5 µM, 25 µM and, finally, to 100 µM, each prior to the addition of Dp44mT at a concentration of 5 µM. Thereafter, the intracellular elemental concentration was determined by means of TXRF (**Figure 6A**). The intracellular content of Cu was

considered to be 100%, and the Cu concentrations applied in the subsequent experiments conducted with the increased Fe(II), Co(II) and Ni(II) treatments were related to this value. Higher concentrations of Fe(II) or Ni(II) in the treatments did not markedly affect the intracellular Cu content. On the contrary, a low Co(II) treatment of 5 μM considerably depleted the Cu intracellular content, i.e. by approximately 50%. However, in the case of 100 μM Co(II), the intracellular Cu content decreased to the levels of control cells in spite of the presence of 5 μM Dp44mT.
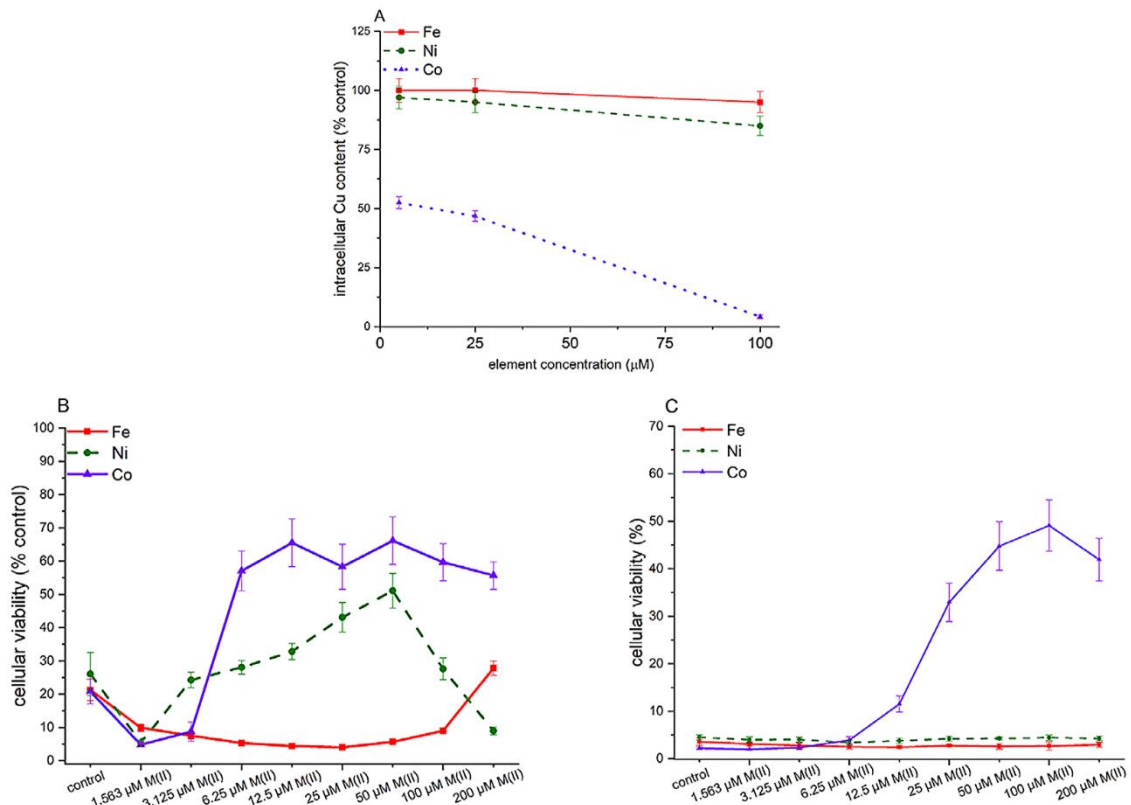
Figure 6. (A) *Intracellular Cu content related to HT-29 cells treated with 2 μM Cu(II) and 5 μM Dp44mT (% control) with increasing concentrations of Fe(II), Ni(II) and Co(II) after 4 h. Dp44mT was added after one-hour incubation with metal ions. **(B-C)** Cellular viability of HT-29 cells related to untreated cells (% control) by MTT assay with increasing concentrations of Fe(II) or Ni(II) or Co(II) and in the presence 5 μM Dp44mT after 24 h. **(B)** First case : with no addition of Cu(II). **(C)** Second case: with addition of 2 μM Cu(II). Copper(II) added simultaneously with the other metal ions; Dp44mT was added after one-hour incubation with metal ions.*

4.1.2.5 *Co(II) could suspend the Cu(II) toxicity, whereas the effect of Ni(II) in this competition context was moderate*

The results of the MTT assay investigating the effect of Fe(II), Co(II) and Ni(II) on the toxicity of Dp44mT in serum-free culture medium with and without 2 μM Cu(II) can be seen in **Figures 6A and 6B**, respectively. In the first series of experiments, the viability

of HT-29 cells was very low in the presence of 5 µM Dp44mT, even if Fe(II) was added at an increasing concentration (**Figure 6B**), e.g. up to 100 µM. By elevating the Fe(II) concentration of the culture medium to 200 µM, the viability hardly exceeded that of the control. Addition of Ni(II) in the concentration range of 6.25 µM to 50 µM steadily increased the viability of HT-29 cell lines to about 50 % compared to the control level. However, above 50 µM Ni(II), no more positive effect was observed. Among the investigated metal ions, Co(II) considerably inhibited the toxicity of Dp44mT, even if it was applied at low concentrations, i.e. 6.25 µM. When the experiment was repeated by adding 2 µM Cu(II) to the culture medium (**Figure 6C**), neither Ni(II) nor Fe(II) could change the cell viability in the applied concentration range, while at least 25 µM Co(II) is required in order to increase the viability.

4.2. Results related to DpC

The DpC chelator show an increased cytotoxicity on the HT-29 colorectal cancer cell line in the presence of different divalent metal ions (Zn^{2+}, Fe^{2+}, Cu^{2+}) (**Figure 7A**). In the presence of 10 µM Cu(II), the toxicity increased markedly, and this *in vitro* anticancer effect can be enhanced further by increasing the amount of Cu(II) (**Figures 7B, 7C**). Increasing Cu(II) concentration (0.5-20 µM) resulted in an increase of Cu content examined over a 4-h time interval, in experiments varying the DpC concentrations (0.1 µM and 5 µM, respectively) (**Figure 7D**). Cu(II) in the concentration range (0.5-20 µM) without the chelator do not cause copper accumulation; only the regular Cu content (3-5 ng/10^6 cells) in cells can be detected (**Figure 7D**).

Figure 7. *In vitro and Cu accumulation data of DpC on HT-29 cell line. DpC increased cytotoxicity in the presence of divalent metal ions (**A**) and increasing Cu(II) concentrations (**B-C**). Cu accumulation could be observed with different DpC concentrations in the presence of increasing Cu(II) concentrations (**D**).*

4.3. Comparative *in vitro* investigation of anticancer copper chelating agents

4.3.1. In vitro results

4.3.1.1 *Toxicity order of the investigated chelators could be established: Dp44mT > neocuproine > APDTC > oxine > 2,2´-biquinoline > dithizone*

2 µM of Cu(II) alone did not affect the cell viability, even for five days. Dp44mT was the most efficient chelating agent (**Table 6**). For the remainder of the chelating agents, the following toxicity order could be established: neocuproine > APDTC > oxine > 2,2´-biquinoline > dithizone. D-penicillamine did not show any toxicity.

Table 6. *In vitro cytotoxic and cytostatic activities of several Cu chelating agents on HT-29 cells through determination of IC$_{50}$ in µM concentration unit.*

Chelating agent	Cytotoxicity		Cytostasis	
	without addition of Cu(II)	+ 2 µM Cu(II)	without addition of Cu(II)	+ 2 µM Cu(II)
D-penicillamine	> 800[**]	> 200[**]	> 100[**]	> 100[**]
Dithizone	52	6.7	69	4.5
2,2´-biquinoline	19	2.8	16	2.0
Oxine	6.5	1.6	3.3	0.44
APDTC	4.5	0.92	1.4	0.14
Neocuproine	1.7	0.12	0.55	0.083
Dp44mT	0.07[*]	0.015	0.34[*]	0.0097

IC$_{50}$ = half maximal inhibitory concentration (µM); overall RSD < 20%;

[*]RSD < 100%; [**]= not toxic (see explanation in text).

4.3.1.2 *Investigated compounds proved to be more cytotoxic in the presence of Cu(II)*

The IC$_{50}$ values decreased drastically in the presence of Cu(II) (**Table 6**). In the present study, the difference in the IC$_{50}$ values for the investigated ligands could even be of two orders of magnitude. However, the cytotoxicity order was not altered by Cu(II) addition. Thus, the increase in cytotoxicity of Dp44mT was 4.8-fold. For the other Cu chelating agents, the increased cytotoxicity ranged between 4.2 (oxine) and 13.9 (neocuproine). Those chelating agents that caused large intracellular Cu accumulation on HT-29 cells, i.e. forming stable coordination compounds of 1:1 metal ion:ligand molar ratio, proved to exert higher cytotoxicity.

Generally, a similar *in vitro* cytotoxicity order was observed when IC$_{50}$ was determined for other cancer lines with the same Cu chelating agents: Dp44mT > APDTC > neocuproine > oxine > 2,2'-biquinoline > dithizone (**Table 6**). The difference in IC$_{50}$ values for the cells could even be one order of magnitude, except for APDTC that proved to cause a similar *in vitro* cytotoxic effect on the different cell lines. The investigated Cu chelating agents exerted a pronounced cytotoxicity on HT-1080, A-375 and MDA-MB-231 cells in the presence of 2 µM Cu(II) (**Table 7**). However, HT-1080 has an extreme glycolytic metabolism [354], while MDA-MB-231 is more resistant to treatments with doxorubicin, commonly used in the treatment of a wide range of cancers according to NCI-60 database [355]. Due to the intermediate cytotoxic effects of chelating agents on

HT-29, this cell line has proven to be an ideal candidate for our study. Therefore, from this point, studies on other cell lines were discontinued for this study.

Table 7. *In vitro cytotoxic activity of several Cu chelating agents on different cancer cells through determination of IC$_{50}$ in the presence of 2 μM Cu(II).*

Chelating agent	MCF-7	MDA-MB-231	ZR-75-7	HT-1080	HCT-15	HCT-116	A-375
Dithizone	>50	0.53	24.3	2.03	71	1.95	7.4
2,2'-biquinoline	4.9	1.5	5.7	0.62	82	10.0	>50
Oxine	1.5	0.39	0.68	0.61	1.12	0.12	0.31
Neocuproine	1.4	0.094	0.24	0.07	0.27	0.015	0.015
APDTC	0.11	0.091	0.092	0.082	0.21	0.31	0.02
Dp44mT	0.08	0.016	0.029	0.016	0.048	0.008	0.005

IC$_{50}$ = half maximal inhibitory concentration (μM); (RSD < 20%).

4.3.1.3 *Cytostasis shows the same tendency as cytotoxicity in the presence of copper*

As in the case of cytotoxicity, a similar tendency could be observed for cytostasis (**Table 6**). Thus, Dp44mT was the most toxic, as the IC$_{50}$ value for characterization of *in vitro* cytostatic effect was 35-fold in the presence of Cu(II) compared to the case when Cu(II) was not intentionally added to the growth medium. For the rest of the Cu chelating agents, the increase in the cytostasis was 6.7-15.3-fold.

4.3.1.4 *Considerable decrease in colony formation for neocuproine and APDTC is observed*

For colony formation, cells could also be grouped according to prevailing coordination species. Therefore, the colony formation was hardly hampered by the combined treatment of Cu(II) with one of the following chelating agents: oxine, dithizone and 2,2´-biquinoline (**Figure 8**). The colony formation ceased for Dp44mT at the end of the experiment. A considerable decrease in colony formation for neocuproine and APDTC was also observed. For Dp44mT and neocuproine, practically no resistant cell line can be developed. For the rest of the Cu chelating agents, long-term survival was obtained (**Figure 8**).
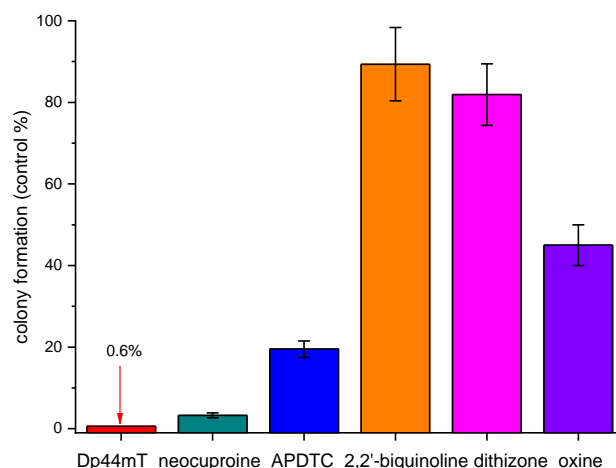
Figure 8. *Effect of Cu chelating agents on the colony formation for HT-29 cells in the presence of 2 μM Cu(II) and each chelating agent in IC_{20} concentration.*

4.3.1.5 *Treatments with APDTC and Dp44mT reduced the spheroid volume dramatically, neocuproine totally disintegrated the spheroids*

During the six-day-long treatment, tumor spheroids treated with oxine showed a slower growth compared to controls, but they remained in tight morphology (**Figure** 3). Treatments with APDTC and Dp44mT reduced the spheroid volume dramatically. On the sixth day, only loosely attached cell aggregates remained, whereas spheroids treated with neocuproine totally disintegrated only three days after exposure to the chelating agent. Dithizone and 2,2'-biquinoline showed no effect compared to controls (**Figure 9**).

The behavior of the chelating agents observed in terms of Cu accumulation, cytotoxicity/cytostasis, and colony formation raises the question of their different toxicity mechanisms. Presumably, the free valence of Cu(II) can attack a proper biological target after formation of the 1:1 metal ion:ligand coordination compound.

Day 3		Day 6	
control	control [+Cu(II)]	control	control [+Cu(II)]
$0.03690 \ mm^3$	$0.03739 \ mm^3$	$0.05863 \ mm^3$	$0.06734 \ mm^3$
Dp44mT	neocuproine	Dp44mT	neocuproine
$0.01917 \ mm^3$	n.a.	$0.00082 \ mm^3$	n.a.
APDTC	oxine	APDTC	oxine
$0.00405 \ mm^3$	$0.00957 \ mm^3$	n.a.	$0.01836 \ mm^3$
dithizone	2,2-biquinoline	dithizone	2,2-biquinoline
$0.03235 \ mm^3$	$0.03424 \ mm^3$	$0.04968 \ mm^3$	$0.05346 \ mm^3$
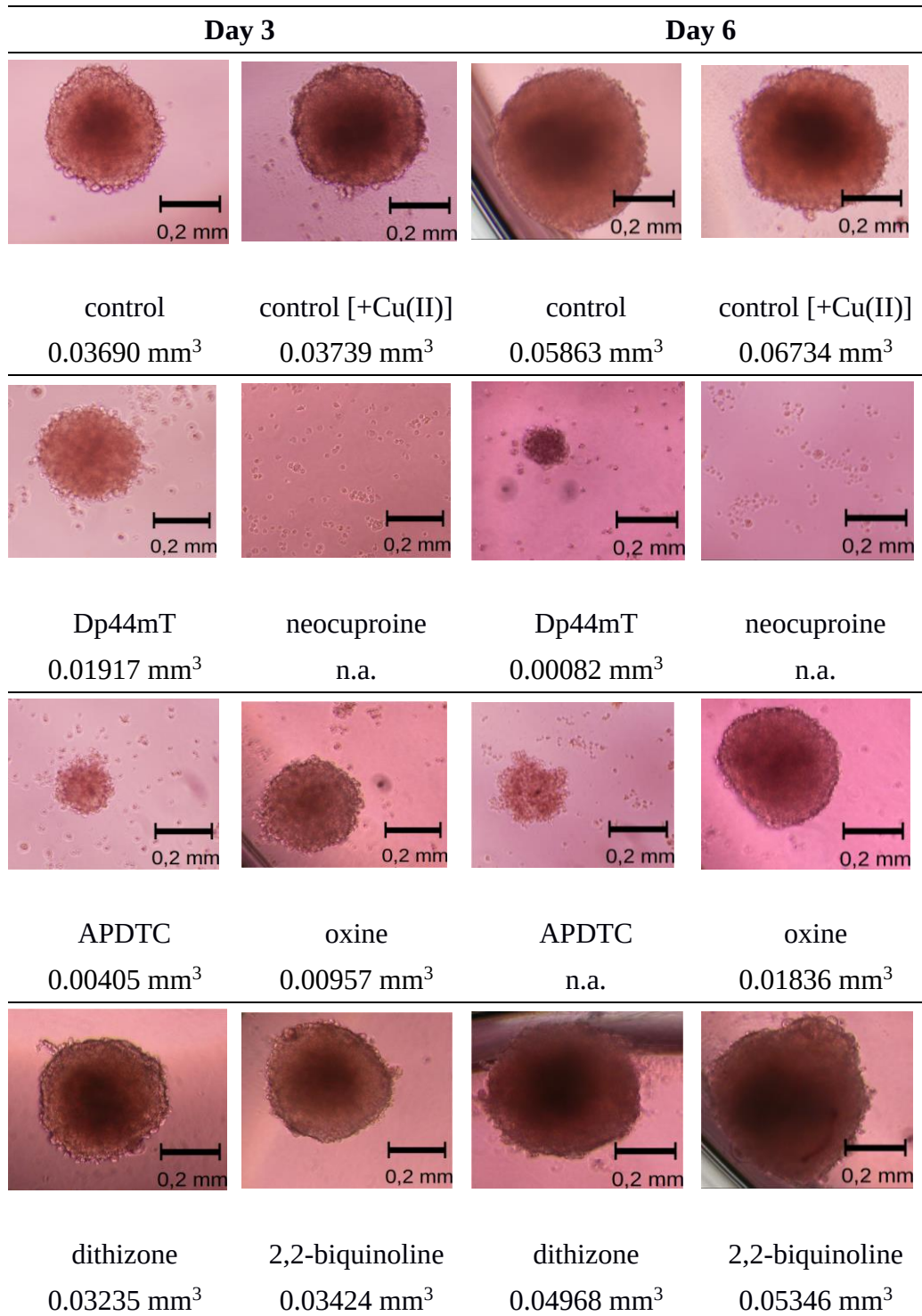
Figure 9. Time-lapse images of control untreated HCT-116 spheroids, and those treated with different chelating agents in a concentration corresponding to the IC_{20} for each and 2 µM Cu(II) three and six days after treatment as well as their estimated volume. Scale bar is 200 µm. (n.a. - loose aggregates).

4.3.1.6 *Apoptosis increased significantly in the presence of Cu (II) in increasing concentration range*

The number of apoptotic cells was low and comparable with that of the control and 0.5 µM Cu(II) when 5 µM Dp44mT and 5 µM oxine as representatives of stable coordination compounds of 1:1 and 1:2 Cu(II)-to-ligand molar ratio respectively were incubated for 20 min with 0.5 µM Cu(II) solution (**Figure 10A**). The number of apoptotic cells increased dramatically with a 10- and 100-fold increase of the added Cu(II) concentration. Interestingly, the ratio of the apoptotic cells was very similar for these two representatives. However, the fluorescent signals characterizing apoptosis increased gradually with the increment of the Cu(II) concentration for oxine, while the plateau was achieved already at a combined 5 µM Cu(II) and 5 µM Dp44mT treatment (**Figure 10B**).
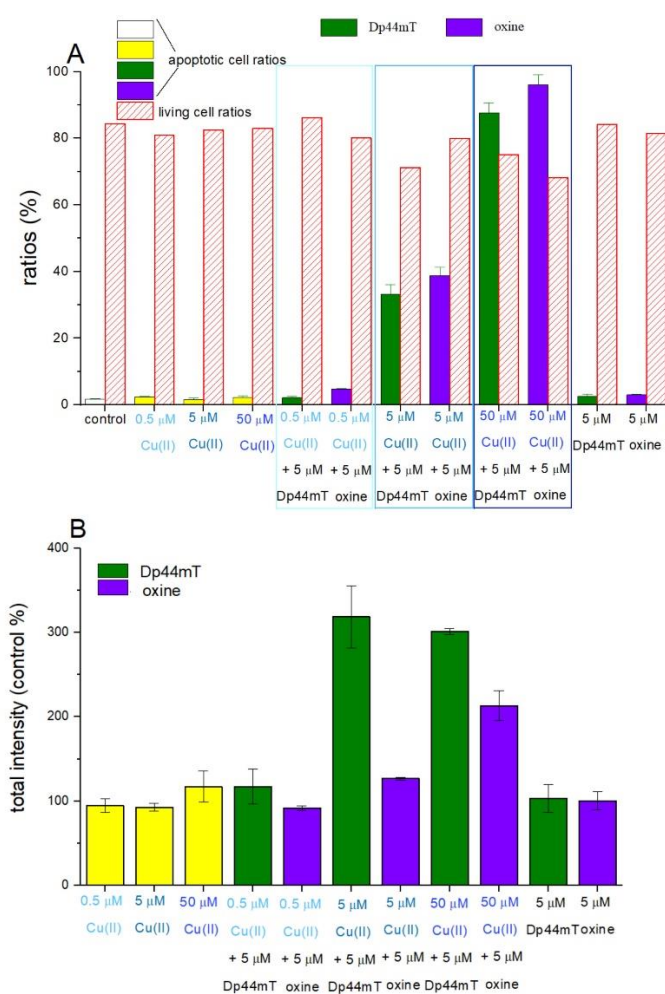
Figure 10. *Ratios of apoptotic HT-29 cells among FITC conjugated Annexin-V-positive cells (**A**) and total intensities (**B**) determined at FITC detection wavelength. Color codes: **yellow bars:** treatment solely with Cu(II) addition; **green and purple bars:** treatment with Dp44mT and oxine with or without addition of Cu(II) in increasing concentrations, respectively.*

4.3.1.7 *ROS generation observed especially for Dp44mT, neocuproine and oxine at increased Cu(II) concentration*

Generation of ROS upon addition of Cu(II) in increased concentration was followed by using H_2DCF-DA. This approach is more convenient than investigation of ROS generation with synthesized Cu(II)-Dp44mT [180, 201]. In the present study, the fluorescent signal upon oxidation of H_2DCF-DA by free radicals was observed especially for Dp44mT, neocuproine and oxine at higher Cu(II) concentration, i.e. 5 µM and 50 µM, compared to D-penicillamine (negative control), indicating a strong ROS generation (**Figure 11**).
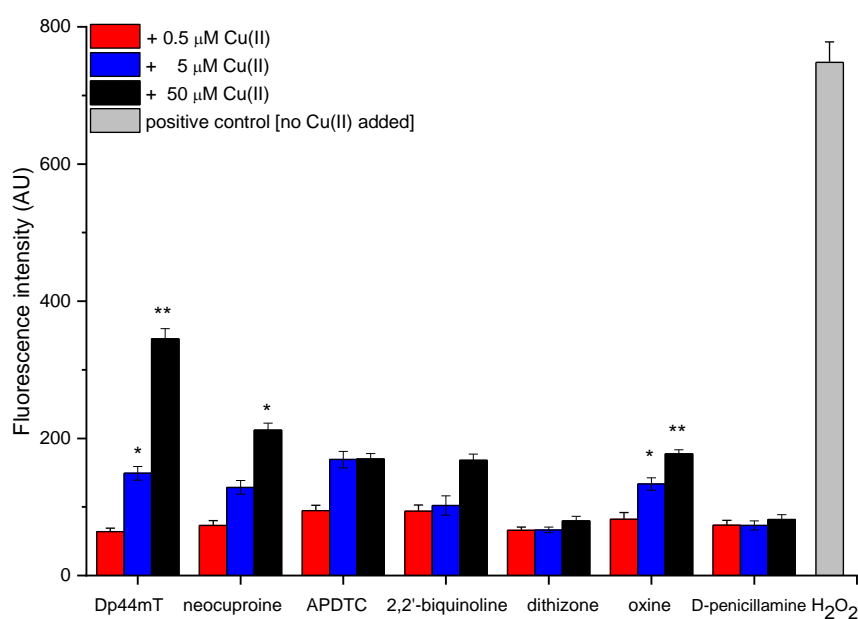
Figure 11. *Oxidative stress by treating HT-29 cells with different chelating agents and Cu(II) in increasing concentrations. D-penicillamine and hydrogen peroxide used as negative and positive controls, respectively.*
*: versus control, p < 0.05; **: versus control, p < 0.01.

4.3.1.8 *DNA intercalation was observed for the Cu(II) and neocuproine system*

The shape of the CD spectra of DNA changed by titrating it with 0.75% w/v Cu(II) (**Figure 12A**). The intensity of the peak at 280 nm decreased, the negative band changed minimally. However, there were no more changes after the addition of 8 µL of Cu(II) stock solution, presumably due to the charge balance achieved between phosphate and Cu(II). Moreover, upon addition of Cu(II), a slight batochromic shift was observed. At the same time, similar UV spectra characterized by a steady increase corresponding to

increasing amounts of added Cu(II) were recorded (results not shown here). The pattern of the CD spectra of DNA was not altered by titration with APDTC, Dp44mT and oxine. The UV absorption increased only with the increasing amounts of the added chelating agent (results not shown). This was not the case for neocuproine, in the CD spectra of which a change in the positive band was observed, likely due to intercalation. From these overlapping bands, the one of lower wavelength was more intense upon addition of neocuproine (**Figure 12B**). Simultaneously, the negative band characteristic to the helical structure did not change significantly. Therefore, it can be supposed that the DNA helical structure is not damaged. Since the UV spectra of neocuproine and DNA overlapped, there was no individual absorption band over 300 nm, thus the appearance of the induced CD spectra was not expected.

In the next step, the interaction between Cu-ligand compounds and DNA was studied. Upon the addition of Cu-ligand complexes to DNA, there was only a slight change in the CD spectra of DNA. For example, by titrating DNA with Cu(II) and Dp44mT mixed in a 1:1 molar ratio, the positive band of the DNA at 280 nm did not change, while the negative peak at 246 nm slightly decreased upon the gradual addition of Dp44mT, and the slight change in the maximum showed a bathochromic shift. The slightly induced CD in the region of the spectra corresponding to the UV absorbance peak at 424 nm was also visible (results not shown here).

When Cu was added to DNA and then titration was performed with each chelating agent (**Figures 12C-F**), change in the CD spectra of DNA indicating intercalation was observed only for the Cu(II) and neocuproine system (**Figure 12C**). In this case, the intensity increase of the positive band was significant. A strong intercalation was observed when the Cu(II):ligand molar ratio was 1:2. It can be supposed that this coordination compound has a planar structure. Next to the maximum value (at 283 nm), a shoulder appeared in the spectra at 300 nm, presumably due to an extended conjugation causing chiral disturbance. The maximum value of the negative band at 246 nm suffered a bathochromic shift of about 3 nm (**Figure 12C**). Mixed ligand Cu(II) complexes containing derivatives of salicylic acid and neocuproine also showed DNA cleavage [52].

In the remainder of the cases, the original spectra of DNA were restored at a Cu(II):ligand molar ratio of about 1 : 3 (**Figure 12. D-F**). Thus it can be concluded that DNA is not the target of the intracellular Cu accumulation. Similar experiments could not

be conducted on dithizone and 2,2'-biquinoline due to their pronounced nonpolar character and, hence, poor water solubility.
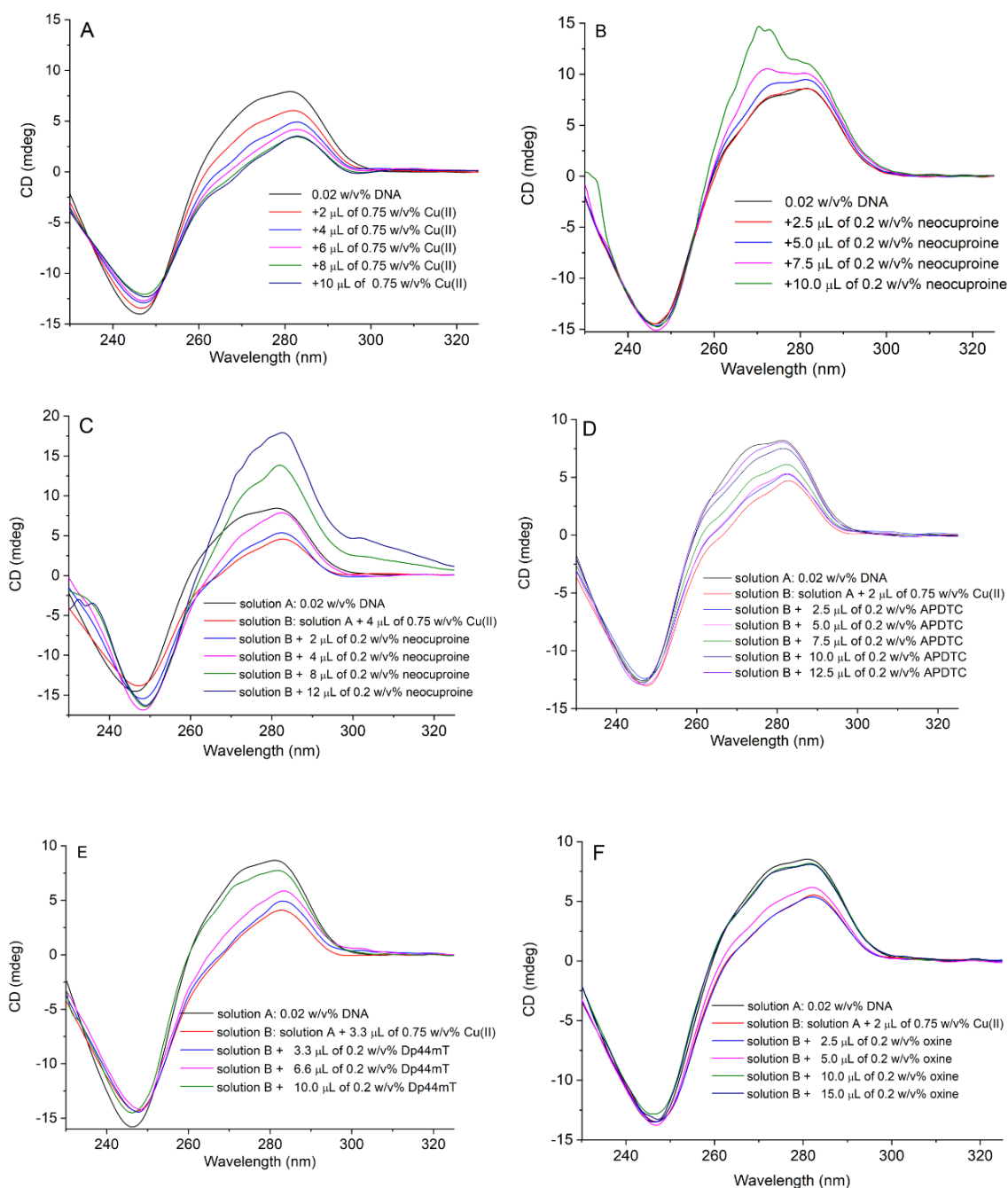

Figure 12. *Changes in the CD spectra of 0.02 w/v % DNA upon addition of Cu(II) (**A**) and neocuproine (**B**) in increasing amounts. In addition to CD spectra of 0.02% w/v DNA (solution A), solution A + 2 - 4 µL of 0.75% w/v Cu(II) (solution B) as well as solution B with increasing amounts of neocuproine (**C**), APDTC (**D**), Dp44mT (**E**) and oxine (**F**).*

4.3.2. *Metal transport capabilities*

4.3.2.1 *Conditional complex stability constants were determined for the investigated chelators related to Cu(II) and Cu(I)*

It is important to define the Cu complex species responsible for the concentration dependent fluctuations in the intracellular Cu content and Cu-dependent *in vitro* antiproliferative data. Thus, the decadic logarithm values for the conditional stability constants for the investigated ligands (L) with Cu(I)/Cu(II), according to the CuL and CuL$_2$ stoichiometry are listed in **Table 8**. The pH was continuously monitored, and it did not decrease below 5.

Neocuproine, APDTC and Dp44mT showed high stability 1:1 Cu(II) to ligand coordination compounds with Cu(II) under physiological conditions (**Table 8**). Among these three chelators, Dp44mT proved to form outstandingly stable 1:1 Cu(II)–to-ligand coordination species under the applied experimental conditions. It is worth mentioning that Dp44mT and neocuproine has proven to be the most toxic under *in vitro* conditions.

At the same time, 2,2'-biquinoline and oxine have more stable 1:2 coordination compounds (**Table 8**) showing similar cumulative stability constants. Similar UV titration could not be carried out for dithizone, due to its non-polar character (see log P values in **Table 8**). However, for dithizone, several literature data exist on thermodynamic complex stability values of Cu:ligand complexes with 1:2 stoichiometry.

The species distribution of the coordination compounds for 2 µM total Cu(II) concentration over six orders of magnitude ligand concentration can be seen in the publication of Gaál et al. [356].

The study of the stability of these ligands with Cu(I) is also important, due to the redox cycling character of Cu ions in the human body. A reduction reaction in the cell occurs when the stability constant for Cu(I) is greater than that of Cu(II) and this is relevant for such Cu(II) complexes as those with neocuproine and 2,2'-biquinoline.

Table 8. *Conditional complex stability constants and partition coefficient (P) expressed as lg β and log $P_{octanol/water}$, respectively.*

Ligand	Cu(II)		Cu(I)		Log $P_{octanol/water}$	
	lg β$_1$ ± SD	lg β$_2$ ± SD	lg β$_1$ ± SD	lg β$_2$ ± SD	Chelator	Cu(II)L
APDTC	7.16 ± 0.08	11.6 ± 0.10	6.09 ± 0.04	12.0 ± 0.08	2.08	n.a.
2,2'-biquinoline	2.73 ± 0.03	9.86 ± 0.05	5.71 ± 0.02	9.76 ± 0.06	1.95	1.15
Dp44mT	8.55 ± 0.06	11.4 ± 0.02	5.35 ± 0.01	n.a.	1.32	0.9
Neocuproine	5.16 ± 0.01	8.53 ± 0.02	n.a.	10.0 ± 0.01	1.44	-0.14
Oxine	3.59 ± 0.01	11.1 ± 0.05	5.91 ± 0.02	10.1 ± 0.01	1.78	0.16

n.a. = not available; SD = standard deviation, Log P values RSD<1%

4.3.2.2 *Cu accumulation rate could be about 2,000% compared to the control*

At the 2 μM Cu(II) and 5 μM chelating agent combined treatment, the intracellular Cu content of HT-29 cells was remarkably high (**Figure 13**) compared to the control. The D-penicillamine was used as control because it plays an important role in the elimination of extracellular Cu. While HT-29 cells were capable of Fe uptake even without co-incubation with any complexing agent [339, 343], Cu(II) in a concentration of 2 μM was not taken up by the cells [352]. Therefore, the presence of the chelating agent is crucial. The presence of Cu in large amounts is expected to be toxic for cells.

Dramatic Cu accumulation was observed especially for Dp44mT, neocuproine and APDTC (**Figure 13**). For these ligands, the Cu accumulation rate could be about 2,000% compared to the control. This finding suggests either a repeated transport followed by an intracellular Cu release, or the opening of a channel for the Cu influx. Copper accumulation was also observed for the remainder of complexing agents (i.e. 2,2'-biquinoline, dithizone and oxine), but at a lesser extent (about 500% – 1,000%). Moreover, the difference in the complexation of Cu(II) of the aforementioned chelating agents and 2,2'-biquinoline, oxine and dithizone is that the former ones form stable complexes of 1:1 Cu(II):ligand molar ratio, while the latter ones form stable coordination compounds of 1:2 Cu(II):ligand molar ratio. For oxine derivatives, it has been shown that the presence of the hydroxyl group for Cu uptake is essential [357].
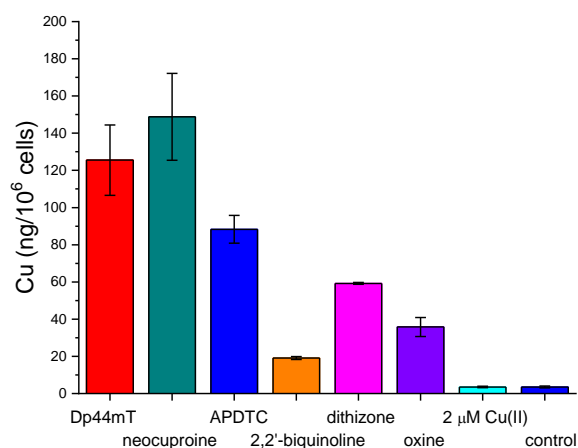
Figure 13. *Effect of 2 μM Cu(II) and 5 μM Cu chelating agent on the intracellular Cu content on HT-29 cell lines in FBS-free culture medium*

4.3.2.3 *Accumulation of Cu can be observed for all tested chelators, closely related to the amount of available external copper*

The intracellular Cu content of the HT-29 cells upon diverse treatments with Cu(II) and Cu chelating agents can be seen in **Figure 14**. If the Cu transport capacity of the investigated chelators is to be studied, free Cu(II) should also be added to the cells. Each investigated chelator increased the intracellular Cu content, causing Cu accumulation depending on the amount of the available Cu(II). By investigating the time dependence of the Cu uptake, a saturation curve was obtained for 1:1 Cu-to-chelator composition, while for oxine that forms a stable 1:2 Cu:chelator complex, the Cu uptake curve reached a peak value (**Figure 14A**). In the case of Dp44mT, cell death was observed after 8hours, thus a similar Cu uptake kinetic curve could not be registered. Therefore, for further experiments, a 4-h long treatment was applied. When the concentration of free Cu(II) to ligand was applied in 1:1 and 4:1 ratios, surprisingly, the extent of accumulation for Cu also increased nearly proportionally for chelators with propensity to form a 1:1 Cu(II):chelator complex. Also, the extent of accumulation for Cu was 159 times higher for Dp44mT compared to the control (**Figure 14B**). Copper accumulation was lower for chelators having lower water-solubility, and consequently, lower *in vitro* cytotoxicity [358]. However, in the case of 2,2'-biquinoline, characterized by the lowest ability to transport Cu, a 7.6-fold increase in Cu uptake was observed, compared to the control (**Figure 14B**). Overall, we could not establish any relationship between the extent of Cu accumulation and the stability of the chelate.
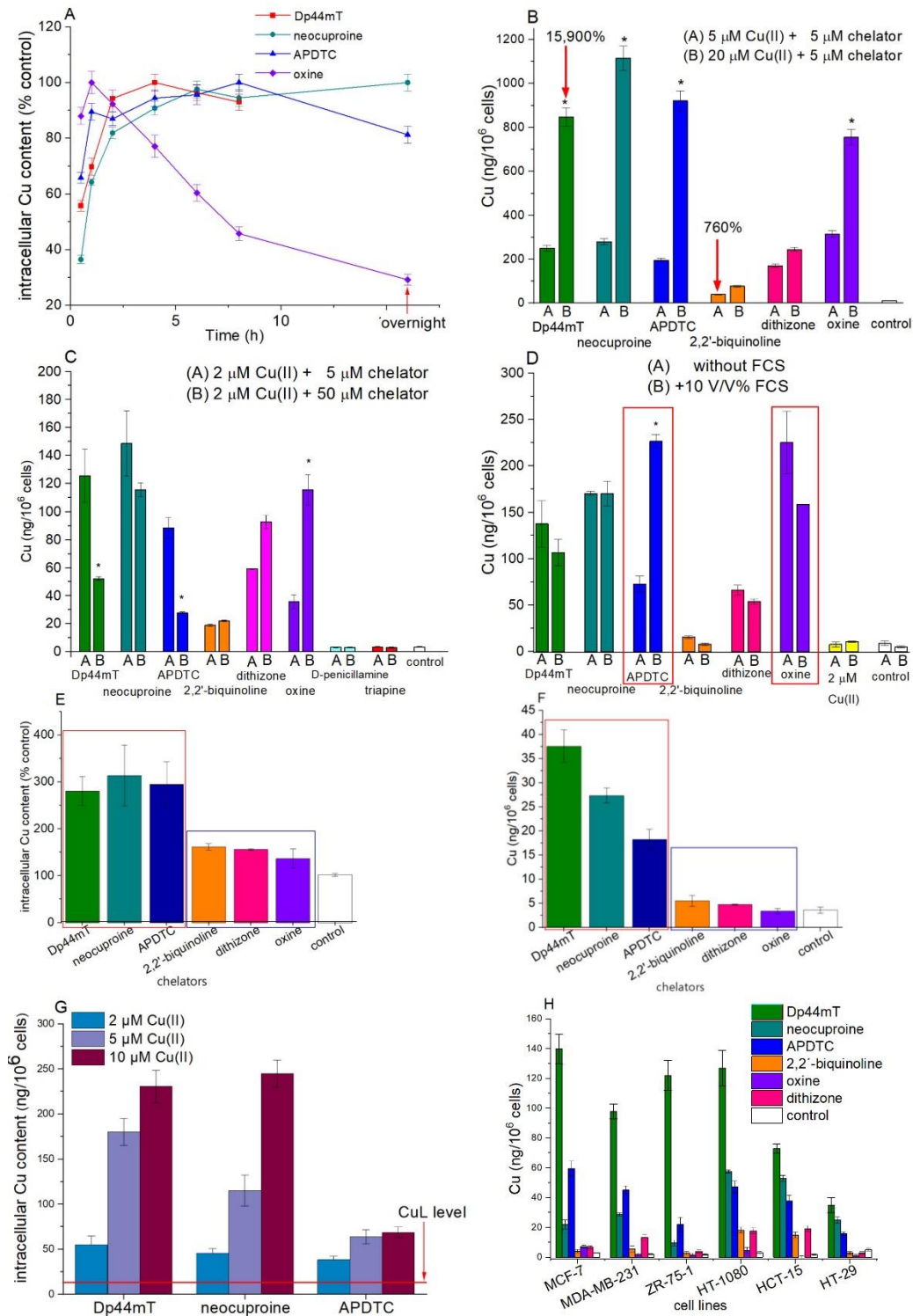
Figure 14. (***A***) *Time dependent Cu uptake;* (***B***) *effect of Cu(II) on a fixed chelator concentration and the opposite (fixed Cu(II) concentration) experiment* (***C***) *on HT-29 cells line.* (***D***) *Effect of 2 μM Cu(II) and 5 μM Cu chelating agent on the intracellular Cu content for an either FBS containing or FBS-free culture medium.* (***E***) *Effect of 0.1 μM Cu(II) and 5 μM Cu chelating agent and that of 2 μM Cu(II) and 0.1 μM Cu chelating agent* (***F***) *on the intracellular Cu content for a 24-hour-long incubation.* (***G***) *Intracellular Cu accumulation with Dp44mT, neocuproine and APDTC in a concentration of 0.1 μM incubated with 2, 5 and 10 μM externally added Cu(II).* (***H***) *Cu accumulation on different cell lines (2 μM Cu(II) and 0.1 μM chelator treatments). Experiments on HT-29 cell line (except H) in FBS-free culture medium (except D) for a four-hour-long incubation (except A and E-F).*

In the next step, the free Cu(II) concentration was fixed to 2 µM and the concentration of the chelator was increased from 5 µM to 50 µM (**Figure 14C**). Copper accumulation decreased for chelators having stable 1:1 Cu(II) complex species, due to a shift towards formation of less stable 1:2 Cu(II)-chelator compounds. Conversely, the accumulation of Cu increased with fixed Cu and increasing chelator concentrations, due to their propensity to form more stable 1:2 Cu(II) to chelator ratio.

It was considered whether the Cu content of the widely used FBS-added media has an effect on the Cu uptake characteristics of the chelators. Thus, in another experiment, the effect of 10% v/v FBS medium on the uptake rate of Cu was studied. The Cu content of 10% v/v FBS was higher (2.5–3 ng/mL) than in the case of the FBS-free treatments (0.1–0.3 ng/mL) [341]. The addition of 10% v/v FBS did not alter significantly the intracellular Cu content for Dp44mT, neocuproine and dithizone (**Figure 14D**). However, the Cu accumulation was higher when the culture medium also contained FBS in 10% v/v for APDTC, and it was lower under the same conditions for 2,2´-biquinoline and oxine (**Figure 14D**). Thus, it seems that APDTC can efficiently mobilize Cu content of the serum. However, for the chelators forming stable 1:2 metal-to-ligand species with Cu(II), the presence of FBS slightly decreased the availability of free Cu and therefore a decrease in the extent of Cu accumulation was observed. In conclusion, the FBS-supplemented media did not affect significantly the Cu uptake for the investigated chelators, except for APDTC.

Intracellular Cu is not available for chelators. However, Finney et al. [359] demonstrated that Cu can be released from its strictly regulated system during angiogenesis. Thus, extracellular Cu in low concentration can be available. Therefore, 0.1 µM Cu(II) concentration, comparable to the Cu level in FBS was applied in the present study and HT-29 cells were treated with 5 µM chelator. Due to the low Cu(II) concentration applied, incubation time was increased from 4 hours to 24 hours. In this case, the investigated chelators could be divided into the same two groups (**Figure 14E**) according to the preference of chelators to form more stable complexes (at 1:1 *vs.* 1:2 metal:chelator molar ratio). For those three chelators that were more cytotoxic *in vitro* (Dp44mT, neocuproine and APDTC) [358], the Cu content was about 300% higher compared to the control. By calculating the Cu(II) amount added to the cells and relating it to the control, it could be estimated that the whole amount of added Cu was taken up.

Simultaneously, for the chelators forming stable CuL_2 species (2,2'-biquinoline, dithizone and oxine), the Cu content was about 120-150%, compared to the control. By estimating the complex species distribution for these Cu(II) and chelator concentrations, the three toxic ligands [358] might be present in CuL form in a range of 50-90%, while the less antiproliferative chelators could be estimated as CuL_2 and not as CuL.

When the opposite experiment was performed, namely, quite highly available Cu(II) with low chelator concentration and, consequently, HT-29 cells were incubated with 2 µM Cu(II) and 0.1 µM chelator separately, a 4-10-fold Cu accumulation was observed for Dp44mT, neocuproine and APDTC (**Figure 14F**). By estimating the complex distribution at this total Cu(II) and ligand concentration, the CuL species allowing Cu transport is already present in about 5% concentration [356]. This finding indicates that low amounts of these chelating agents is capable of Cu accumulation, suggesting at the same time either a repeated transport or intracellular Cu release inside the cells, or the opening of a channel for the Cu influx. In the case of the other three chelators showing low intracellular Cu accumulation, formation of complex species did not occur because the low chelator concentration does not favor formation of a complex with CuL_2 stoichiometry.

4.3.2.4 *Cu accumulation far exceeded the base level of 0.1 µM chelator which is the maximum amount of copper that a chelator can transport*

The question arises of whether either the ligands or Cu is accumulated in the cells. In order to decide this, low ligand concentration (0.1 µM) and relatively high Cu(II) concentrations (2-10 µM) were applied (**Figure 14G**). It could be calculated that the chelator in 0.1 µM concentration would allow only 12.7 ng Cu in the cells in 2 mL cell media if Cu accumulated in the form of complex species. We demonstrated that Cu levels were far exceeding this base level in the cells. Thus, the chelator is responsible for the intracellular Cu accumulation. In the case of effective chelators (Dp44mT, neocuproine, APDTC), accumulation of Cu in the presence of low chelator concentration (0.1 µM) is observed in all tested cell lines (**Figure 14H**).

4.3.2.5 *Cu accumulation arises with similar values in the presence of a reducing agent*

The two study compounds, namely neocuprine and 2,2'-biquinoline, are known as Cu(I) chelators. We also examined whether there was a difference in the copper uptake and toxicity of the cells, when the experiments were performed with Cu(I), instead of Cu(II). We found that there was no significant difference in the intracellular Cu content,

when Cu(II) was reduced to Cu(I), using 2 µM Cu and 5 µM chelator concentrations (**Figure 15**). It is important to mention that there is no difference in IC$_{50}$ values in the presence of 2 µM Cu(II) and 20 µM ascorbic acid with increasing chelator concentration (data not shown here).
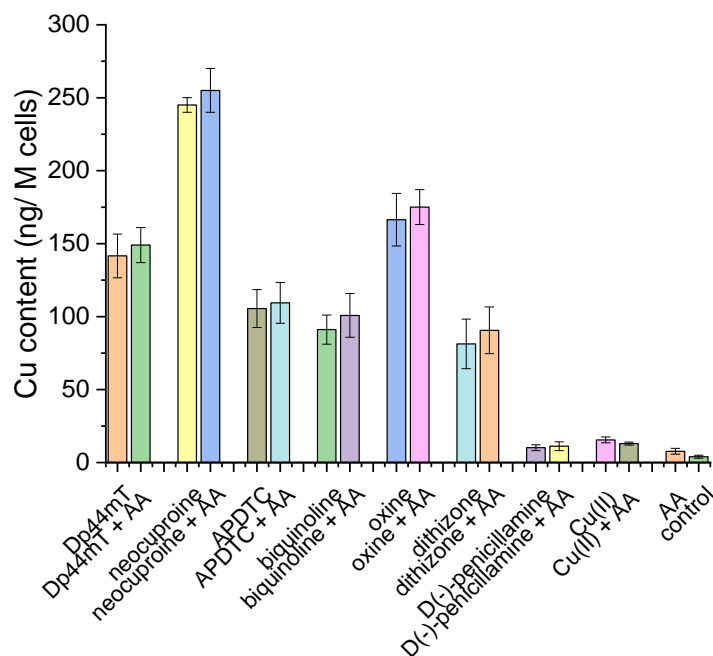
Figure 15. Treatments with 2 µM Cu(II) and 5 µM chelator with or without ascorbic acid (AA) as a reducing agent in 20 µM concentration on HT-29 cell line.

4.3.2.6 *No metal accumulation was measured for Co, Ni and Hg, but Pb, Zn and Fe accumulation was observed*

It is also important to determine whether the investigated chelators are exclusively responsible for Cu accumulation. After incubating the identical cells with other possible competing divalent transition metals (**Table 9**) in concentrations of 2 µM with 5 µM chelators, surprisingly no metal accumulation was observed at all for Co, Ni and Hg with APDTC, oxine and Dp44mT. In a previous study, we demonstrated that Dp44mT had stable Ni and Co complexes [352]. However, intracellular accumulation of Cd was observed for two chelators, due to possible binding to metallothioneins. The accumulation of Pb, Zn and Fe was also observed (**Table 9**).

Table 9. *Observed intracellular metal ion accumulation using 2 μM metal ion and 5 μM ligand incubated for 4h.*

Ligand	Extent of intracellular metal ion accumulation							
	Cd	**Co**	**Ni**	**Hg**	**Pb**	**Fe**	**Cu**	**Zn**
Dp44mT	✓✓	x	x	x	x	x	✓✓	✓
Neocuproine	x	x	x	x	x	x	✓✓	x
APDTC	✓✓	x	x	x	✓	x	✓✓	x
Oxine	x	x	x	x	x	✓✓	✓✓	x

x: < 15 ng/M cells ;

✓: 15 ng – 50 ng/M cells;

✓✓: >50 ng/M cells

4.3.2.7 *Intracellular Zn content slightly decreased for MCF-7 cells, while dramatically decreasing for MDA-MB-231. The same trends can be observed on HT-29 and HCT-116 cell line pair*

Simultaneously, with Cu uptake, another reproducible phenomenon could be observed, namely intracellular Zn depletion (**Figure 16**). In contrast, all other detectable element (e.g., Ca, K, Fe) levels were not altered substantially. Interestingly, the extent of Zn depletion was cell line dependent. Intracellular Zn content slightly decreased for MCF-7 cells, while a dramatic decrease was observed for MDA-MB-231 cells (**Figure 16**). This effect was slightly dependent on the type of the applied chelator. A similar decrease was observed for HCT-116, while Zn depletion for HT-29 corresponded to an intermediate level.
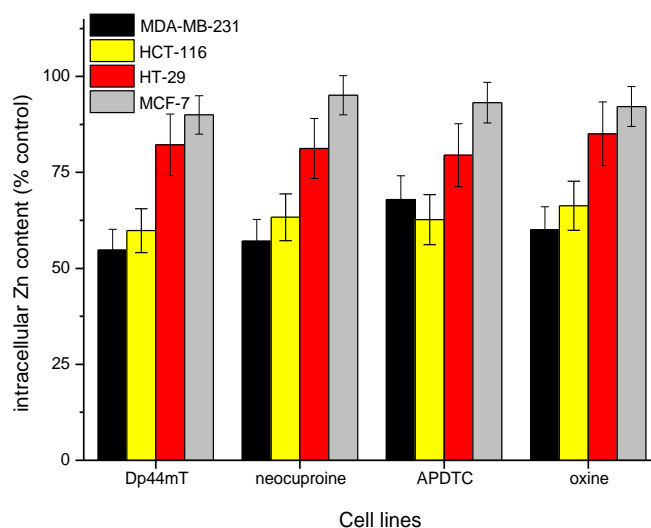
Figure 16. *Cellular Zn depletion after incubation of Dp44mT, neocuproine, APDTC and oxine 5 μM each with 2 μM external Cu(II) for 4 h.*

In the present study, IC_{50} values were registered for the four investigated cell lines by means of increasing stepwise the Cu(II) concentration for Dp44mT and oxine as representatives for 1:1 and 1:2 metal:ligand stable complexes (**Figure 17A, 17B**). Unsurprisingly, the IC_{50} values decreased with increasing external Cu(II) concentration. However, the extent of Zn depletion was inversely proportional to *in vitro* cytotoxicity. Thus, the MDA-MB-231 cells had the lowest IC_{50} values in the nM concentration range and these cells lost about half of their Zn content. It has been reported that the intracellular Zn content is distributed between different fractions; among them, one is the metallothionein associated Zn fraction [360]. It is also known that the MDA-MB-231 cells have considerable Zn pool [361] and the expression of Zn transporter ZIP10 mRNA is higher in this invasive breast cell line [362].
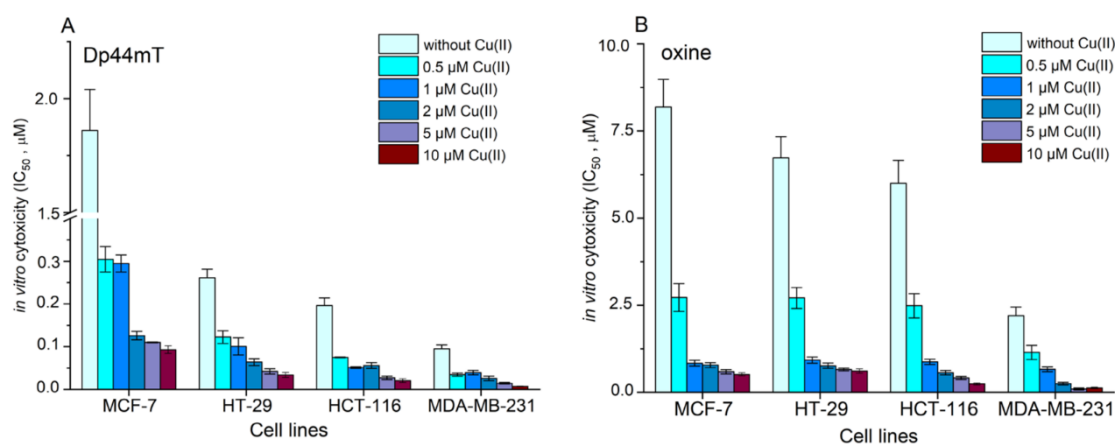
Figure 17. *In vitro cytotoxic activity expressed as IC_{50} (µM) for Dp44mT (**A**) and oxine (**B**) with Cu(II) in increasing concentration.*

4.3.2.8 *Copper depletion less pronounced in the presence of the two most cytotoxic ligands (Dp44mT and neocuproine)*

By investigating the fate of the intracellular Cu 24 hours after the Cu(II)/chelator treatment and replacement of the culture media with a Cu(II)- and chelator-free one, Cu depletion was observed for all ligands (**Figure 18**). Copper depletion was less pronounced in the presence of the two most cytotoxic ligands, i.e. Dp44mT and neocuproine. Therefore, the considerable intracellular Cu content hampers the survival of cells even after 24 hours. Usually the presence of FBS slightly decreased the intracellular Cu content. For Dp44mT and neocuproine, intracellular Cu content decreased by about 50-70% depending on the presence or absence of FBS. However, the intracellular Cu content decreased drastically for the remainder of the chelators, practically to the control level for

2,2'-biquinoline and oxine. In these cases, higher survival rates for cells were expected. In conclusion, the extent of Cu depletion was lower for chelators forming stable 1:1 Cu(II)-to-chelator complexes compared to those forming stable 1:2 Cu(II)-to-chelator ones. This is an intriguing result indicating diverse Cu accumulation mechanisms, mediated by chelators.
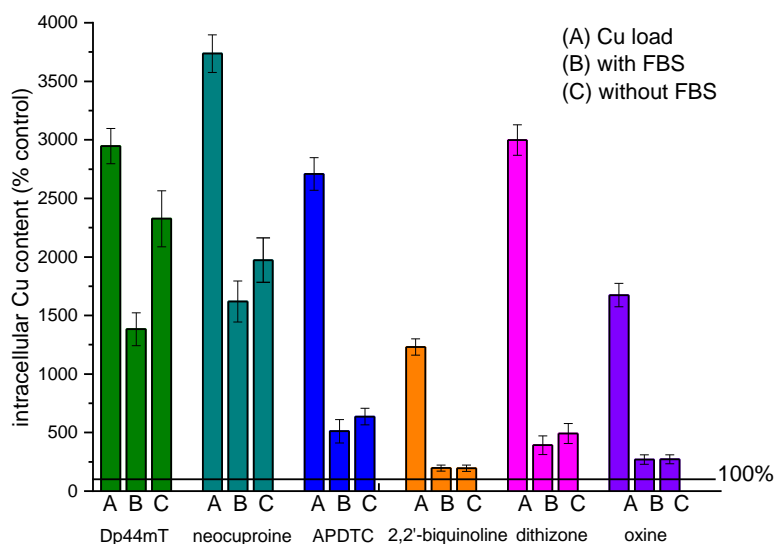
Figure 18. *Copper depletion studied on HT-29 cell lines by incubating 2 μM Cu(II) and 5 μM Cu chelating agent ("A" treatments) 24 h after a 4-h-long incubation followed by replacement of FBS free culture medium ("B" condition) or replacement of the completed media (complemented by 10% FBS, "C" condition) in every 6 h.*

4.3.2.9 *Colocalization of Cu and Zn was observed in several cases measured by Micro X-ray fluorescence spectroscopy and pixel-by-pixel by Pearson correlation setting*

Micro X-ray fluorescence spectroscopy is a well-established method for performing non-destructive elemental analysis down to the submicron scale of length for elemental localization studies. Focused beams are used for scanning samples in order to build-up the elemental maps point-by-point [343, 363]. The X-ray focusing optics can be used with submicrometric beams of high photon densities and allow X-ray fluorescence imaging. Elemental imaging was made on MCF-7 and HT-29 cell lines in the presence of Cu(II) and oxine and Dp44mT chelators separately. From these elements, images for P, S and K serve for delimitation of the cells (**Figure 19**). As it can be seen in **Figure 19**, considerable amounts of Cu could be localized, mainly in the nuclei, but in a diffuse way. Moreover, colocalization of Cu and Zn could be observed in several cases. Therefore, the extent of

colocalization was investigated pixel-by-pixel by Pearson correlation setting at 30% threshold, compared to the maximum intensity for the fluorescent intensity data. Loose correlation was observed for the MCF-7 cells, independent of the applied chelator (correlation coefficient of 0.57) (**Figure 19A**). Similarly, weak correlation was observed for HT-29 cells treated with Cu(II) and oxine (correlation coefficient of 0.47) (**Figure 19B**). Colocalization of Cu and Zn in the nucleus of HT-29 cells was observed in the case of 2 µM Cu(II) treatments with Dp44mT, proved by a strong correlation coefficient of 0.85 (**Figure 19C**).

Figure 19. *False-color XRF image showing phosphorus, sulfur, potassium copper and zinc distribution in MCF-7 cells supplemented with 2 µM Cu(II) sulfate and 5 µM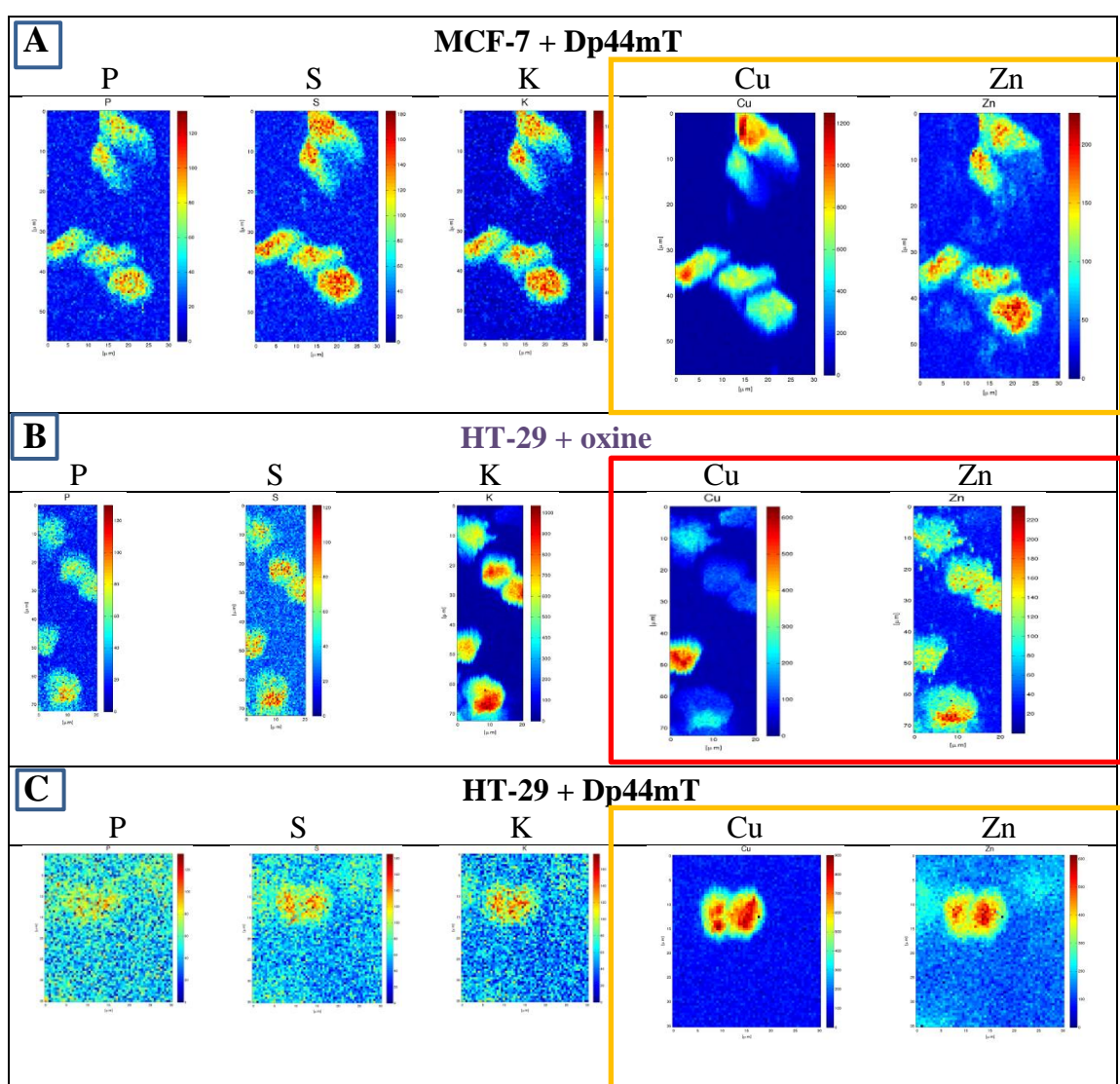 Dp44mT (**A**); HT-29 cells supplemented with 2 µM Cu(II) sulfate and 5 µM oxine (**B**); and HT-29 cells supplemented with 2 µM Cu(II) sulfate and 5 µM Dp44mT (**C**). The relative intensities increase in the order blue, green, yellow, orange and red.*

4.4. Cytotoxic effect on resistant cell lines

The investigated ligands showed wide antitumor activity and could overcome resistance to established antitumor agents (doxorubicin, vinblastine). The obtained IC_{50} values highlighted an increased or unchanged IC_{50} value on doxorubicin (MES-SA/Dx5) and vinblastine resistant (KB-V1) cell lines both without addition of Cu(II) and in the presence of 2 μM Cu(II) (**Table 10A, 10B**). The determined collateral sensitivity is not related to P-gp (data not shown here). In order to confirm that the resistance was maintained, doxorubicin and vinblastine were included as relevant controls. The chelators markedly inhibited growth of resistance cell lines and overcame resistance to other cytotoxic agents. In summary, these chelators can overcome resistance to established chemotherapeutics due to their unique mechanism of action.

Table 10. *IC_{50} values for 72 hours according to the investigated chelators without Cu(II) or in the presence of 2 μM Cu(II) on sensitive-resistant cell line pairs (MES-SA and MES-SA/Dx5 doxorubicin sensitive-resistant pair, KB-3-1 and KB-V vinblastine sensitive-resistant cell line pair). n.a.: not available.*

A	IC$_{50}$ values (PrestoBlue assay, 72 hours, RSD<20%) [μM]			
	without Cu(II)		with 2 μM Cu(II)	
Chelator / drug	MES-SA	MES-SA/Dx5	MES-SA	MES-SA/Dx5
Dp44mT	0.13	0.036	0.031	0.0085
Neocuproine	0.42	0.43	0.095	0.12
APDTC	0.89	0.57	0.34	0.31
Oxine	2.4	0.95	0.61	0.15
Cisplatin	7.3	14.8	n.a.	
Doxorubicin	0.65	18.4		

B	IC$_{50}$ values (PrestoBlue, 72 hours, RSD<20%) [μM]			
	without Cu(II)		with 2 μM Cu(II)	
Chelator	KB-3-1	KB-V1	KB-3-1	KB-V1
Dp44mT	0.039	0.018	0.27	0.019
Neocuproine	2.0	1.2	0.15	0.16
APDTC	1.9	0.83	0.65	0.48
Oxine	11	7.6	3.2	1.3
Vinblastine	0.0019	1.1	n.a.	n.a.

4.5. Liposomal formulations

4.5.1. *Neocuproine loading into a Cu(II)-containing liposome*

4.5.1.1 *Optimization of the liposomal formulation*

The main goal of this work was to characterize and test the *in vivo* anticancer activity of a novel copper-ionophore encapsulated in a temperature sensitive liposomal drug delivery system. The first step of the preparation of copper-neocuproine complex containing thermosensitive liposomes was the formation of unilamellar liposomes in $CuSO_4$ solution, which was followed by replacing the external solution with 100 mM HEPES-Na (pH 7.7-7.8) buffer using gel filtration. Next, neocuproine was added to the solution, which resulted in the formation of a Cu(I) - neocuproine complex within the liposomes [364]. In order to achieve maximal loading efficiency while maintaining the stability and temperature sensitivity of the liposomal drug delivery system, the Cu(II) concentration, the neocuproine-to-lipid ratio, and the lipid composition were optimized, and the resulting system was thoroughly characterized by DLS, IR spectroscopy, and DSC.

4.5.1.1.1 *Optimal copper(II) concentration*

Different lipid-based copper containing PEGylated liposomes (using LIPO1, **Table 4.**) were prepared by the hydration of the dry lipid film with $CuSO_4$ solutions at 10 mM, 100 mM, 300 mM concentrations at 35 mg/mL lipid concentration. After extrusion through a polycarbonate membrane with nominal 100 nm pore size, the size distributions of the liposomal systems were measured by means of DLS. Loading with 300 mM $CuSO_4$ resulted in unstable liposomal formulation (**Table 11**), while the lowest concentration of 10 mM $CuSO_4$ loading resulted in significantly lower copper concentration and decreased cytotoxicity as measured after gel filtration with TXRF and PrestoBlue assay respectively (**Table 11**). Hydration of the lipid films with 100 mM $CuSO_4$ in MQ water solution was optimal, i.e. resulted in a stable, monodisperse liposome system with an average diameter of 103±13 nm (polydispersity index (PDI) = 12%) with encapsulated Cu(II) concentration of 1.0±0.2 mM, according to TXRF measurements.

Table 11. *Optimization of the copper(II) concentration for the preparation of thermosensitive liposomal formulation. Loading a dose of 300 mM CuSO₄ resulted in unstable liposomal formulation according to DLS results, while the lowest loading concentration of 10 mM CuSO₄ resulted in significantly lower Cu concentration (as measured after gel filtration with TXRF method) and markedly decreased in vitro cytotoxic effect (one-day experiment using PrestoBlue assay, D$_{avr}$=average diameter).*

LIPO1				
	Cu (mM)	IC$_{50}$ (µM) 24-h (RSD<20%)	D$_{avr}$ ±SD (nm)	PDI (%)
10 mM CuSO$_4$	0.5 ± 0.1	25.8	94 ± 12	13
100 mM CuSO$_4$	1.0 ± 0.2	3.3	103 ± 13	12
300 mM CuSO$_4$	2.5 ± 0.3	2.8	120 ± 24	20

4.5.1.1.2 Optimal drug to phospholipid ratio

The lipophilic character of neocuproine implies its interaction with phospholipids. Therefore, the optimal drug-to-lipid concentration was investigated in the 0.2-0.8 mol neocuproine to 1 mol lipid concentration range. Neocuproine stock solution was added to the HSPC lipid-based PEGylated liposomes (HEAT RES LIPO and HEAT SENS LIPO) encapsulating 100 mM CuSO₄ solution and suspended in 100 mM HEPES-Na buffer, and the DLS measurements were performed after overnight incubation. In the final step of the preparation, the non-encapsulated drug was removed with gel filtration using sterile 0.9% NaCl solution as eluent. Except for the conditions ensuring a 0.2 neocuproine-to-lipid molar ratio, all the investigated drug concentrations resulted in unstable liposome systems, as indicated by visible precipitation, and IC$_{50}$ values did not improve further (**Table 12**), Therefore, 0.2 mol of neocuproine per 1 mol of phospholipid was selected for further investigation.

Table 12. *Optimization of drug to phospholipid ratio during the liposomal formulation process. The optimal drug-to-lipid concentration was investigated in the 0.2-0.8 mol neocuproine to 1 mol lipid concentration range. An amount of 0.2 mol of neocuproine per 1 mol of phospholipid was selected for further experiments. IC_{50} value was a good selection parameter: The difference between 0.1 mol and 0.2 mol neocuproine amount (to 1 mol phospholipid content) is still significant, but does not change substantially at higher neocuproine mol ratio. However, the polydispersity (PDI) of the liposome may increase, resulting in a more unstable liposome (D_{avr}=average diameter).*

Liposomal formulation	Neocuproine (mol) to 1 mol lipid	IC_{50} (µM) 24-h (RSD<20%)	$D_{avr} \pm$ SD (nm)	PDI (%)
HEAT SENS LIPO	0.1	5.9	92±10	10
	0.2	3.5	97±8	9
	0.4	3.2	98±14	16
	0.8	4.1	95±13	15
HEAT RES LIPO	0.1	9.1	104±13	14
	0.2	4.2	103±13	12
	0.4	3.9	102±12	14
	0.8	4.8	103±12	14

4.5.1.1.3 Optimization of the lipid composition of thermosensitive liposomes

The main lipid component of HSPC-based liposomal formulations is 1,2-distearoyl-sn-glycero-3-phosphocholine (DSPC), which has a phase transition temperature at 55°C [365, 366]. Mild hyperthermia applications require a phase transition temperature slightly above the physiological body temperature (39-40°C). Therefore, lipids with shorter fatty acid chains are added to the formulations to lower the phase transition temperature. Liposomes with different compositions were prepared by varying the weight percentage of DPPC and HSPC (**Table 4**). In our first experiments, *in vitro* IC_{50} values of the liposome samples were measured with and without a 10 min. heat treatment at 45°C. IC_{50} values were recorded after 4 hours and 24 hours in both cases. The results show that without heat treatment the liposomal formulations are devoid of any cytotoxic effect after 4 hours (**Table 13**). Lack of toxicity after 4 hours of incubation indicates that the copper-neocuproine complex was successfully encapsulated, as the free form is already highly toxic within this relatively short time frame (**Table 13**). After heating the liposomes at 45°C for 10 min, the cytotoxicity of all liposomal forms was increased. As expected, HEAT RES LIPO formulations (LIPO1) containing exclusively HSPC were relatively resistant to heat activation (IC_{50} changes from 33.1 µM to 27.5 µM), while the highest

increase in toxicity was observed with LIPO6 (contains DPPC only, IC_{50} changes from >40 µM to 5.2 µM).

Table 13. *In vitro IC_{50} values (µM) of drug loaded liposomes (LIPO1-LIPO6) with different compositions and Cu(II)-neocuproine preformed complex 1:1. PrestoBlue assay on HT-29 cells were applied to identify IC_{50} values in 4h and 24h treatment with intact and with preheated (10 minutes, 45°C) liposomes. No significant difference in IC_{50} values (µM) was observed between the different lipid compositions regardless of pretreatment and duration of the assay, but the liposome containing 100% HSPC was the least effective (n.a.=not available).*

different liposomal formulations	lipid composition		IC_{50} (µM) 4h (RSD<10%)		IC_{50} (µM) 24h (RSD<20%)	
	DPPC w/w%	HSPC w/w%	without previous heating	heating to 45 °C for 10 min. before the experiment	without previous heating	heating to 45 °C for 10 min. before the experiment
LIPO1 HEAT RES LIPO	0	100	33.1	27.5	4.3	2.6
LIPO2	50	50	>40	10.1	2.1	0.98
LIPO3 HEAT SENS LIPO	70	30	> 40	9.2	2.2	0.94
LIPO4	80	20	> 40	6.5	2.0	0.91
LIPO5	90	10	> 40	5.5	1.5	0.62
LIPO6	100	0	> 40	5.2	1.7	0.71
Cu(II)-neocuproine preformed complex 1:1	-	-	1.15	n.a.	0.6	n.a.

In order to find the ideal DPPC:HSPC w/w% for hyperthermia applications, short term (4-h) cytotoxicity assays were repeated with heat treatment of the samples at increasing temperatures (**Table 14**). LIPO1 and LIPO2 (containing no or 50% DPPC, respectively) were not cytotoxic even after a heat treatment at 39°C, whereas LIPO4, LIPO5 and LIPO6 (containing 80%, 90% and 100% DPPC, respectively) proved to be cytotoxic by preheating the samples at 38°C. In conclusion, LIPO3 (70 w/w% DPPC: 30 w/w% HSPC, denoted as HEAT SENS LIPO) was chosen as the heat sensitive liposome, because this formulation showed the desired drug-release behavior, i.e. it has no cytotoxicity at 37°C and 38°C, but starts to release the drug at 39°C.

Table 14. *Phase transition temperature optimization of the liposomal formulation using the different w/w% DPPC and HSPC mixtures (Table 1) for using hyperthermic treatment. In vitro data using PrestoBlue assay on HT-29 cell line in a four-hour experiment. The optimal lipid content of the PEGylated liposomal formulation contains 70w/w% DPPC and 30 w/w% HSPC (HEAT SENS LIPO), because it has no noticeable cytotoxic effect at 38°C, but at 39°C the liposome release the entrapped drug. Thus, a significant release of the drug can be achieved as a result of hyperthermic treatment.*

Liposome formulation	IC_{50} (µM) (RSD<20%)		
	37 °C	38 °C	39 °C
LIPO1 HEAT RES LIPO	>40	>40	~40
LIPO2	>40	>40	~40
LIPO3 HEAT SENS LIPO	>40	>40	36.8
LIPO4	>40	30.9	15.5
LIPO5	>40	9.9	5.2
LIPO6	~40	5.9	4.6

4.5.1.1.4 Characterization of the optimized liposomal formulations

The mean hydrodynamic diameter was 103 nm ±13 nm (PDI: 12 %) and 97 nm ± 8 nm (PDI: 9 %) for HEAT RES LIPO and HEAT SENS LIPO, respectively. The mean hydrodynamic diameter of HEAT SENS LIPO was further measured by means of MRPS (**Figure 20A**). In this case the mean diameter was 72 ± 0.25 and SD was 32.5 ±0.73 according to the best fit. (**Figure 20A**). The difference can be attributed to the thickness of hydration layer of the liposomes, because DLS determined the hydrodynamic diameter, whereas MRPS determined the diameter corresponding to the excluded volume [367]. With the assistance of MRPS, we could also determine the particle concentration of $4.22 \times 10^{10} \pm 0.8\%$ particle/ml.

The copper/neocuproine content of HEAT SENS LIPO was determined by TXRF and UV-Vis spectroscopy, respectively. The copper concentration of the HEAT SENS LIPO and HEAT RES LIPO was found to be similar (1 mM ± 0.05 mM). The neocuproine was 1 mM ± 0.1 mM, with an encapsulation efficacy of 64% for HEAT SENS LIPO, thus there is an excess of copper in the liposomes, since the complex ratio is 1:2 for Cu:neocuproine. In the case of HEAT RES LIPO, the neucoproine concentration was slightly lower 0.9 mM ± 0.1 mM, with an encapsulation efficacy of 55%.

IR measurements with the copper-neocuproine complex, HEAT SENS LIPO before the addition of neocuproine, and after the final gel purification clearly indicate the presence of the complex in the final product (**Figure 20B**). Detailed spectral analysis of the C=O stretching vibrational bands at 1750-1720 cm^{-1} [368, 369] in the liposome sample before the addition of neocuproine indicates that copper ions reduce the number of H-bonds around the carbonyl groups of the phospholipids, presumably because of the binding of the metal ions to the hydrophobic – polar interface of the lipid bilayer (**Figure 20C**). After the addition of neocuproine, the number of H-bonds around the carbonyl groups significantly increased (**Figure 20D**), indicating the formation of the copper-neocuproine complex.

The DSC measurements were carried out in order to reveal the thermotropic behavior of the optimized liposomal system (HEAT SENS LIPO). In parallel, investigation of the drug release was performed in the temperature range of 37-45°C using gel filtration to separate liposomes from released copper-neocuproine complex and UV-Vis spectroscopy to quantify the drug release (**Figure 20E**). Based on the DSC measurements, the HEAT SENS LIPO sample has two phase transitions; one at 38.55 °C (onset) with 0.01 J/g enthalpy change, and another at 41.46 °C (onset) with 0.23 J/g enthalpy change (**Figure 20E**). The inflection point of the drug release curve coincides with the first phase transition, which indicates that the release of the drug is not connected to the main chain-melting transition of the lipid bilayer.
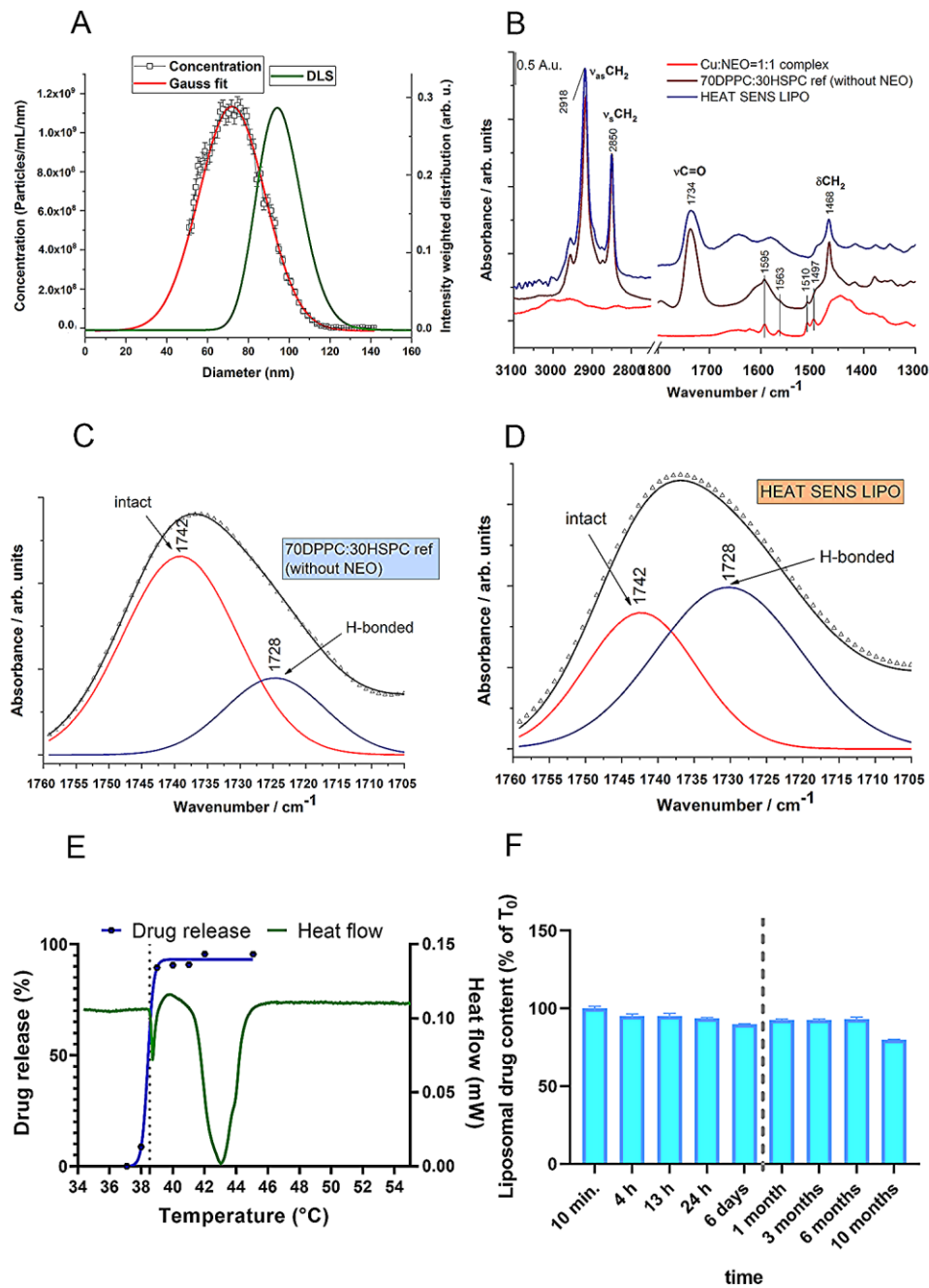
Figure 20. *Characterization of the liposomal formulation HEAT SENS LIPO. (**A**) Size distributions obtained by DLS and MRPS. This figure denotes the evolution of particles with diameter sizes (nm) in the function of intensity (DLS) or concentration (MRPS) in the range of 0–160 nm. (**B**) IR spectra of HEAT SENS LIPO with and without the addition of neocuproine chelator compared to Cu(II)-neocuproine preformed complex IR spectra. (**C, D**) Part of IR spectra of Cu LIPO without adding neocuproine chelator (**C**) and HEAT SENS LIPO (**D**) samples. (**E**) Comparison between the heat flow (mW) measured by means of the DSC method for HEAT SENS LIPO and its drug release profile. Tests were carried out with normal 0.9% NaCl infusion. The pre-phase transition onset temperature for HEAT SENS LIPO release was relatively narrow to the expected one, the measured value was 38.55 °C. (**F**) Stability of the liposomal formulation using gel filtration. After 10 months, 80% of the active ingredient is still present in the liposome.*

4.5.1.2 *Stability of the prepared liposomes*

The HEAT SENS LIPO sample was subjected to a stability test (**Figure 20F**). The sample was stored at 4 °C, and the ratio of free to liposome bound copper-neocuproine complex was determined at pre-defined time points using gel-filtration and UV-Vis spectroscopy. It can be seen that the liposome has proven to be completely stable for six months. After 10 months, 80% of the active ingredients is still present in the liposome. Then we compared the short time stability of the liposomes at 37°C, but no difference was found, the drug was not released in 4 hours (liposomal drug content of 98%). Furthermore, the liposomes were then mixed with cell completed medium (DMEM + 10% FBS) modeling cell culture conditions, and SEC method combined with UV/Vis spectrophotometry was used to check the integrity of the liposomes. In this case we obtained the same results, i.e. the active ingredient was not released by the liposomes in a 4 hours experiment incubating the liposomes in FBS containing media (SEC chromatograms not shown).

4.5.1.3 *Cytotoxic effect of the liposomes on colorectal cancer cells*

PrestoBlue assay was used to evaluate the cytotoxic effect of neocuproine chelator, neocuproine-copper complexes, and their liposomal forms (HEAT RES LIPO and HEAT SENS LIPO) on C-26 and HT-29 cells (**Table 15**). Toxicity of the samples was assessed at three different time points (4-h, 24-h and 72-h) to determine the anticancer potential of the liposomal formulations, the active drug neocuproine and the different mixtures of neocuproine-copper(II). Liposomal formulations were tested with and without pre-heating to 42°C to model the added benefit of tumor hyperthermia treatments In line with the stability of the liposomes, both liposomal formulations showed minimal toxicity without pre-heating. In contrast, after heating the liposomes to 42°C, HEAT SENS LIPO was twice as effective as HEAT RES LIPO in the four-hour-long assay. In contrast, the toxicity of the heat-sensitive and heat-resistant formulations was identical after 24-h and 72-h incubation with cells, irrespective of the hyperthermia pretreatments. After 24-hour-long treatments, both of the liposomal formulations were more toxic than neocuproine, but less toxic than neocuproine-copper complexes. The toxicity of the combined copper and neocuproine treatment is due to the excess amount of the metal (2 μM Cu(II)) added to neucoproine. This is in line with earlier findings showing a considerable increase in the toxicity of intracellular copper ionophores in the presence of free copper ions [370].

We found that the copper (II)-neocuproine complex with 1:1 or 1:2 stoichiometric ratio exhibits similar activity to the liposomal forms, with the exception that 1: 2 preformed complex proved to be less effective in the 24-hour-long experiment. Of note, the observation that a chelator cannot be in excess if a rapid effect is required is in line with earlier results [356]. Excess of Cu(II) in both the short and the long-term experiments resulted in lower IC_{50} values, indicating greater antitumor effects. In the longer 72-h experiment, each investigated treatment showed comparable IC_{50} values against HT-29 and C-26 cells.

Table 15. *The 4-h, 24-h and 72-h IC_{50} values (RSD<20%) on HT-29 and C-26 cells of the prepared liposomes (HEAT SENS LIPO and HEAT RES LIPO) at different temperatures compared to neocuproine chelator, to copper-neocuproine preformed complexes (various ratios: 1:1 and 1:2) and to neocuproine chelator in the presence of 2 µM copper(II). NEO=neocuproine.*

Treatment Parameters		IC50 values (µM) on HT-29 and C-26 cell lines (RSD<20%)							
		HEAT SENS LIPO		HEAT RES LIPO		compared to other treatments			
Cell line	Time	Without pre-heating 37°C	Heating to 42°C	Without pre-heating 37°C	Heating to 42°C	Neocuproine	2 µM Cu(II) + neocuproine	Cu(II)-NEO preformed complex 1:1	Cu(II)-NEO preformed complex 1:2
HT-29	4 h	>40	19.4	>40	>40	>500	1.6	1.15	n.a.
	24 h	5	2.8	9.8	10.1	~300	0.16	0.6	>25
	72 h	0.2	0.2	0.2	0.3	0.083	0.025	0.05	0.053
C-26	4 h	>40	18.6	>40	>40	>500	1.8	1.05	n.a.
	24 h	3.6	3	4.2	4.1	~500	0.21	0.49	>25
	72 h	0.2	0.15	0.3	0.2	0.15	0.037	0.13	0.12

4.5.1.4 *Cu accumulation by liposomal formulation in vitro*

In order to investigate the molecular background of *in vitro* toxicity, copper accumulation induced by the chelator neocuproine or its liposomal formulations was followed by means of TXRF. Treatment with increasing volumes of liposomes (HEAT RES LIPO and HEAT SENS LIPO) resulted in increasing copper content in C-26 cells (**Figure 21**). Clearly, the copper uptake of HEAT SENS LIPO in this time range (4-h) was much higher, as compared to the copper uptake mediated by HEAT RES LIPO, in agreement with the IC_{50} values measured at 24 hours. To understand the phenomena, a

series of different stability tests were performed by modeling cell culture conditions (see Section 3.1.5.). However, we have found that both liposomes are stable in the presence of a completed medium. This indicates that HEAT SENS LIPO transmits copper more efficiently than the HEAT RES LIPO without using mild hyperthermia. Of note, the only difference between HEAT SENS LIPO and HEAT RES LIPO is the higher DPPC content of HEAT SENS LIPO. It should be noted that the highest copper uptake could be observed, when treating the cells with neocuproine itself in the presence of free copper [356].
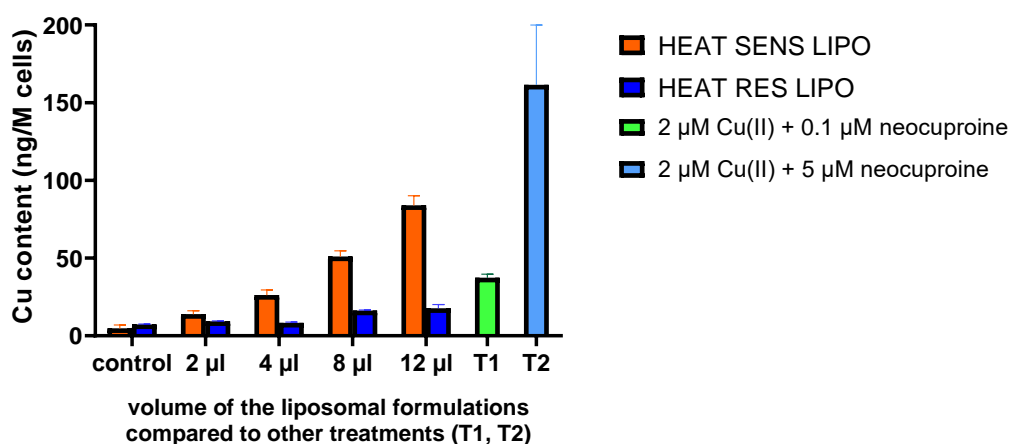

Figure 21. *The Cu content (determined by means of TXRF) of C-26 cell line treated with various volumes of the liposomal formulations (HEAT SENS LIPO and HEAT RES LIPO) compared with the treatment of 0.1 μM (T1) and 5 μM neocuproine (T2) in the presence of 2 μM Cu(II).*

4.5.1.5 *In vivo effects of the liposomal formulations*

In vivo antitumor activity of the liposomal formulations (HEAT SENS LIPO and HEAT RES LIPO pegylated liposomes subjected to the appropriate formulation for mild and nonhyperthermic treatments, respectively) was tested in BALB/c mice bearing C-26 tumors. In agreement with the literature data [179], we have found that 1 mg/kg neocuproine-copper(II) complex is well tolerated, but has no *in vivo* antitumor effect. Administration of the liposomal formulations was designed to achieve the maximum dose of neocuproine-copper(II) complex (2.8 mg/kg), which was still tolerable for the studied animals. In the first experiment, the efficacy of HEAT SENS LIPO and HEAT RES LIPO was compared without applying heat treatments. Treatments with the liposomes showed a profound antitumor effect, reaching significance (p=0.046) in the HEAT SENS LIPO group (**Figure 22A**). The antitumor effect was detectable in the weight of the dried tumor

in both of the treated groups (**Figure 22C**), in terms of 65% and 50% tumor mass reduction in the HEAT SENS LIPO and HEAT RES LIPO groups, respectively. In the second experiment, our aim was to investigate whether using a smaller dose of thermosensitive liposome formulation combined with local heating of the tumor could show appropriate antitumor effects. Hence, the thermosensitive liposome formulation (HEAT SENS LIPO) was administered in parallel with mild heat treatment in two doses (2.8 mg/kg and 1.4 mg/kg) and compared to the group receiving higher dose treatment without mild heating (**Figure 22B**). The mild hyperthermia by itself does not show any antitumor effect (data not shown here). All three treated groups showed reduced tumor growth as compared to the control group (**Figure 22B**). Surprisingly, the strongest antitumor effect was observed as a result of treatment with 1.4 mg/kg liposome combined with mild heat treatment (p=0.0145) or without heat treatment (p=0.0376) (HEAT SENS LIPO). At the beginning of the treatment, the "HEAT SENS LIPO + mild hyperthermia" group appeared to be less responsive to the treatment, but over time the effect levelled off (p=0.0382). Referring to time-dependent *in vitro* experiments (**Table 15**), it should be noted that IC_{50} values of the cells treated with heated and non-heated liposomes became similar over time (72 hours). Dried tumor masses (**Figure 22E**) in all groups were significantly lower (p values in the range of 0.0132-0.0153) than in the control group. Curves for each individual animal's tumor volume is presented in **Figure 23.** No decrease in body weight was observed during the experiments in mice receiving any of the liposomal treatments as above (**Figure 22D, 22F**).
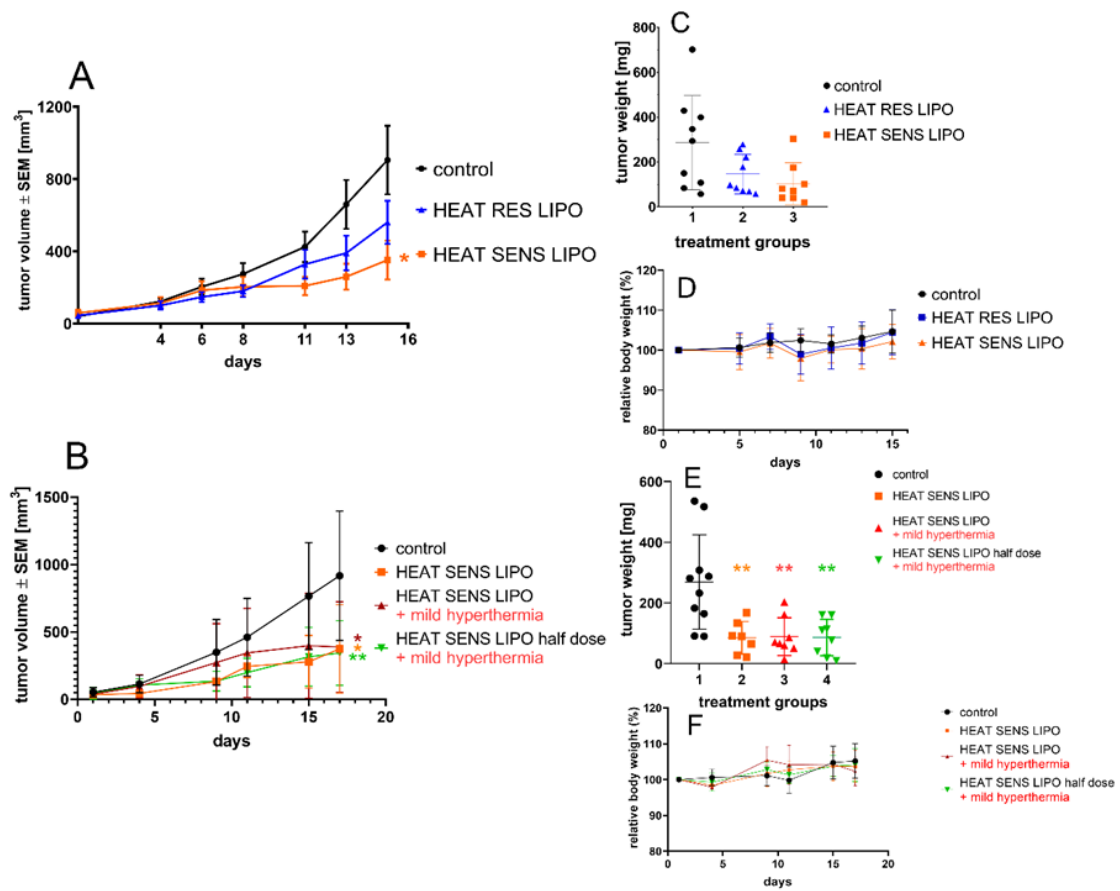
Figure 22. *Antitumor efficacy of HEAT RES LIPO and HEAT SENS LIPO on C-26 tumors in BALB/c animal model. (**A**) Average tumor volume and (**C**) dry tumor weight of vehicle, 2.8 mg/kg HEAT SENS LIPO and 2.5 mg/kg HEAT RES LIPO treated mice. Treatment groups received 10 μL liposome/1 g body weight or physiological saline solution intravenously (i.v.) on the 1st and 8th day of the treatment. (**B**) Average tumor volume and (**E**) dry tumor weight of vehicle, 2.8 mg/kg HEAT SENS LIPO, 2.8 mg/kg HEAT SENS LIPO + mild hyperthermia, 1.4 mg/kg HEAT SENS LIPO + mild hyperthermia mice. The treatments were implemented on the 1st and 10th day of the in vivo experiment. The local mild heat treatment was given immediately following drug injection (41-42°C, 20 min). The data (**A and B**) presented as average ± standard error of the mean (SEM); * p < 0.05, **p < 0.02. and (**D and F**) Relative body weight data of animals during experiments.*
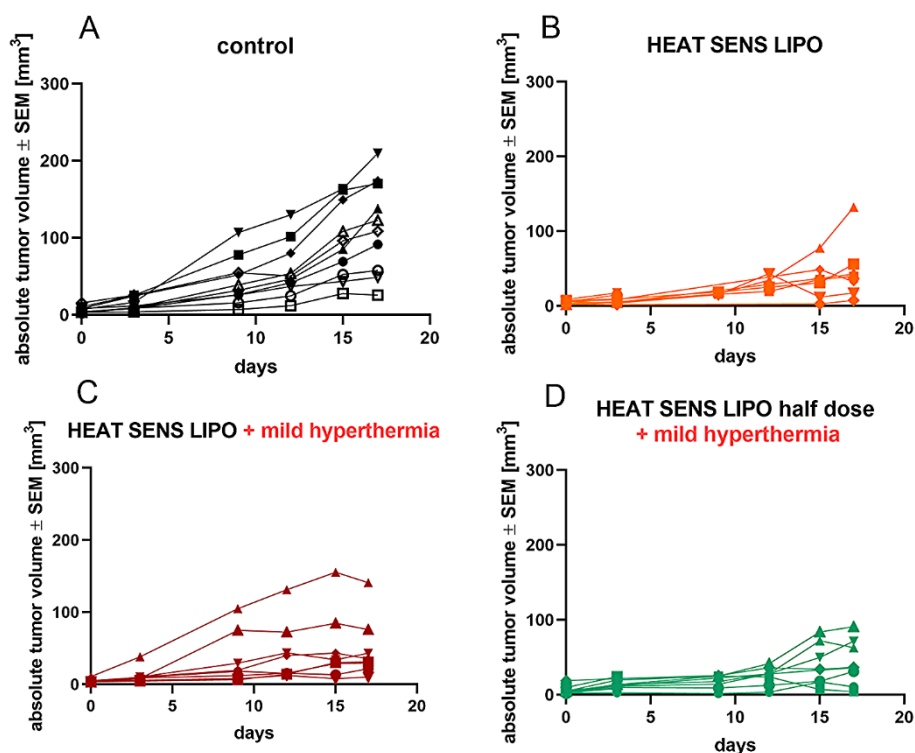
104

*Figure 23. Growth curves of individual tumors (from Figure 22B) in control (**A**), HEAT SENS LIPO (**B**), HEAT SENS LIPO + mild hyperthermia (**C**), half dose of HEAT SENS LIPO + mild hyperthermia treated mice (**D**).*

4.5.1.6   PET/CT results

The *in vivo* distribution of [^{64}Cu]-neocuproine liposomes is evaluated in a U251-HRE mouse xenograft model (n=3). Representative PET/CT images are shown in **Figure 24**. the tumor activity concentration to whole body activity concentration ratio was 0.61 and 1.16 for the control animals for 1-h and 4-h post injection (p.i.), respectively, whereas it was 1.3 for the animal that received hyperthermic treatment for 3-h p.i. High activity concentrations were observed in the livers and intestines of the three mice. High spleen uptake was observed in a control animal for 4-h post injection. This organ uptake pattern is similar to other liposomal drug delivery systems [371, 372]. Although the biodistribution of liposomes is varying and greatly influenced by their sizes, lipid composition and surface modification [373, 374], it is likely that the high intestinal activity observed in these animals is caused by the hepatic clearance of free ^{64}Cu ions [372, 375, 376] or ^{64}Cu-neocuproine released from the liposomes. The tumor-to-muscle ratios (representing the target-to-background ratio) were 4.47 and 9.70 for the control animals (p.i. 1-h and p.i. 4-h respectively) and 4.64 for the hyperthermic treated animal indicating good target visibility (a ratio of at least 1.5 is necessary for the identification

of a lesion [377]). The imaging results suggest efficient tumor uptake of the drug; however, further studies are required to accurately determine the amount of released free or neocuproine-bound copper in the circulation and how it can be affected by means of hyperthermic treatment.
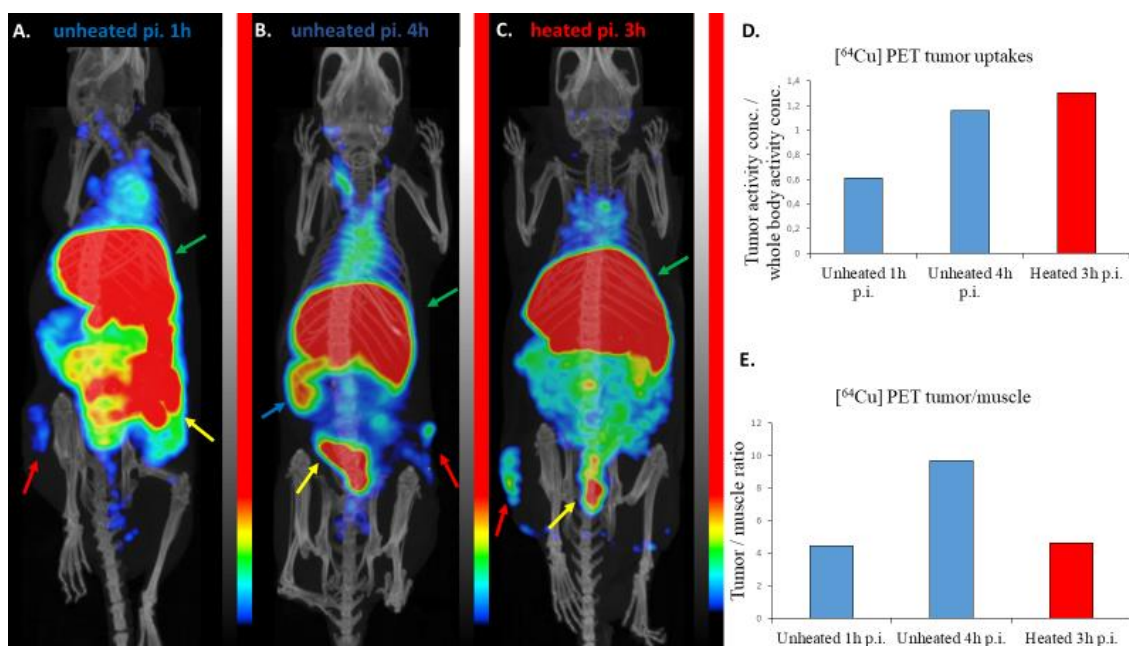

Figure 24. *PET/CT imaging results. Maximum intensity projections of PET/CT images showing the biodistribution of [^{64}Cu]Cu-neocuproine liposomes (HEAT SENS LIPO) in control, unheated (**A** and **B**) and mild hyperthermia treated (**C**) mice. The liver (green arrows) and intestine (yellow arrows) of all animals show high activities. The tumor (red arrows) also shows increased uptake and is easily distinguishable from its surroundings on all images. The spleen (blue arrow) of a control animal shows high uptake 4-h p.i. (**B**). There is a marked difference between the tumor activity concentrations (normalized to whole body concentrations) between the 1-h p.i. and 4-h p.i. control animals (**D**). Graph **E** shows the tumor-to-muscle uptake values.*

4.5.2. Q4 chelator loading into a Cu(II)-containing liposome

The drug (Q4) is an MDR-selective compound [378], showing an increased cytotoxic effect on the MES-SA/Dx5 and ME-SA/B1 cell line. As shown in **Figure 24A**, in the presence of different transition metal ions, Fe(II), Fe(III), Cu(II), Mn(II), or Zn(II), the chelator shows mostly decreased IC$_{50}$ values with an increasing selectivity ratio (SR). Based on this *in vitro* cytotoxic effect, each complex may be suitable for liposomal formulation. Based on the preparation protocol of neocuproine-containing liposome described above, the drug was loaded into a Cu(II)-containing liposome by the same

procedure, but with one difference: using an aqueous solution of Q4 instead of an aqueous solution of the hydrochloric acid salt of neocuproine. Loading resulted in monodisperse CuQ4 LIPO formulation (**Figure 24C**). The average hydrodynamic diameter was observed to be 100 nm ± 9 nm (PDI: 13 %), determined by means of DLS. The mean diameter, measured by the MRPS method, was found to be 79 nm ± 11 nm. By this method, we could also obtain the particle concentration, i.e. $1.152 \times 10^{13} \pm 0.6\%$ particle/ml (recalculated with the dilution). The difference between the two measurements can be explained as described earlier. *In vitro* results were obtained using the doxorubicin sensitive-resistant cell line pairs: MES-SA and MES-SA/B1; P388 and P388/ADR, respectively. The liposomal formulation showed a significant *in vitro* cytotoxic effect as early as 4-h (**Figure 24A, 24B**). In the 72-h experiment, the IC_{50} value was comparable with the efficacy of Q4 chelator.

Two animal experiments were performed. The masses of the animals were in the appropriate range, the formulation could be used *in vivo* at a dose of 10 μL per 10 g animals. First, the antitumor activity of the CuQ4 liposome was examined in BALB/c mice harboring tumors induced by C-26 cells. With regard to this animal experiment, at 17 days including 2 treatments, the CuQ4 LIPO reduced the tumor volume in tumorized mice (**Figure 24D, 24E**). The transplanted P388 leukemia model did not respond satisfactorily to treatment. When the chemotherapeutic activity of the CuQ4 LIPO was evaluated against P388 and P388/ADR tumor-bearing mice, borderline responses were observed with increased survival of only 2 days beyond controls in the case of P388 and 1 day in the case of P388/ADR (data not shown here).
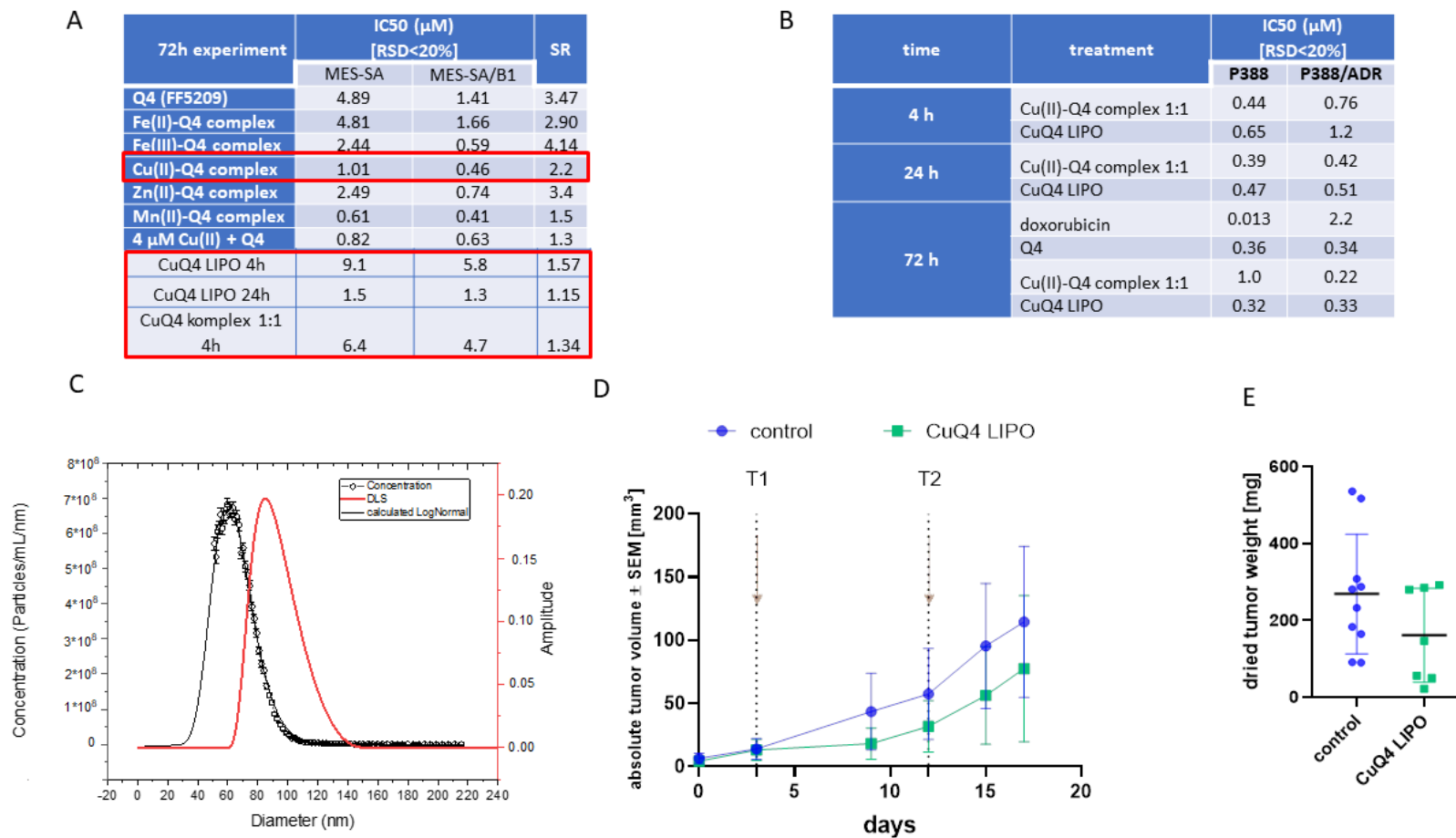
Figure 25. *Results related to the formulation of Q4 in the presence of Cu(II). (**A**) 72-h IC$_{50}$ values using PrestoBlue assay with preformed complexes with different transition metal ions. (**B**) In vitro cytotoxic effect of preformed Cu(II)-Q4 complex and CuQ4 LIPO in different time points (4-h, 24-h, 72-h) on doxorubicin sensitive-resistant P388 and P388/ADR cell line. (**C**) DLS and MRPS results related to the liposomal formulation. (**D**) In vivo antitumor effect of CuQ4 LIPO on BALB/C C-26 tumor bearing mice. (**E**) Tumor weights of animal experiment D.*

5. Discussion

The first and only success story of metal-based chemotherapy, the discovery of cisplatin, allowed the treatment of advanced solid tumors, and has been used for the treatment of various types of human cancer, especially in testicular tumors. Historically, the research in this field has focused on platinum and DNA targeting. However, anticancer drug research may be expanded to include alternative metal compounds with different modes of action, resulting in markedly different cytotoxic response profiles. Copper complexes with selected ligands are being extensively studied as agents for the treatment of cancer [379]. Probably the most important and most studied compounds are the thiosemicarbazones.

Our first test compound was a thiosemicarbazone compound, Dp44mT, a member of a series synthesized as an antitumor iron chelator. The protonation constants for Dp44mT in the current study are slightly lower than those previously reported [180]. However, we agree that the neutral ligand is the sole species at physiological pH. The only available stability constants for Mn(II), Cu(II), Ni(II) and Zn(II) with Dp44mT at pH 7.4 have recently been reported [380]. The lg β values for [Cu(Dp44mT)$_2$], [Ni(Dp44mT)$_2$], [Zn(Dp44mT)$_2$] and [Mn(Dp44mT)$_2$] were 12.49, 11.21, 10.20 and 7.76, respectively. According to our results, there is no stable ML$_2$ complex of this chelator with Cu(II), but only ML or M$_2$L complexes. M$_2$L can be formed only if the metal concentration is much higher than μM range. Except for Zn, the stability of Fe(II) with the Dp44mT complex was lower than with the other investigated metal ions. Moreover, the stability constant of ML$_2$ for Zn is approximately five and six orders of magnitude lower than the values determined for [Fe(II)(Dp44mT)$_2$] and [Ni(Dp44mT)$_2$], respectively. We compared the stability constants determined in the above study with the literature data for Fe, Cu and Zn triapine complexes. The triapine (3-aminopyridine-2-carbaldehyde thiosemicarbazone) structure is somewhat similar to that of Dp44mT, and the authors found the same order of stability for the ligand (Zn<Fe<Cu) [381]. According to our calculations, the maximum concentration of the free complex forming ligand cannot exceed 10% of the input concentration at the equilibrium, the stability of the [Fe(Dp44mT)$_2$] and [CuDp44mT] can be compared by multiplying the lg β_2 of the 1-to-2 M:L complex for Fe(II) by the free ligand concentration, while the lg β_1 for Cu(II) is left unchanged. In this way, the decadic logarithm of the conditional stability constant for Fe(II), lg β_1', is equal to lg (β_2 × [Dp44mT]) = lg β_2 + lg [Dp44mT]. The maximum value

that can be calculated for this mathematical expression is $10.25 - 6 = 4.25$, which is approximately three orders of magnitude lower than the lg β_1 value for Cu.

According to our calculations on complex formation constants (**Table 5** and Ref. 352), Fe(II) can be bound to Dp44mT in a reductive medium in the presence of Cu(II) only at unrealistically high Fe-to-Cu ratios [352]. The mean elemental concentration of the culture medium [340, 353] proved that Fe is not present in excessively large amounts when compared to Cu, implying that the extracellular metal ion ratios do not allow complex formation for Fe with Dp44mT at physiological pH. The Fe-to-Cu ratios can be established at which Dp44mT functions as an iron chelator, because cells can take up high amounts of Fe [339], if there is not any available extra/intracellular Cu at physiological pH.

When easily available extracellular Cu(II) was introduced into the system, Dp44mT forms a complex with Cu, due to the high stability of [Cu(II)Dp44mT], and Cu was transported by Dp44mT into the cells, where it accumulated **(Figure 4B)**. In the case of a low concentration Cu(II), e.g., 2 µM, an extremely high intracellular Cu level was observed. According to our calculations, the added Cu(II) was mostly taken up. When the concentration of the Cu(II) in the treatment was increased, the Cu uptake was higher and the cellular death was accelerated (**Figure 5**). Although the applied Dp44mT concentration (0.0625 µM) was far lower than IC_{50} at 24-h, it was enough to induce cellular death (**Figure 5B**). By comparing the amounts of Cu taken up and the total chelator, it can be estimated that even 0.2 nmol of Dp44mT is capable of an uptake of 1-15 nmol Cu. One possible explanation for this may be that Dp44mT is released after the Cu transfer and it is again capable of repeating the Cu transport. However, triggering of a copper-transport system by the ligand cannot be excluded. Furthermore, there was no difference in the Cu(II) uptake or its toxicity effect for both [Cu(II)Dp44mT] and when Cu(II) sulfate was added to the culture medium one hour before the addition of Dp44mT. It should be mentioned that free amino acids found in the culture medium form complexes with the added Cu(II) sulfate. However, it is well-known that the conditional stability constants of these Cu complexes with amino acids are generally lower than those of Cu with Dp44mT. Moreover, the equilibrium may be shifted, due to the fact that, with the assistance of Dp44mT, Cu ions are transported into the cells, where they are trapped.

Therefore, in our opinion, there is not any real competition between Dp44mT and amino acids found in the culture medium.

An attempt was made to suspend the uptake of Cu by considerably increasing the Fe(II) concentration, and subsequently, the cell viability. It could be established that the intracellular Cu concentration related to control could not be decreased in the presence of high Fe concentration, and consequently, its toxicity could not be inhibited (**Figure 6**). This finding is in agreement with the values of the complex formation constants (**Table 5**). As the strength of the stability of [Co(II)(Dp44mT)$_2$] is comparable with that of [Cu(II)Dp44mT], it is understandable that Co(II) could suspend the Cu(II) toxicity, when the Co-to-Cu ratio was 10:1. The effect of Ni(II) was moderate in the same experiment compared to Co(II), but in every case, a greater decrease in the Cu concentration and higher cell viability could be registered than for Fe. Competition studies with Zn(II) were not performed in this study as the formation constant of Zn with Dp44mT is very low (**Table 5**). Copper can be bound extracellularly by other Cu chelators, such as tetrathiomolybdate, and the Cu-mediated cell toxicity can be suspended [382, 383]. In this case, Dp44mT can act as an Fe chelator.

In conclusion, our results indicate that Dp44mT is mainly a Cu chelator in a biological system also containing Fe, which is understandable as the complex formation constant of [Cu(II)Dp44mT] is higher than that of [Fe(II)(Dp44mT)$_2$]. If Dp44mT is used as a Fe chelator, it causes Cu poisoning in the cells, unless Cu is completely bound to another chelator, which forms a complex of higher stability. According to our results, it would be important to investigate the Cu-mediated toxicity of other molecules synthesized with the purpose of chelating the Fe(II).

Two additional thiosemicarbazone derivatives were tested in the present investigation, DpC and Triapine. Both of them are presently under clinical trials. DpC and Triapine are subject to intensive testing due to their ability to bind zinc and iron, respectively [202, 381]. Our results show that DpC behaves similarly in many ways to Dp44mT, in that it causes significant accumulation of copper in cancer cells in the presence of free copper (**Figure 7D**), and also increases significantly its toxicity in the presence of increasing amounts of Cu(II) (**Figure 7B,C**). In addition, *in vitro* cytotoxicity also increased in the presence of Fe(II) and Zn(II) (**Figure 7A**). Triapine, on the other hand, is significantly

different to DpC and Dp44mT in that it does not cause intracellular copper accumulation in the presence of free copper (**Figure 14C**).

In addition to Dp44mT, members of several additional chelator groups of chemical compounds, such as neocuproine, ammonium pyrrolidine dithiocarbamate, 2,2′-biquinoline, 8-hydroxyquinoline and dithizone were also tested (**Table 3**). It has long been known that these structures have been shown to be more cytotoxic in the presence of copper(II) [179, 384–386]. So, our results are in good agreement with the work of Chen et al. [387] on cytotoxicity of neocuproine in the presence of Cu(II) added in increasing concentration for cultured rat cortical astrocytes. The same was observed for pyrrolidine dithiocarbamate on MDA-MB-231 breast cancer [386] and for oxine on Jurkat T cells [215]. Very similar IC_{50} values to that of ours were found for Cu-oxine complex on HeLa and PC3 cells [388]. For Dp44mT, several research groups have previously reported on Cu-dependent toxicity of Dp44mT [180, 389].

However, for the first time in the literature, we systematically investigated their effects in the context of quantitative copper uptake (**Figure 13, 14, 15, 18**). The Zn and Fe levels (**Figure 4, 16**) were also found to be related to the mechanism of the chelating processes. The most common instrumental analytical techniques applied nowadays for the quantification of Cu, Fe and Zn from biological samples *in vitro* and *ex vivo* include inductive coupled plasma mass spectrometry (ICP-MS), atomic absorption spectrometry (AAS), total reflection X-ray fluorescence (TXRF) and colorimetric assays by UV-Vis [390] or fluorescence spectrometry [391]. The major advantage of the TXRF method, applied in the current studies, is that the S, Cu, Fe and Zn content can be determined simultaneously in the low ppm range.

The D(-)-penicillamine, an extracellular iron chelator, was used as a control, since this compound causes only minimal cellular copper accumulation based on our results. To determine whether their toxicity is related to copper or to determine whether the efficiency can be increased by the addition of Cu(II), we used a 2 µM $CuSO_4$ pre-treatment before adding chelators. It should be noted that 2 µM Cu(II) does not show cytotoxicity even after long-term treatment of 72hours. The IC_{50} values in the 24-hour experiment (**Table 6**) showed a significant decrease for all chelators in the presence of 2 µM Cu(II). A small increase in toxicity was also observed with penicillamine due to the uptake of a small amount of copper.

It is important to mention that it was difficult to determine the IC_{50} values of chelators (especially in the case of Dp44mT), due to the high standard deviations. The standard deviation of these measurements can be more than 100% (**Table 6**). The reason for this is presumably to be found in the variable copper content of the media used for cell culture, since small metal contamination is unavoidable during cell culture and the toxicity of the test compounds is clearly related to the copper content of the media. In contrast, well reproducible values (<10% RSD) were obtained in the presence of 2 μM copper.

Cytostatic activity was studied in the context of a 6-h treatment, and the treatment solutions were carefully removed. After that, the cells were kept for another three day period under normal cell culture conditions. Again, a drastic decrease in IC_{50} values was observed in the presence of copper (**Table 6**), showing that the copper accumulation induced cytotoxic effect could occur in a few hours. Based on our time-lapse video microscopy experiments, this cell death can occur in less than 2 hours (data not shown here).

It can be seen from the results that a clear correlation can be established between copper accumulation and toxicity. Thus, a detailed series of experiments were performed to investigate the copper uptake. Examination of copper uptake using a combination of different Cu(II) and chelator concentrations revealed copper accumulation (**Figure 14A-H**), which may be closely related to the induced cytotoxic effect discussed above. However, if Cu uptake is achieved with complexing agents, toxicity does not necessarily develop. For example, regarding the intracellular uptake of Rh by HT-29 cells in the presence of chelating agents with different Rh ion:ligand molar ratios ranging from 1:1 to 1:4, the development of toxicity depended on the Rh:complexing agent molar ratio [141].

The first condition investigated was a low amount of the chelator in the presence of 2 μM Cu (**Figure 14F**). This very low amount of 0.1 μM chelator showed more than 1,000% copper accumulation for Dp44mT, neocuproine and APDTC, compared to control cells. So these chelators are very efficient, even when applied in small amounts, as they can cause the accumulation of large amounts of copper. In other words, these chelators are able to move more copper than their own molar amount, a phenomenon for which two explanations are possible. Either they "release" the copper from the cell and

introduce another copper ion, or they open a channel through which the copper can flow into the cell.

In subsequent experiments, the treatment conditions were opposite, as a small amount of copper (0.1 µM) was applied with significantly increased chelator concentration (5 µM) (**Figure 14E**). In this case, the maximum amount of accumulated Cu can be calculated as the treatment volume is 2 mL, so approximately 12-13 ng, i.e. 200-400% of the percentage of the control. It can be seen in **Figure 14E** that the same three chelators are able to accumulate all available copper in the cells, while the three less toxic molecules achieve a much smaller effect. Thus the ranking of the chelators related to their copper accumulation properties is similar.

However, a different order is obtained under the third condition: a treatment concentration of 5 µM chelator with 2 µM Cu(II) (**Figure 13**). In this case, each chelator proved to be more effective. This effect is actually well understood, since all copper here is in a complex form with all chelators, according to the stability constants. Here, we also studied whether there is a difference in the copper uptake of the cells when treated with a medium containing 10% FBS instead of an FBS-free medium (**Figure 14D**). It is important to note that based on our TXRF measurements the copper content of the medium containing 10% FBS was significantly higher (2.5–3 ng/mL) than the medium without FBS (0.1–0.3 ng/mL). We found that similar copper data were obtained for 4 chelators (Dp44mT, neocuproine, 2,2′-biquinoline, dithizone), but for APDTC the copper accumulation was greatly increased in the medium containing 10% FBS, and for oxine there was a slight decrease. The explanation for this is presumably to be found in the stability of the copper complexes of the chelators. The most stable chelator (APDTC) presumably forms a sufficiently stable complex to extract some of the copper from the serum. The time scale of copper uptake was also examined under this condition. Copper measurements were performed at different time points. It can be seen in **Figure 14A** that the copper uptake grows rapidly and shows a maximum in 1 hour in the cases of the more toxic chelators.

We also examined whether the accumulated copper could be removed from the cells. A treatment similar to the cytostasis experiment was used after 4 hours of treatment; the cells were washed three times, and the intracellular copper content was determined after 24 hours. The most important result is that while Dp44mT, neocuproine, and APDTC

removed only a small fraction of the copper content, the other three chelators showed a large decrease in intracellular copper content after multiple washes (**Figure 18**).

Two compounds that were studied, neocuproine and 2,2′-biquinoline, are known as Cu(I) chelators. A very important question is which oxidation state of the same complex is more toxic or shows greater Cu accumulation. In the case of neocuproine, both oxidation states can be prepared. Therefore, we also examined whether there was a difference in the copper uptake and toxicity of the cells when the experiments were performed with Cu(I) instead of Cu(II), using ascorbic acid as a reducing agent. We found that there was no significant difference in intracellular copper content when Cu(II) containing complexes were reduced to Cu(I) (**Figure 15**). In the case of neocuproine, we observed a negligibly small increase only, but no difference in the cytotoxicity (data not shown here). Finally, we found that the formation of more stable Cu(I) complexes does not cause enhanced effects in terms of metal uptake and toxicity. This result is not surprising, since it is known that Cu(II) compounds are converted to Cu(I) compounds in the cell and then cause oxidative stress in similar pathways.

Bio-metals imaging and speciation become possible in single cells using proton and synchrotron radiation X-Ray microscopy. Platinum drug bio-distribution can be investigated in cancer cells or spheroid tumor models [29, 30]. With regard to copper imaging, the quantity and distribution of some elements has been investigated, in particular, copper in primary breast cancer has been assessed by Farquharson et al. [32]. μ-XRF imaging proved that Cu is localized diffusely in the cell. However, it may be useful to explain the chelator efficiency in combination with Cu, because colocalization of Cu and Zn was observed in several cases. This phenomenon may have implication in the targeting of Zn-containing peptides/proteins. The most remarkable Cu transporters were those forming stable 1:1 Cu(II) to ligand coordination compounds, i.e. Dp44mT, neocuproine and APDTC. Colocalization of Cu and Zn was observed at the highest extent for Dp44mT indicating replacement of Zn from their peptides/proteins by Cu. Intracellular zinc depletion was also observed examining cell line pairs (**Figure 16**). It should be noted that we have not as yet found such high-resolution metal measurements with copper complexes in the relevant literature.

To investigate the mechanism of action of copper chelators involved in the cytotoxic effect, annexin V-based FACS measurements were performed. Fluorescent signals

indicating apoptosis increased significantly with a 10- and 100-fold increase of the added Cu(II) concentration for the two investigated chelators (**Figure 10**). However, we were able to induce necrosis by increasing the copper-to-chelator ratio. In this case, in the presence of 50 µM Cu ions, even 2 µM Dp44mT can cause a significant necrotic effect, while up to 100 µM chelator alone causes apoptosis (data not shown). The current experiments (**Figure 10**) have indicated an apoptotic cell death mechanism for both Dp44mT and oxine, while paraptotic features were highlighted for oxine and its derivatives [388, 392]. Thus, the key point of toxicity is to be found in the intracellular accumulation of copper. It has been said that apoptosis which has been induced by various cytotoxic agents is the desired mechanism for cell death in the development of therapeutic agents [393, 394], because necrosis leads to local inflammation [395]. Recent studies have shown [396–398] that necrotic cell death is neither a "clean death" nor a "quiet death". It comes to the attention of the immune system, which triggers both of its major responses, the adaptive and the innate. Therefore, controlled necrosis is a possible tool for immunotherapy of human cancer [399]. It is important to note that the dysregulation of apoptosis is related to the development of human cancer and the resistance to anticancer therapy. The findings of Guerriero et al. [378] show that in apoptosis-deficient tumors, necrosis may play a fundamental role in tumor clearance by stimulating the innate immune response [400].

In general, the literature reports that in most cases the toxic effects of copper complexes lead to cell death, due to the activation of the apoptotic process [401–407]. Evidence is increasing on the ability of some copper compounds to induce alternative non-apoptotic forms described as „programmed cell death", and „paraptotic-like" [401]. In addition, a study by Ahmad et al. clearly demonstrated that a Cu(II) complex treatment caused a higher percentage of the necrotic area in the tumor xenografts of treated groups when compared to control groups, and that the percentage necrosis was concentration dependent [190]. A further study found that apoptotic cell death was followed by necrosis to a significant level, and finally to cells losing their plasma integrity [404].

Another well-known *in vitro* effect related to copper complexes is that they generate reactive oxygen species (ROS) [178, 408–413]. As shown **in Figure 11,** ROS release measurements support this conclusion, since increasing the copper concentration significantly increased the amount of ROS release found. Our result is in agreement with

the literature data concerning neocuproine chelator, in which the production of free radicals decreased by increasing the ratio of neocuproine in the investigated system [387]. This is understandable, since the chelating agent reduces the toxic effects of Cu by formation of coordination compounds.

From data related to cytotoxicity, copper uptake, colony formation, and spheroid experiments, it can be concluded that Dp44mT and neocuproine are most effective. The APDTC and 8-hydroxyquinoline proved to be relatively effective. The 2,2′-biquinoline and dithizone compounds were not shown to be useful, mainly due to their poor water solubility. We have shown that some compounds with different toxicity induced similar intracellular Cu concentrations. The Dp44mT, neocuproine and APDTC are each capable of forming 1:1 metal to ligand complexes of similar stability. Therefore, these last three ligands can accumulate Cu in the same way.

The data in the literature concerning copper chelators talks of using preformed complexes in most cases. A copper-chelator complex, which does not have high stability may dissociate intracellularly. Additionally, the mechanism of action of copper transport that we have shown may also play a vital role. In the case of the Cu(II)-neocuproine system, a complex with a molar ratio of 1: 2 can be prepared. It can be clearly seen that when cells are treated with this preformed complex, it is less effective than the treatment with the one at 1:1 ratio (**Table 15**) in the case of short-term cytotoxicity. This observation suggests that in the case of a complex at 1:1 molar ratio, an excess of copper is formed, which increases the *in vitro* cytotoxic efficiency.

To date, there have been several *in vivo* experiments with antitumor Cu(II), or Cu(I) complexes (see **Section 1.5.4.2.**). For example, Gandin et al. [414] synthesized Cu(I) complexes with tridentate tris(pyrazolyl)borate and auxiliary monodentate phosphine ligands. These compounds were insoluble in water, so in their animal experiments a solution of 50% (v/v) Cremophor EL and 50% (v/v) PEG400 was used as a vehicle for dissolution. Treatment with the most efficient anticancer compound in the experiment on LLC (Lewis lung carcinoma)-bearing mice gave a 78% reduction of tumor mass as compared to control animals without signs of toxicity, whereas mice treated with cisplatin showed less effect and substantial weight loss [414]. Additionally, in another study, a different phosphino Cu(I) complex, HydroCuP was examined by the same research group. This compound has shown excellent water solubility (>2.0 mg/mL at pH 7.4) and

good solution stability, enabling *in vivo* formulation using 0.9% NaCl normal saline solution. This complex suppressed tumor growth in both the syngeneic and xenograft models (LoVo colorectal oxaliplatin-sensitive and oxaliplatin-resistant xenograft), being also able to overcome oxaliplatin-resistance without causing evident toxic or side effects [415]. In the above mentioned *in vivo* experiments, the antitumor effect of stable Cu(I)-complexes have been investigated, but the cellular copper accumulation could be due to either the copper, or the complex accumulation. However, the mechanism of action of these complexes does not show the ability of copper accumulation caused by the ionophore release, due to the dissociation of the complex.

The most relevant research in the literature related to our study of the copper and ionophore derived copper accumulation mechanism is the work related to disulfiram (DSF). Firstly, an *in vitro* study by Safi et al. [385] investigated the antitumor effect of the FDA approved drug, disulfiram which, when complexed with Cu(II), induced ROS-dependent apoptosis of malignant, but not normal, prostate cells. Of note is the fact that disulfiram without copper has previously yielded disappointing results in clinical trials conducted with patients with recurrent prostate cancer (PCa). Since dithiocarbamate can be a metabolite of disulfiram, the dithiocarbamate/copper complexes are likely to be effective for the treatment of PCa patients, whose disease is resistant to classical androgen ablation therapies. Not surprisingly, a robust CTR1-dependent uptake of copper into PCa cells was observed [385]. In this study, the DSF/copper group received 100 mL of DSF (30 mg/kg in DMSO-Corn oil) and 100 mL of $CuSO_4$ (0.5 mg/kg) in physiologic saline solution. In another study, Xu et al. administered copper and DSF separately: Cu (0.15 mg/kg/day) each morning (8 o'clock) and DSF (50 mg/kg/day) each evening (18:00) [416]. The different copper and DSF administrations in the two studies mentioned above have reached the level of clinical trial [417–420]. The mechanism of action of DSF in the presence of copper is closely related to anticancer ionophores in the presence of copper, the latter of which we have studied. The copper complex of disulfiram is identical after entering the cell to the DDTC-copper complex, the structure of which is closely related to APDTC-Cu(II) complex [421]. Mohindru et al. [179] published a study related to neocuproine, which is another substance that we have examined. The antitumor effect of neocuproine-Cu(II) complex was evaluated against two types of leukemia tumor-bearing mice. Intraperitoneal injections were administered using 20 µmoles/kg neocuproine

dissolved in 25% propylene glycol and 10 µmol/kg $CuSO_4$ with 20 µmol/kg nitrilotriacetic acid to reduce copper toxicity [422]. The Cu(II)-neocuproine complex is only marginally effective against the L1210 leukemia xenograft *in vivo*, but significantly increased the life span of P388 leukemia-bearing mice [423].

Many other cases related to different copper complexes have experienced high toxicity or insufficiently effective antitumor effects. Mohindru et al. explained the reason for the separate administration of neocuprine and Cu(II) sulfate: the goal was to establish the active complex inside the tumor cells, thus avoiding the formation of the toxic Cu(II)-neocuproine complex in the extracellular milieu [424]. For such toxic complexes, drug delivery systems, especially liposomes, can be an obvious solution. Wehbe et al. showed for the first time that liposomal formulation and *in vivo* utility is possible in the case of precipitated copper complexes [184, 289]. Laine et. al has previously suggested liposomal formulations for the *in vivo* use of poorly soluble metal-based complexes [425]. We aimed to formulate a water-soluble complex, which is the reverse to that of Wehbe et al., namely a neocuproine-copper complex. This complex has a marked cytotoxic effect and a devastating effect on HT-29 spheroids (**Figure 9**), as well as the ability to bind to DNA (**Figure 12**), assuming an even more versatile mechanism of action. The water-soluble hydrochloric acid salt of neocuproine is also available, so this compound was chosen for liposomal formulation. Liposomal formulation of copper(II) is a known method. Moreover, other chemotherapeutic drugs are co-formulated with copper in liposomes [293, 294, 300, 426]. We have shown in the **Sections 3.8.1. and 4.5.1.1.** how to trap the neucoproine in the liposome by application of pH gradient (summarized in **Figure 26**). This is performed by adding the hydrochloric acid salt of neocuproine to an HEPES buffer with pH 7.8. It is then deprotonated, thus being able to dissolve in the lipid bilayer, where it can bind with high affinity to Cu(II) inside the liposomes. We performed this "saturation" at room temperature overnight. Already after half an hour, an increasingly intense orange color is observed, instead of the initial greenish color of the Cu(II)-complex. This apparently indicates the reduction of Cu(II) to Cu(I) in the neocuproine complex, resulting in the orange color. The color of the complex can also be used for the quantitative determination of ascorbic acid by the spectrophotometric method [427]. The external HEPES buffer may play a role in this reduction step [364, 428], which is able to reduce the Cu(II)-neocuproine complex. Moreover, the lipids present in the liposomes

may also play a role due to possible lipid peroxidation (LPO) [429]. Of note, the LPO may play a role in the effect of several copper complexes. Hussain et al. found a substantial increase in LPO levels, which was dependent on the concentration of Cu(II) complexes [404]. Purification of the resulting orange liposome from untrapped drug by gel-filtration and replacement of the external solution with 0.9% NaCl infusion established a monodisperse system suitable for *in vivo*, which was also supported by DLS and MRPS measurements. The steps of liposome preparation are summarized in **Figure 26**. The method can also be used to formulate other chelators, such as Q4 quinoline derivate in the presence of Cu(II) ions (**Section 3.8.2.** and results in **Figure 25**).
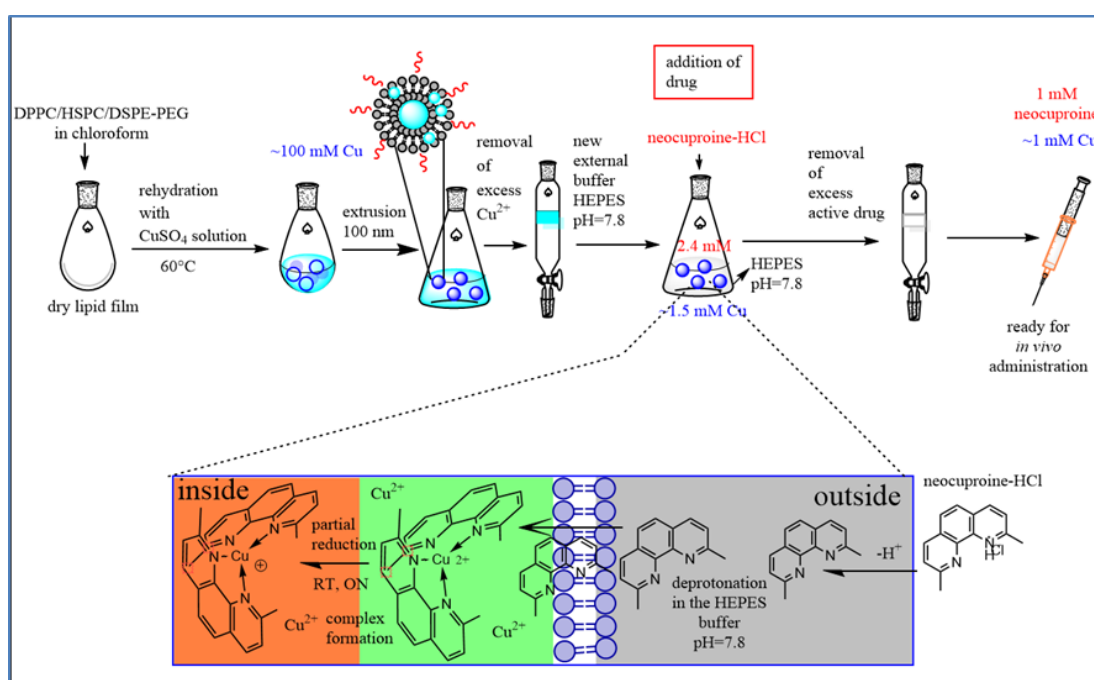

Figure 26. *Schematic representation of the preparation of HEAT SENS LIPO via thin film hydration method.*

It should be noted that the developed color also depends on the lipid composition. It is important to notice that part of the copper is present in reduced form in the liposome, which is measurable by spectrophotometric determination using reducing agents. According to our results, 60% of Cu(II) remained in oxidized form. The transition between Cu(I) and Cu(II) can result in the generation of hydroxyl radicals, which can damage cellular constituents. Generally, the intracellular generation of reactive oxygen species (ROS) via thiol-mediated reduction of Cu(II) to Cu(I) has been assumed to be one of the major mechanisms underlying the anticancer activity of Cu(II) complexes [430].

In the case of our liposome samples, an excess of copper exists compared to that of the Cu-(neocuproine)$_2$ complex, resulting in a more efficient formulation, as shown in **Tables 6 and 15** and discussed in detail in the Results Section. No similar formulation has been found in the literature so far. In addition to the general benefits of liposome (increased vasculature permeability, the minimization of systemic toxicity, with PEG results in prolonged circulation times), we have also examined a drug delivery possibility using mild hyperthermia treatment by heating the tumor to a temperature of 40-42°C (**Section 3.9.1.** and related results in **Figure 22**). To this aim, an appropriate liposomal composition is required. Widely used DSPC or HSPC-containing pegylated liposomes are not suitable for this purpose [431–433]. Replacing HSPC with DPPC did not lead to a solution, as the liposomes release the drug at 37°C. We systematically tested the proportions of these two constituents and 70% DPPC: 30% HSPC was found to be suitable (**Table 14 and Figure 20E**). Based on the IC$_{50}$ values, our pegylated liposome, which did not show any cytotoxic effect at 38°C, apparently did so at 41°C. In order to find the appropriate composition of liposomes, both the copper concentration and the drug to lipid ratio had to be optimized and 0.2 mol of neocuproine per mol of lipid were found to be suitable (**Table 12**). This is in good agreement with the literature data [433]. The liposome proved to be effective *in vitro*. It should be noted that it did not show any cytotoxic effect in the studied range for 4 hours, which indicates the proper encapsulation of the drug. The free complex induces a cytotoxic effect in 4 hours. The DPPC based thermosensitive liposomal formulations (TSL) have been published in the literature. As an example, DPPC/DSPC/DSPE-PEG2000 in a molar ratio of 55:40:5 as the slow release TSL formulation, and in a molar ratio of 80:15:5 as the fast release TSL formulation [434]. Thus, a faster release can be achieved by increasing the amount of DPPC in the different lipid mixtures. This is related to our Cu determination results; the HEAT SENS LIPO accumulated significant amounts of copper in a 4-hour-long experiment (**Figure 21**). The addition of lysolipid (MPPC or MSPC) components is also possible. Kong et al. [318] and Kheirolomoom et al. [294] prepared the low temperature sensitive liposome of DPPC:MPPC:DSPE-PEG-2000 in different molar ratios [305]. There have been further studies where copper is used for thermosensitive liposome formulations, e.g. doxorubicin, 5-fluorouracil and gemcitabin [294, 295, 435]. However, no TSL was found in the literature related to water-soluble copper complexes. It should be noted that each of the three above-mentioned compounds

form complexes with Cu(II) [436]. Cu(II) is used to create the appropriate formulation with more effective loading, but it is the Cu(II)-complex itself that is the key to the antitumor effect.

For animal experiments, Colon-26 carcinoma tumor-bearing BALB/c mouse model was selected, a model which is also suitable as a model for the study of cancer cachexia [437]. Two *in vivo* experiments were conducted in the thesis related to the formulated liposomes (**Figure 22**). First, the antitumor effects of the two selected formulations were compared: the HSPC-based pegylated liposome (HEAT RES LIPO), which is unsuitable for hyperthermia, and the liposome (HEAT SENS LIPO), which is suitable for combination with mild hyperthermia (**Figure 22A,C,D**). An antitumor effect was observed in both cases, but more significantly in the case of HEAT SENS LIPO. This can be explained by the significant difference in Cu accumulation related to TXRF data (**Figure 21**). In a second *in vivo* experiment (**Figure 22B, E,F**) our aim was to investigate whether a smaller dose could reach the desired antitumor effect applied together with mild hyperthermic treatment, so a half-dose administered group was also investigated. This group without controlled release shows probably an even less satisfactory antitumor effect, compared to the first *in vivo* experiment (**Figure 22A, C**). The major finding is that a significant antitumor effect was observed in every treated group compared to control. Surprisingly, the strongest antitumor effect was observed as a result of treatment with half dose (1.4 mg/kg) liposome combined with hyperthermia (**Figure 22B, E**). It should be emphasized that the antitumor effect could not be increased by hyperthermia treatment in the full dose group. This is in agreement with the *in vitro* data (**Table 15**), where the initial difference in toxicity totally disappears after 72-hours. In summary, with minimal toxicity, we formulated a moderately *in vivo* efficacious Cu based antitumor therapy through liposomal drug administration combined with mild hyperthermia to trigger intravascular release of drug (**Section 4.5**).

6. Conclusions

In conclusion, the following results as new findings can be highlighted:

1.   Intracellular Cu content increased under the influence of 50 µM Dp44mT and increased more than 30 times in 8 different cancer cells in the presence of 5 µM Dp44mT and 2 µM CuSO$_4$ solution.

2.   Co(II) decreases Dp44mT mediated Cu accumulation and reduces the toxicity of Dp44mT.

3.   The uptake and cytotoxicity of Cu mediated by Dp44mT depends on extracellular Cu(II) concentration.

4.   Low concentration (0.1 µM) of Dp44mT can deliver high amounts of copper inside the cells.

5.   Detailed intracellular copper uptake and depletion data in the case of Dp44mT, neocuproine, APDTC, oxine, 2,2'-biquinoline and dithizone chelators are presented. Moreover, cellular localization of copper is shown using Dp44mT and oxine.

6.   Copper localization and its colocalization with Zn were determined by µ-XRF imaging. Colocalization of Cu and Zn in the nucleus of HT-29 cells was observed for Dp44mT (correlation coefficient as high as 0.85).

7.   Cu uptake with respect to different chelators has been shown to be a relatively universal process and that among all possible divalent metals, only cadmium will accumulate in the same way.

8.   Compounds with similar intracellular Cu uptake have been shown to induce very different values of cytotoxicity.

9.   The Cu uptake results in a cell type dependent intracellular Zn depletion, which is in correlation with the toxicity of the chelator.

10.   The Cu(II) concentration-dependent, fast apoptosis could be detected with the application of Dp44mT and oxine chelators.

11.   The chelating agents – except for neocuproine – restored the DNA damage induced by free Cu(II).

12.   The feasibility of using a liposome preparation containing a copper nanotoxin and excess of copper ion in a water-soluble form for tumor targeting has been demonstrated. I have developed liposomal formulation of copper-neocuproine complex HEAT SENS LIPO as thermosensitive and HEAT RES LIPO as „thermoresistant", which are suitable for *in vivo* application

13.   I have shown that both the thermosensitive and the "thermoresistant" formulations induce intracellular copper accumulation and related *in vitro* cytotoxic effects. *In vivo* antitumor activity could be detected with both liposomes, but the effect of HEAT SENS LIPO was found to be more pronounced. Mild hyperthermia treatment combined with the HEAT SENS LIPO formulation allowed the reduction of the applied dose.

7. Summary

Since the initial clinical success of platinum-containing anticancer compounds, considerable attention has been paid to the research of various transition metal-containing complexes and chelator-like structures. Many of these compounds have also been the subjects of clinical trials.

During my doctoral research, I investigated antitumor chelators, including thiosemicarbazone, thiocarbazone, thiocarbamate, quinoline, and phenanthroline structures. I have shown that the investigated chelators cause high cellular accumulation of copper, even at low chelator concentrations. They are able to accumulate multiples of their own amounts in the presence of free copper, and the copper content appears in the nuclei in a diffuse manner. The amount of accumulated copper within the cell can be up to thirty times higher than that of the control. I have also demonstrated that there is no strong correlation between copper accumulation and toxicity alone. I observed that, for more potent compounds, copper content could not be removed from cells, and zinc depletion could also be observed. I have demonstrated that Dp44mT, which is known as an iron chelator, also causes copper accumulation in the presence of copper, which can be suspended with cobalt ions. The localization of copper in the case of Dp44mT shows significant colocalization with zinc. I have shown that their cytotoxicity is greatly increased in the presence of free copper(II), and fast (20 min) copper-dependent apoptosis can be detected. I have pointed out that the *in vitro* cytotoxic effect does not depend on the cell line type; they are similarly toxic in several different tumor cell lines and also in resistant tumor models. I have shown that when examining toxic metals, a process similar to copper accumulation occurs only in the case of cadmium, but also to a much lesser extent. Many antitumor complex compounds and chelators do not have appropriate pharmacological parameters for successful *in vivo* applicability. Liposomal formulations have shown several advantages in terms of the *in vivo* applicability of chemotherapeutic agents. I have developed the preparation method of liposomes containing copper ionophore (neocuproine). I have recognized the formulation of a thermosensitive liposome for the purpose of targeted drug release (combination with hyperthermia treatment). Liposomes containing neocuproine Cu(II) were shown to be effective *in vivo* (BALB / c C-26 colon adenocarcinoma) in a mouse tumor model, with significant tumor growth inhibition observed in all cases. Hyperthermia treatment with the use of thermosensitive liposomes allowed dose reduction.

8. Summary in Hungarian (Összefoglalás)

A platina tartalmú rákellenes vegyületek klinikai sikere óta jelentős figyelem fordult a különböző átmenetifém-komplexek illetve kelátor jellegű struktúrák kutatásának irányába. Számos közülük klinikai vizsgálatokba is bekerült.

Doktori kutatásaim során tumorellenes kelátorokat, közöttük tioszemikarbazon-, tiokarbazon-, tiokarbamát-, kinolin- és fenantrolin-vázas struktúrákat vizsgáltam. Bemutattam, hogy a vizsgált kelátorok nagymértékű rézfelhalmozódást okoznak rákos sejtvonalakon, még kis kelátorkoncentrációnál is képesek szabad réz jelenlétében a saját mennyiségük többszörösét felhalmozni, és az réztartalom a sejtmagokban diffúz módon jelenik meg. Kimutattam, hogy a felhalmozott réz mennyisége a sejten belül akár harmincszorosa is lehet a kontrollnak, és bizonyítottam, hogy önmagában a rézfelhalmozódás és a toxicitás között nincs szoros összefüggés. Megfigyeltem, hogy a hatékonyabb vegyületek esetén a réztartalom nem távolítható el a sejtekből, továbbá a cink depléciója is megfigyelhető. Bizonyítottam, hogy a vaskelátorként ismert Dp44mT is rézfelhalmozódást okoz megfelelő mennyiségű réz jelenlétében, ami kobalt ionokkal felfüggeszthető. A réz lokalizációja Dp44mT esetén jelentős egybeesést mutat a cinkkel. Bemutattam, hogy citotoxikus hatásuk szabad réz(II) jelenlétében nagymértékben növelhető és rézfüggő apoptózis mutatható ki már 20 perc eltelte után. Megállapítottam, hogy *in vitro* citotoxikus hatásuk nem függ a sejtvonal típusától, számos különböző tumor sejtvonalon, rezisztens tumor modelleket is vizsgálva hasonlóan toxikusnak mutatkozik. Bemutattam, hogy megvizsgálva a toxikus fémeket, a rézfelhalmozódáshoz hasonló folyamat csak kadmium esetében játszódik le, de az is jóval kisebb mértékben.

Számos tumorellenes komplex vegyület, vagy kelátor nem rendelkezik a megfelelő farmokológiai paraméterekkel a sikeres *in vivo* alkalmazhatósághoz. A liposzómás formulációk számos előnye mutatkozott meg a kemoterápiás szerek *in vivo* alkalmazhatóságának tekintetében. Réz-ionofór (neokuproin) tartalmú liposzómák preparálásához módszereket dolgoztam ki és javasoltam. A célzott hatóanyag felszabadítás (kombináció hipertermiás kezeléssel) céljából termoszenzitív liposzóma formulálását is megvalósítottam. A neokuproin-Cu(II)-t tartalmazó liposzómák hatékonynak bizonyult *in vivo* (BALB/c C-26 kolon adenokarcinóma) egér tumormodellen, mivel szignifikáns tumornövekedés-gátlást figyeltem meg minden esetben. A hipertermiás kezelés a termoszenzitív liposzóma alkalmazása során lehetővé tette a dózis csökkentését.

9. Bibliography

1.   WHO/Europe | Home. http://www.euro.who.int/en/home. Accessed 29 Feb 2020

2.   Cancer today. http://gco.iarc.fr/today/home. Accessed 29 Feb 2020

3.   Ferlay J, Colombet M, Soerjomataram I, Mathers C, Parkin DM, Piñeros M, Znaor A, Bray F (2019) Estimating the global cancer incidence and mortality in 2018: GLOBOCAN sources and methods. Int J Cancer, 144: 1941–1953.

4.   Blackadar CB (2016) Historical review of the causes of cancer. World J Clin Oncol, 7: 54–86.

5.   Ferlay J, Colombet M, Soerjomataram I, Dyba T, Randi G, Bettio M, Gavin A, Visser O, Bray F (2018) Cancer incidence and mortality patterns in Europe: Estimates for 40 countries and 25 major cancers in 2018. Eur J Cancer, 103: 356–387.

6.   Ferlay J, Colombet M, Soerjomataram I, Dyba T, Randi G, Bettio M, Gavin A, Visser O, Bray F (2018) Cancer incidence and mortality patterns in Europe: Estimates for 40 countries and 25 major cancers in 2018. Eur J Cancer Oxf Engl 1990, 103: 356–387.

7.   Címlap | www.stat.nrr.hu. http://stat.nrr.hu/. Accessed 19 Feb 2020

8.   Menyhárt O, Fekete JT, Győrffy B (2018) Demographic shift disproportionately increases cancer burden in an aging nation: current and expected incidence and mortality in Hungary up to 2030. Clin Epidemiol, 10: 1093–1108.

9.   GBD 2017 Causes of Death Collaborators (2018) Global, regional, and national age-sex-specific mortality for 282 causes of death in 195 countries and territories, 1980–2017: a systematic analysis for the Global Burden of Disease Study 2017. The Lancet, 392: 1736–1788.

10.   Dagenais GR, Leong DP, Rangarajan S, Lanas F, Lopez-Jaramillo P, Gupta R, Diaz R, Avezum A, Oliveira GBF, Wielgosz A, Parambath SR, Mony P, Alhabib KF, Temizhan A, Ismail N, Chifamba J, Yeates K, Khatib R, Rahman O, Zatonska K, Kazmi K, Wei L, Zhu J, Rosengren A, Vijayakumar K, Kaur M, Mohan V, Yusufali A, Kelishadi R, Teo KK, Joseph P, Yusuf S (2020) Variations in common diseases, hospital admissions, and deaths in middle-aged adults in 21 countries from five continents (PURE): a prospective cohort study. The Lancet, 395: 785–794.

11.   Shah SC, Kayamba V, Peek RM, Heimburger D (2019) Cancer Control in Low- and Middle-Income Countries: Is It Time to Consider Screening? J Glob Oncol, 5: 1–8.

12.   Worldometer - real time world statistics. In: Worldometer. http://www.worldometers.info/. Accessed 19 Feb 2020

13. Prager GW, Braga S, Bystricky B, Qvortrup C, Criscitiello C, Esin E, Sonke GS, Martínez GA, Frenel J-S, Karamouzis M, Strijbos M, Yazici O, Bossi P, Banerjee S, Troiani T, Eniu A, Ciardiello F, Tabernero J, Zielinski CC, Casali PG, Cardoso F, Douillard J-Y, Jezdic S, McGregor K, Bricalli G, Vyas M, Ilbawi A (2018) Global cancer control: responding to the growing burden, rising costs and inequalities in access. ESMO Open, 3: e000285.

14. Puricelli Perin DM, Vogel AL, Taplin SH (2019) Assessing Knowledge Sharing in Cancer Screening Among High-, Middle-, and Low-Income Countries: Insights From the International Cancer Screening Network. J Glob Oncol, 5: 1–8.

15. Siegel RL, Miller KD, Jemal A (2019) Cancer statistics, 2019. CA Cancer J Clin, 69: 7–34.

16. Pizzoli S, Renzi C, Arnaboldi P, Russell-Edu W, Pravettoni G (2019) From life-threatening to chronic disease: Is this the case of cancers? A systematic review. Cogent Psychol, 6: 1–17.

17. (2007) What Is Cancer? In: Natl. Cancer Inst. https://www.cancer.gov/about-cancer/understanding/what-is-cancer. Accessed 19 Feb 2020

18. Hanahan D, Weinberg RA (2011) Hallmarks of cancer: the next generation. Cell, 144: 646–674.

19. AACR Cancer Progress Report. https://www.cancerprogressreport.org:443/Pages/default.aspx. Accessed 4 Apr 2020

20. Hiller JG, Perry NJ, Poulogiannis G, Riedel B, Sloan EK (2018) Perioperative events influence cancer recurrence risk after surgery. Nat Rev Clin Oncol, 15: 205–218.

21. Wyld L, Audisio RA, Poston GJ (2015) The evolution of cancer surgery and future perspectives. Nat Rev Clin Oncol, 12: 115–124.

22. Baskar R, Lee KA, Yeo R, Yeoh K-W (2012) Cancer and Radiation Therapy: Current Advances and Future Directions. Int J Med Sci, 9: 193–199.

23. Chen HHW, Kuo MT (2017) Improving radiotherapy in cancer treatment: Promises and challenges. Oncotarget, 8: 62742–62758.

24. Gilman A, Philips FS (1946) The Biological Actions and Therapeutic Applications of the B-Chloroethyl Amines and Sulfides. Science, 103: 409–436.

25. Link W (2015) Anti-cancer Drugs: Discovery, Development and Therapy. Int Man Oncol Pract, 81–94.

26. Rosenberg B, VanCamp L, Trosko JE, Mansour VH (1969) Platinum compounds: a new class of potent antitumour agents. Nature, 222: 385–386.

27. Lajous H, Lelièvre B, Vauléon E, Lecomte P, Garcion E (2019) Rethinking Alkylating(-Like) Agents for Solid Tumor Management. Trends Pharmacol Sci, 40: 342–357.

28.   Galanski M, Jakupec MA, Keppler BK (2005) Update of the preclinical situation of anticancer platinum complexes: novel design strategies and innovative analytical approaches. Curr Med Chem, 12: 2075–2094.

29.   Ndagi U, Mhlongo N, Soliman ME (2017) Metal complexes in cancer therapy – an update from drug design perspective. Drug Des Devel Ther, 11: 599–616.

30.   Huang M, Shen A, Ding J, Geng M (2014) Molecularly targeted cancer therapy: some lessons from the past decade. Trends Pharmacol Sci, 35: 41–50.

31.   Hudziak RM, Lewis GD, Winget M, Fendly BM, Shepard HM, Ullrich A (1989) p185HER2 monoclonal antibody has antiproliferative effects in vitro and sensitizes human breast tumor cells to tumor necrosis factor. Mol Cell Biol, 9: 1165–1172.

32.   Gharwan H, Groninger H (2016) Kinase inhibitors and monoclonal antibodies in oncology: clinical implications. Nat Rev Clin Oncol, 13: 209–227.

33.   Santos R, Ursu O, Gaulton A, Bento AP, Donadi RS, Bologa CG, Karlsson A, Al-Lazikani B, Hersey A, Oprea TI, Overington JP (2017) A comprehensive map of molecular drug targets. Nat Rev Drug Discov, 16: 19–34.

34.   Bai X, Yang X, Wu L, Zuo B, Lin J, Wang S, Bian J, Sang X, He Y, Yang Z, Zhao H (2019) CMTTdb: the cancer molecular targeted therapy database. Ann Transl Med, 7: 667.

35.   Ke X, Shen L (2017) Molecular targeted therapy of cancer: The progress and future prospect. Front Lab Med, 1: 69–75.

36.   Sjoquist KM, Martyn J, Edmondson RJ, Friedlander ML (2011) The role of hormonal therapy in gynecological cancers-current status and future directions. Int J Gynecol Cancer, 21: 1328–1333.

37.   Whitmore WF (1956) Hormone therapy in prostatic cancer. Am J Med, 21: 697–713.

38.   Zhao J, Chen Y, Ding Z-Y, Liu J-Y (2019) Safety and Efficacy of Therapeutic Cancer Vaccines Alone or in Combination With Immune Checkpoint Inhibitors in Cancer Treatment. Front Pharmacol, 10: 1184.

39.   Schirrmacher V (2019) From chemotherapy to biological therapy: A review of novel concepts to reduce the side effects of systemic cancer treatment (Review). Int J Oncol, 54: 407–419.

40.   Wu J, Waxman DJ (2018) Immunogenic chemotherapy: Dose and schedule dependence and combination with immunotherapy. Cancer Lett, 419: 210–221.

41.   Emens LA (2010) Chemoimmunotherapy. Cancer J Sudbury Mass, 16: 295–303.

42.   Englinger B, Pirker C, Heffeter P, Terenzi A, Kowol CR, Keppler BK, Berger W (2019) Metal Drugs and the Anticancer Immune Response. Chem Rev, 119: 1519–1624.

43.   Shin J, Chung J-H, Kim SH, Lee KS, Suh KJ, Lee JY, Kim J-W, Lee J-O, Kim J-W, Kim Y-J, Lee K-W, Kim JH, Bang S-M, Lee J-S (2019) Effect of Platinum-Based Chemotherapy on PD-L1 Expression on Tumor Cells in Non-small Cell Lung Cancer. Cancer Res, 51: 1086–1097.

44.   Jiang T, Zhou C, Hu J, Song Y (2019) Combination immune checkpoint inhibitors with platinum-based chemotherapy in advanced non-small cell lung cancer: what's known and what's next. Transl Lung Cancer Res, 8: S447–S450.

45.   Liu MC, Oxnard GR, Klein EA, Swanton C, Seiden MV & on behalf of the CCGA Consortium (2020) Sensitive and specific multi-cancer detection and localization using methylation signatures in cell-free DNA. Ann Oncol, 31: 745–759.

46.   Szakács G, Paterson JK, Ludwig JA, Booth-Genthe C, Gottesman MM (2006) Targeting multidrug resistance in cancer. Nat Rev Drug Discov, 5: 219–234.

47.   Szakács G, Hall MD, Gottesman MM, Boumendjel A, Kachadourian R, Day BJ, Baubichon-Cortay H, Di Pietro A (2014) Targeting the Achilles Heel of Multidrug-Resistant Cancer by Exploiting the Fitness Cost of Resistance. Chem Rev, 114: 5753–5774.

48.   Ludwig JA, Szakács G, Martin SE, Chu BF, Cardarelli C, Sauna ZE, Caplen NJ, Fales HM, Ambudkar SV, Weinstein JN, Gottesman MM (2006) Selective Toxicity of NSC73306 in MDR1-Positive Cells as a New Strategy to Circumvent Multidrug Resistance in Cancer. Cancer Res, 66: 4808–4815.

49.   Pluchino KM, Hall MD, Goldsborough AS, Callaghan R, Gottesman MM (2012) Collateral sensitivity as a strategy against cancer multidrug resistance. Drug Resist Updat, 15: 98–105.

50.   Türk D, Hall MD, Chu BF, Ludwig JA, Fales HM, Gottesman MM, Szakács G (2009) Identification of compounds selectively killing multidrug resistant cancer cells. Cancer Res, 69: 8293–8301.

51.   Satoh M, Cherian MG, Imura N, Shimizu H (1994) Modulation of resistance to anticancer drugs by inhibition of metallothionein synthesis. Cancer Res, 54: 5255–5257.

52.   Heffeter P, Pape VFS, Enyedy ÉA, Keppler BK, Szakacs G, Kowol CR (2019) Anticancer Thiosemicarbazones: Chemical Properties, Interaction with Iron Metabolism, and Resistance Development. Antioxid Redox Signal, 30: 1062–1082.

53.   Wehbe M, Lo C, Leung AWY, Dragowska WH, Ryan GM, Bally MB (2017) Copper (II) complexes of bidentate ligands exhibit potent anti-cancer activity regardless of platinum sensitivity status. Invest New Drugs, 35: 682–690.

54.   Schwartz MK (1975) Role of trace elements in cancer. Cancer Res, 35: 3481–3487.

55.   Gupte A, Mumper RJ (2009) Elevated copper and oxidative stress in cancer cells as a target for cancer treatment. Cancer Treat Rev, 35: 32–46.

56. Carpentieri U, Myers J, Thorpe L, Daeschner CW, Haggard ME (1986) Copper, zinc, and iron in normal and leukemic lymphocytes from children. Cancer Res, 46: 981–984.

57. Kuo HW, Chen SF, Wu CC, Chen DR, Lee JH (2002) Serum and tissue trace elements in patients with breast cancer in Taiwan. Biol Trace Elem Res, 89: 1–11.

58. Gupta SK, Shukla VK, Vaidya MP, Roy SK, Gupta S (1993) Serum and tissue trace elements in colorectal cancer. J Surg Oncol, 52: 172–175.

59. K S, Dk M, Rc K, Vp K, Chowdhery (1994) Diagnostic and prognostic significance of serum and tissue trace elements in breast malignancy. Indian J Med Sci, 48: 227–232.

60. Majumder S, Chatterjee S, Pal S, Biswas J, Efferth T, Choudhuri SK (2009) The role of copper in drug-resistant murine and human tumors. Biometals Int J Role Met Ions Biol Biochem Med, 22: 377–384.

61. Ishida S, Lee J, Thiele DJ, Herskowitz I (2002) Uptake of the anticancer drug cisplatin mediated by the copper transporter Ctr1 in yeast and mammals. Proc Natl Acad Sci U S A, 99: 14298–14302.

62. Zhu S, Shanbhag V, Wang Y, Lee J, Petris M (2017) A Role for The ATP7A Copper Transporter in Tumorigenesis and Cisplatin Resistance. J Cancer, 8: 1952–1958.

63. Li Y-Q, Yin J-Y, Liu Z-Q, Li X-P (2018) Copper efflux transporters ATP7A and ATP7B: Novel biomarkers for platinum drug resistance and targets for therapy. IUBMB Life, 70: 183–191.

64. Kwok JC, Richardson DR (2002) The iron metabolism of neoplastic cells: alterations that facilitate proliferation? Crit Rev Oncol Hematol, 42: 65–78.

65. Campbell JA (1940) Effects of Precipitated Silica and of Iron Oxide on the Incidence of Primary Lung Tumours in Mice. Br Med J, 2: 275–280.

66. Richmond HG (1959) Induction of sarcoma in the rat by iron-dextran complex. Br Med J, 1: 947–949.

67. Hann HW, Stahlhut MW, Blumberg BS (1988) Iron nutrition and tumor growth: decreased tumor growth in iron-deficient mice. Cancer Res, 48: 4168–4170.

68. Shen Y, Li X, Dong D, Zhang B, Xue Y, Shang P (2018) Transferrin receptor 1 in cancer: a new sight for cancer therapy. Am J Cancer Res, 8: 916–931.

69. Stevens RG, Graubard BI, Micozzi MS, Neriishi K, Blumberg BS (1994) Moderate elevation of body iron level and increased risk of cancer occurrence and death. Int J Cancer, 56: 364–369.

70. Stevens RG, Jones DY, Micozzi MS, Taylor PR (1988) Body iron stores and the risk of cancer. N Engl J Med, 319: 1047–1052.

71.   van Asperen IA, Feskens EJ, Bowles CH, Kromhout D (1995) Body iron stores and mortality due to cancer and ischaemic heart disease: a 17-year follow-up study of elderly men and women. Int J Epidemiol, 24: 665–670.

72.   Knekt P, Reunanen A, Takkunen H, Aromaa A, Heliövaara M, Hakulinen T (1994) Body iron stores and risk of cancer. Int J Cancer, 56: 379–382.

73.   Nelson RL (2001) Iron and colorectal cancer risk: human studies. Nutr Rev, 59: 140–148.

74.   Torti SV, Torti FM (2013) Iron and cancer: more ore to be mined. Nat Rev Cancer, 13: 342–355.

75.   Costello LC, Franklin RB (2016) A comprehensive review of the role of zinc in normal prostate function and metabolism; and its implications in prostate cancer. Arch Biochem Biophys, 611: 100–112.

76.   Skrajnowska D, Bobrowska-Korczak B (2019) Role of Zinc in Immune System and Anti-Cancer Defense Mechanisms. Nutrients, 11: 2273.

77.   Ho E (2004) Zinc deficiency, DNA damage and cancer risk. J Nutr Biochem, 15: 572–578.

78.   Inutsuka S, Araki S (1978) Plasma copper and zinc levels in patients with malignant tumors of digestive organs. Clinical evaluation of the Cu/Zn ratio. Cancer, 42: 626–631.

79.   Mawson CA, Fischer MI (1952) The occurrence of zinc in the human prostate gland. Can J Med Sci, 30: 336–339.

80.   Song Y, Ho E (2009) Zinc and prostatic cancer. Curr Opin Clin Nutr Metab Care, 12: 640–645.

81.   Li D, Stovall DB, Wang W, Sui G (2020) Advances of Zinc Signaling Studies in Prostate Cancer. Int J Mol Sci, 21: 667.

82.   Franklin RB, Feng P, Milon B, Desouki MM, Singh KK, Kajdacsy-Balla A, Bagasra O, Costello LC (2005) hZIP1 zinc uptake transporter down regulation and zinc depletion in prostate cancer. Mol Cancer, 4: 32.

83.   Chakravarty PK (2011) Evaluation of Serum Zinc Level Under Malignant Condition and its Possible Implication on Improving Cell-Mediated Immunity During Cancer Progression. World J Oncol, 2: 16–23.

84.   Prasad AS, Beck FWJ, Snell DC, Kucuk O (2009) Zinc in cancer prevention. Nutr Cancer, 61: 879–887.

85.   Mahmoud AM, Al-Alem U, Dabbous F, Ali MM, Batai K, Shah E, Kittles RA (2016) Zinc Intake and Risk of Prostate Cancer: Case-Control Study and Meta-Analysis. PLoS ONE, 11: e0165956.

86.   N. Loh S (2010) The missing Zinc : p53 misfolding and cancer. Metallomics, 2: 442–449.

87.   Krizkova S, Ryvolova M, Hrabeta J, Adam V, Stiborova M, Eckschlager T, Kizek R (2012) Metallothioneins and zinc in cancer diagnosis and therapy. Drug Metab Rev, 44: 287–301.

88.   Kondo Y, Kuo SM, Watkins SC, Lazo JS (1995) Metallothionein localization and cisplatin resistance in human hormone-independent prostatic tumor cell lines. Cancer Res, 55: 474–477.

89.   Yap X, Tan H-Y, Huang J, Lai Y, Yip GW-C, Tan P-H, Bay B-H (2009) Over-expression of metallothionein predicts chemoresistance in breast cancer. J Pathol, 217: 563–570.

90.   Kontoghiorghes GJ (2020) Advances on Chelation and Chelator Metal Complexes in Medicine. Int J Mol Sci, 21: 2499.

91.   SEER Cancer Statistics Review 1975-2008 - Previous Version - SEER Cancer Statistics. In: SEER. https://seer.cancer.gov/archive/csr/1975_2008/index.html. Accessed 10 Apr 2020

92.   Bucher-Johannessen C, Page CM, Haugen TB, Wojewodzic MW, Fosså SD, Grotmol T, Haugnes HS, Rounge TB (2019) Cisplatin treatment of testicular cancer patients introduces long-term changes in the epigenome. Clin Epigenetics, 11: 179.

93.   Raudenska M, Balvan J, Fojtu M, Gumulec J, Masarik M (2019) Unexpected therapeutic effects of cisplatin. Metallomics, 11: 1182–1199.

94.   Johnstone TC, Suntharalingam K, Lippard SJ (2016) The Next Generation of Platinum Drugs: Targeted Pt(II) Agents, Nanoparticle Delivery, and Pt(IV) Prodrugs. Chem Rev, 116: 3436–3486.

95.   Gandara DR, Wiebe VJ, Perez EA, Makuch RW, DeGregorio MW (1990) Cisplatin rescue therapy: Experience with sodium thiosulfate, WR2721, and diethyldithiocarbamate. Crit Rev Oncol Hematol, 10: 353–365.

96.   Wheate NJ, Walker S, Craig GE, Oun R (2010) The status of platinum anticancer drugs in the clinic and in clinical trials. Dalton Trans Camb Engl 2003, 39: 8113–8127.

97.   Stathopoulos GP (2010) Liposomal cisplatin: a new cisplatin formulation. Anticancer Drugs, 21: 732–736.

98.   Boros E, Dyson PJ, Gasser G (2020) Classification of Metal-Based Drugs according to Their Mechanisms of Action. Chem, 6: 41–60.

99.   Deilami-nezhad L, Moghaddam-Banaem L, Sadeghi M, Asgari M (2016) Production and purification of Scandium-47: A potential radioisotope for cancer theranostics. Appl Radiat Isot, 118: 124–130.

100. Caporale A, Palma G, Mariconda A, Del Vecchio V, Iacopetta D, Parisi OI, Sinicropi MS, Puoci F, Arra C, Longo P, Saturnino C (2017) Synthesis and Antitumor Activity of New Group 3 Metallocene Complexes. Mol Basel Switz, 22: 526.

101. Chitambar CR. Gallium Complexes as Anticancer Drugs. In: Astrid Sigel, Helmut Sigel, Eva Freisinger and Roland K. O. Sigel (ed) Metallo-Drugs: Development and Action of Anticancer Agents. Met Ions Life Sci, Walter de Gruyter GmbH, Berlin, Germany, 2018: 282-297.

102. Chitambar CR, Antholine WE (2013) Iron-targeting antitumor activity of gallium compounds and novel insights into triapine(®)-metal complexes. Antioxid Redox Signal, 18: 956–972.

103. Ellahioui Y, Prashar S, Gómez-Ruiz S (2017) Anticancer Applications and Recent Investigations of Metallodrugs Based on Gallium, Tin and Titanium. Inorganics, 5: 4.

104. Esmail SAA, Shamsi M, Chen T, Al-asbahy WM (2019) Design, synthesis and characterization of tin-based cancer chemotherapy drug entity: In vitro DNA binding, cleavage, induction of cancer cell apoptosis by triggering DNA damage-mediated p53 phosphorylation and molecular docking. Appl Organomet Chem, 33: e4651.

105. Crowe AJ (1990) Tin Compounds and their Potential as Pharmaceutical Agents. In: Gielen M (ed) Tin-Based Antitumour Drugs. Springer, Berlin, Heidelberg, pp 69–114

106. Rocamora-Reverte L, Carrasco-García E, Ceballos-Torres J, Prashar S, Kaluđerović GN, Ferragut JA, Gómez-Ruiz S (2012) Study of the anticancer properties of tin(IV) carboxylate complexes on a panel of human tumor cell lines. ChemMedChem, 7: 301–310.

107. Sharma P, Perez D, Cabrera A, Rosas N, Arias JL (2008) Perspectives of antimony compounds in oncology. Acta Pharmacol Sin, 29: 881–890.

108. Tiekink ERT (2002) Antimony and bismuth compounds in oncology. Crit Rev Oncol Hematol, 42: 217–224.

109. Hadjikakou SK, Antoniadis CD, Hadjiliadis N, Kubicki M, Binolis J, Karkabounas S, Charalabopoulos K (2005) Synthesis and characterization of new water stable antimony(III) complex with pyrimidine-2-thione and in vitro biological study. Inorganica Chim Acta, 358: 2861–2866.

110. Reis DC, Pinto MCX, Souza-Fagundes EM, Rocha LF, Pereira VRA, Melo CML, Beraldo H (2011) Investigation on the pharmacological profile of antimony(III) complexes with hydroxyquinoline derivatives: anti-trypanosomal activity and cytotoxicity against human leukemia cell lines. Biometals Int J Role Met Ions Biol Biochem Med, 24: 595–601.

111. Axelson O (1980) Arsenic compounds and cancer. J Toxicol Environ Health, 6: 1229–1235.

112. Martinez VD, Vucic EA, Becker-Santos DD, Gil L, Lam WL (2011) Arsenic Exposure and the Induction of Human Cancers. J Toxicol, 2011: 431287.

113. Antman KH (2001) Introduction: the history of arsenic trioxide in cancer therapy. The Oncologist, 6 Suppl 2: 1–2.

114. Emadi A, Gore SD (2010) Arsenic trioxide - An old drug rediscovered. Blood Rev, 24: 191–199.

115. Wang Z-Y, Chen Z (2008) Acute promyelocytic leukemia: from highly fatal to highly curable. Blood, 111: 2505–2515.

116. Berenson JR, Yeh HS (2006) Arsenic compounds in the treatment of multiple myeloma: a new role for a historical remedy. Clin Lymphoma Myeloma, 7: 192–198.

117. Liu Y-F, Zhu Y-M, Shi Z-Z, Li J-M, Wang L, Chen Y, Shen Z-X, Hu J (2006) Long-Term Follow-Up Confirms the Benefit of All-Trans Retinoic Acid (ATRA) and Arsenic Trioxide (As_2O_3) as Front Line Therapy for Newly Diagnosed Acute Promyelocytic Leukemia (APL). Blood, 108: 565–565.

118. Sun RC, Board PG, Blackburn AC (2011) Targeting metabolism with arsenic trioxide and dichloroacetate in breast cancer cells. Mol Cancer, 10: 142.

119. Chen H, Pazicni S, Krett NL, Ahn RW, Penner-Hahn JE, Rosen ST, O'Halloran TV (2009) Coencapsulation of Arsenic- and Platinum-based Drugs for Targeted Cancer Treatment. Angew Chem Int Ed, 48: 9295–9299.

120. Hernandez-Delgadillo R, García-Cuéllar CM, Sánchez-Pérez Y, Pineda-Aguilar N, Martínez-Martínez MA, Rangel-Padilla EE, Nakagoshi-Cepeda SE, Solís-Soto JM, Sánchez-Nájera RI, Nakagoshi-Cepeda MAA, Chellam S, Cabral-Romero C (2018) In vitro evaluation of the antitumor effect of bismuth lipophilic nanoparticles (BisBAL NPs) on breast cancer cells. Int J Nanomedicine, 13: 6089–6097.

121. Lümmen G, Sperling H, Luboldt H, Otto T, Rübben H (1998) Phase II trial of titanocene dichloride in advanced renal-cell carcinoma. Cancer Chemother Pharmacol, 42: 415–417.

122. Kröger N, Kleeberg U, Mross K, Edler L, Hossfeld D (2000) Phase II Clinical Trial of Titanocene Dichloride in Patients with Metastatic Breast Cancer. Onkologie, 23: 60–62.

123. Kostova I (2009) Titanium and vanadium complexes as anticancer agents. Anticancer Agents Med Chem, 9: 827–842.

124. Leon IE, Cadavid-Vargas JF, Di Virgilio AL, Etcheverry SB (2017) Vanadium, Ruthenium and Copper Compounds: A New Class of Nonplatinum Metallodrugs with Anticancer Activity. Curr Med Chem, 24: 112–148.

125. Nair RS, Kuriakose M, Somasundaram V, Shenoi V, Kurup MRP, Srinivas P (2014) The molecular response of vanadium complexes of nicotinoyl hydrazone in

cervical cancers--a possible interference with HPV oncogenic markers. Life Sci, 116: 90–97.

126. Bakhshi Aliabad H, Khanamani Falahati-pour S, Ahmadirad H, Mohamadi M, Hajizadeh MR, Mahmoodi M (2018) Vanadium complex: an appropriate candidate for killing hepatocellular carcinoma cancerous cells. Biometals, 31: 981–990.

127. Vojtek M, Marques MPM, Ferreira IMPLVO, Mota-Filipe H, Diniz C (2019) Anticancer activity of palladium-based complexes against triple-negative breast cancer. Drug Discov Today, 24: 1044–1058.

128. Jahromi EZ, Divsalar A, Saboury AA, Khaleghizadeh S, Mansouri-Torshizi H, Kostova I (2016) Palladium complexes: new candidates for anti-cancer drugs. J Iran Chem Soc, 13: 967–989.

129. Ulukaya E, Ari F, Dimas K, Ikitimur EI, Guney E, Yilmaz VT (2011) Anti-cancer activity of a novel palladium(II) complex on human breast cancer cells in vitro and in vivo. Eur J Med Chem, 46: 4957–4963.

130. Lin K, Zhao Z-Z, Bo H-B, Hao X-J, Wang J-Q (2018) Applications of Ruthenium Complex in Tumor Diagnosis and Therapy. Front Pharmacol, 9: 1323.

131. Pierroz V, Joshi T, Leonidova A, Mari C, Schur J, Ott I, Spiccia L, Ferrari S, Gasser G (2012) Molecular and Cellular Characterization of the Biological Effects of Ruthenium(II) Complexes Incorporating 2-Pyridyl-2-pyrimidine-4-carboxylic Acid. J Am Chem Soc, 134: 20376–20387.

132. Wang J-Q, Zhang P-Y, Ji L-N, Chao H (2015) A ruthenium(II) complex inhibits tumor growth in vivo with fewer side-effects compared with cisplatin. J Inorg Biochem, 146: 89–96.

133. Zeng L, Gupta P, Chen Y, Wang E, Ji L, Chao H, Chen Z-S (2017) The development of anticancer ruthenium(II) complexes: from single molecule compounds to nanomaterials. Chem Soc Rev, 46: 5771–5804.

134. Hartinger CG, Groessl M, Meier SM, Casini A, Dyson PJ (2013) Application of mass spectrometric techniques to delineate the modes-of-action of anticancer metallodrugs. Chem Soc Rev, 42: 6186–6199.

135. Bergamo A, Gava B, Alessio E, Mestroni G, Serli B, Cocchietto M, Zorzet S, Sava G (2002) Ruthenium-based NAMI-A type complexes with in vivo selective metastasis reduction and in vitro invasion inhibition unrelated to cell cytotoxicity. Int J Oncol, 21: 1331–1338.

136. Bacac M, Vadori M, Sava G, Pacor S (2004) Cocultures of metastatic and host immune cells: selective effects of NAMI-A for tumor cells. Cancer Immunol Immunother CII, 53: 1101–1110.

137. Alessio E, Messori L (2019) NAMI-A and KP1019/1339, Two Iconic Ruthenium Anticancer Drug Candidates Face-to-Face: A Case Story in Medicinal Inorganic Chemistry. Molecules, 24: 1995.

138. Schmitt F, Govindaswamy P, Süss-Fink G, Ang WH, Dyson PJ, Juillerat-Jeanneret L, Therrien B (2008) Ruthenium Porphyrin Compounds for Photodynamic Therapy of Cancer. J Med Chem, 51: 1811–1816.

139. Frasconi M, Liu Z, Lei J, Wu Y, Strekalova E, Malin D, Ambrogio MW, Chen X, Botros YY, Cryns VL, Sauvage J-P, Stoddart JF (2013) Photoexpulsion of surface-grafted ruthenium complexes and subsequent release of cytotoxic cargos to cancer cells from mesoporous silica nanoparticles. J Am Chem Soc, 135: 11603–11613.

140. Lu X, Wu Y-M, Yang J-M, Ma F-E, Li L-P, Chen S, Zhang Y, Ni Q-L, Pan Y-M, Hong X, Peng Y (2018) Preparation of Rhodium(III) complexes with 2(1H)-quinolinone derivatives and evaluation of their in vitro and in vivo antitumor activity. Eur J Med Chem, 151: 226–236.

141. Majer Z, Bősze S, Szabó I, Mihucz VG, Gaál A, Szilvágyi G, Pepponi G, Meirer F, Wobrauschek P, Szoboszlai N, Ingerle D, Streli C (2015) Study of dinuclear Rh(II) complexes of phenylalanine derivatives as potential anticancer agents by using X-ray fluorescence and X-ray absorption. Microchem J, 120: 51–57.

142. Katsaros N, Anagnostopoulou A (2002) Rhodium and its compounds as potential agents in cancer treatment. Crit Rev Oncol Hematol, 42: 297–308.

143. Khan T-M, Gul NS, Lu X, Kumar R, Choudhary MI, Liang H, Chen Z-F (2019) Rhodium(III) complexes with isoquinoline derivatives as potential anticancer agents: in vitro and in vivo activity studies. Dalton Trans, 48: 11469–11479.

144. Calamai P, Carotti S, Guerri A, Messori L, Mini E, Orioli P, Speroni GP (1997) Biological properties of two gold(III) complexes: AuCl3(Hpm) and AuCl2(pm). J Inorg Biochem, 66: 103–109.

145. Bertrand B, Williams MRM, Bochmann M (2018) Gold(III) Complexes for Antitumor Applications: An Overview. Chem – Eur J, 24: 11840–11851.

146. Jain S, Hirst DG, O'Sullivan JM (2012) Gold nanoparticles as novel agents for cancer therapy. Br J Radiol, 85: 101–113.

147. Mohd Sofyan NRF, Nordin FJ, Mohd Abd Razak MR, Abdul Halim SN 'Ain, Mohd Khir NAF, Muhammad A, Rajab NF, Sarip R (2018) New Silver Complexes with Mixed Thiazolidine and Phosphine Ligands as Highly Potent Antimalarial and Anticancer Agents. In: J. Chem. 18: 1-10.

148. Holmes J, Kearsey RJ, Paske KA, Singer FN, Atallah S, Pask CM, Phillips RM, Willans CE (2019) Tethered N-Heterocyclic Carbene-Carboranyl Silver Complexes for Cancer Therapy. Organometallics, 38: 2530–2538.

149. Vlăsceanu GM, Marin Ş, Ţiplea RE, Bucur IR, Lemnaru M, Marin MM, Grumezescu AM, Andronescu E (2016) Chapter 2 - Silver nanoparticles in cancer therapy. In: Grumezescu AM (ed) Nanobiomaterials in Cancer Therapy. William Andrew Publishing, pp 29–56.

150. Wani WA, Baig U, Shreaz S, Shiekh RA, Iqbal PF, Jameel E, Ahmad A, Mohd-Setapar SH, Mushtaque M, Hun LT (2016) Recent advances in iron complexes as potential anticancer agents. New J Chem, 40: 1063–1090.

151. Zhang P, Sadler PJ (2017) Redox-Active Metal Complexes for Anticancer Therapy. Eur J Inorg Chem, 2017: 1541–1548.

152. Mojžišová G, Mojžiš J, Vašková J (2014) Organometallic iron complexes as potential cancer therapeutics. Acta Biochim Pol, 61: 651–654.

153. Carmona-Negrón JA, Santana A, Rheingold AL, Meléndez E (2019) Synthesis, structure, docking and cytotoxic studies of ferrocene-hormone conjugates for hormone-dependent breast cancer application. Dalton Trans Camb Engl 2003, 48: 5952–5964.

154. Milosavljevic V, Haddad Y, Merlos Rodrigo MA, Moulick A, Polanska H, Hynek D, Heger Z, Kopel P, Adam V (2016) The Zinc-Schiff Base-Novicidin Complex as a Potential Prostate Cancer Therapy. PLoS ONE, 11: e0204441.

155. Lee Y-H, Tuyet P-T (2019) Synthesis and biological evaluation of quercetin–zinc (II) complex for anti-cancer and anti-metastasis of human bladder cancer cells. Vitro Cell Dev Biol - Anim, 55: 395–404.

156. Marloye M, Berger G, Gelbcke M, Dufrasne F (2016) A survey of the mechanisms of action of anticancer transition metal complexes. Future Med Chem, 8: 2263–2286.

157. Frezza M, Hindo S, Chen D, Davenport A, Schmitt S, Tomco D, Dou QP (2010) Novel Metals and Metal Complexes as Platforms for Cancer Therapy. Curr Pharm Des, 16: 1813–1825.

158. Jung M, Mertens C, Tomat E, Brüne B (2019) Iron as a Central Player and Promising Target in Cancer Progression. Int J Mol Sci, 20: 273.

159. Cserepes M, Türk D, Tóth S, Pape VFS, Gaál A, Gera M, Szabó JE, Kucsma N, Várady G, Vértessy BG, Streli C, Szabó PT, Tovari J, Szoboszlai N, Szakács G (2020) Unshielding Multidrug Resistant Cancer through Selective Iron Depletion of P-Glycoprotein-Expressing Cells. Cancer Res, 80: 663–674.

160. Costello LC, Franklin RB (2012) Cytotoxic/tumor suppressor role of zinc for the treatment of cancer: an enigma and an opportunity. Expert Rev Anticancer Ther, 12: 121–128.

161. Hashemi M, Ghavami S, Eshraghi M, Booy EP, Los M (2007) Cytotoxic effects of intra and extracellular zinc chelation on human breast cancer cells. Eur J Pharmacol, 557: 9–19.

162. Xue J, Moyer A, Peng B, Wu J, Hannafon BN, Ding W-Q (2014) Chloroquine Is a Zinc Ionophore. PLoS ONE, 9: e109180.

163. Velthuis AJW te, Worm SHE van den, Sims AC, Baric RS, Snijder EJ, Hemert MJ van (2010) Zn2+ Inhibits Coronavirus and Arterivirus RNA Polymerase Activity In Vitro and Zinc Ionophores Block the Replication of These Viruses in Cell Culture. PLOS Pathog, 6: e1001176.

164. Yu X, Vazquez A, Levine AJ, Carpizo DR (2012) Allele-specific p53 mutant reactivation. Cancer Cell, 21: 614–625.

165. Kogan S, Carpizo DR (2018) Zinc Metallochaperones as Mutant p53 Reactivators: A New Paradigm in Cancer Therapeutics. Cancers, 10: 166.

166. Salim KY, Maleki Vareki S, Danter WR, Koropatnick J (2016) COTI-2, a novel small molecule that is active against multiple human cancer cell lines in vitro and in vivo. Oncotarget, 7: 41363–41379.

167. Zaman S, Yu X, Bencivenga AF, Blanden AR, Liu Y, Withers T, Na B, Blayney AJ, Gilleran J, Boothman DA, Loh SN, Kimball SD, Carpizo DR (2019) Combinatorial Therapy of Zinc Metallochaperones with Mutant p53 Reactivation and Diminished Copper Binding. Mol Cancer Ther, 18: 1355–1365.

168. Denoyer D, Masaldan S, La Fontaine S, Cater MA (2015) Targeting copper in cancer therapy: "Copper That Cancer." Met Integr Biometal Sci, 7: 1459–1476.

169. Lopez J, Ramchandani D, Vahdat L. Copper Depletion as a Therapeutic Strategy in Cancer. In: Peggy L. (ed) CarverEssential Metals in Medicine: Therapeutic Use and Toxicity of Metal Ions in the Clinic. Met Ions Life Sci, 19: 304-322.

170. Kim Y-J, Tsang T, Anderson GR, Posimo JM, Brady DC (2020) Inhibition of BCL2 family members increases the efficacy of copper chelation in BRAFV600E-driven melanoma. Cancer Res. https://doi.org/10.1158/0008-5472.CAN-19-1784

171. Ishida S, McCormick F, Smith-McCune K, Hanahan D (2010) Enhancing Tumor-Specific Uptake of the Anticancer Drug Cisplatin with a Copper Chelator. Cancer Cell, 17: 574–583.

172. Sinha W, Sommer MG, Deibel N, Ehret F, Bauer M, Sarkar B, Kar S (2015) Experimental and Theoretical Investigations of the Existence of CuII, CuIII, and CuIV in Copper Corrolato Complexes. Angew Chem Int Ed, 54: 13769–13774.

173. Marzano C, Pellei M, Santini FT and C (2009) Copper Complexes as Anticancer Agents. Anticancer Agents Med. Chem, 9: 185-211.

174. Padhyé S, Kauffman GB (1985) Transition metal complexes of semicarbazones and thiosemicarbazones. Coord Chem Rev, 63: 127–160.

175. Denoyer D, Clatworthy SAS, Cater MA (2018) Copper Complexes in Cancer Therapy. Met Ions Life Sci, 18: 469–506.

176.   Santini C, Pellei M, Gandin V, Porchia M, Tisato F, Marzano C (2014) Advances in copper complexes as anticancer agents. Chem Rev, 114: 815–862.

177.   Tisato F, Marzano C, Porchia M, Pellei M, Santini C (2010) Copper in diseases and treatments, and copper-based anticancer strategies. Med Res Rev, 30: 708–749.

178.   Sîrbu A, Palamarciuc O, Babak MV, Lim JM, Ohui K, Enyedy EA, Shova S, Darvasiová D, Rapta P, Ang WH, Arion VB (2017) Copper(II) thiosemicarbazone complexes induce marked ROS accumulation and promote nrf2-mediated antioxidant response in highly resistant breast cancer cells. Dalton Trans, 46: 3833–3847.

179.   Mohindru A, Fisher JM, Rabinovitz M (1983) 2,9-Dimethyl-1,10-phenanthroline (neocuproine): a potent, copper-dependent cytotoxin with anti-tumor activity. Biochem Pharmacol, 32: 3627–3632.

180.   Lovejoy DB, Jansson PJ, Brunk UT, Wong J, Ponka P, Richardson DR (2011) Antitumor activity of metal-chelating compound Dp44mT is mediated by formation of a redox-active copper complex that accumulates in lysosomes. Cancer Res, 71: 5871–5880.

181.   Mohindru A, Fisher JM, Rabinovitz M (1983) Bathocuproine sulphonate: a tissue culture-compatible indicator of copper-mediated toxicity. Nature, 303: 64–65.

182.   Van Giessen GJ, Crim JA, Petering DH, Petering HG (1973) Effect of heavy metals on the in vitro cytotoxicity of 3-ethoxy-2-oxobutyraldehyde bis (thiosemicarbazone) and related compounds. J Natl Cancer Inst, 51: 139–146.

183.   Bhuyan BK, Betz T (1968) Studies on the Mode of Action of the Copper(II)Chelate of 2-Keto-3-ethoxybutyraldehyde-bis(thiosemicarbazone). Cancer Res, 28: 758–763.

184.   Wehbe M, Leung AWY, Abrams MJ, Orvig C, Bally MB (2017) A Perspective – can copper complexes be developed as a novel class of therapeutics? Dalton Trans, 46: 10758–10773.

185.   Berners-Price SJ, Sadler PJ. Phosphines and metal phosphine complexes: Relationship of chemistry to anticancer and other biological activity. In: Aisen P. (ed) Bioinorganic Chemistry. Springer, Berlin, Heidelberg, 1988: 27–102.

186.   Ruiz-Azuara L, Bastian G, Bravo-Gómez ME, Cañas RC, Flores-Alamo M, Fuentes I, Mejia C, García-Ramos JC, Serrano A (2014) Abstract CT408: Phase I study of one mixed chelates copper(II) compound, Casiopeína CasIIIia with antitumor activity and its mechanism of action. Cancer Res, 74: CT408–CT408.

187.   Alemón-Medina R, Breña-Valle M, Muñoz-Sánchez JL, Gracia-Mora MI, Ruiz-Azuara L (2007) Induction of oxidative damage by copper-based antineoplastic drugs (Casiopeínas). Cancer Chemother Pharmacol, 60: 219–228.

188.   Kamah S, Vilaplana R, Moreno J, Akdi K, García-Herdugo G, González-Vílchez F (2000) Isolation, Characterization and Antitumour Propirties of the 1,2-Popylenediaminetetraacetate trans-Diaqua-Copper (II). Met-Based Drugs, 7: 219–24.

189. Gou Y, Zhang Y, Qi J, Chen S, Zhou Z, Wu X, Liang H, Yang F (2016) Developing an anticancer copper(II) pro-drug based on the nature of cancer cell and human serum albumin carrier IIA subdomain: mouse model of breast cancer. Oncotarget, 7: 67004–67019.

190. Ahmad M, Suhaimi S-N, Chu T-L, Aziz NA, Kornain N-KM, Samiulla DS, Lo K-W, Ng C-H, Khoo AS-B (2018) Ternary copper(II) complex: NCI60 screening, toxicity studies, and evaluation of efficacy in xenograft models of nasopharyngeal carcinoma. PLOS ONE, 13: e0191295.

191. Palanimuthu D, Shinde SV, Somasundaram K, Samuelson AG (2013) In Vitro and in Vivo Anticancer Activity of Copper Bis(thiosemicarbazone) Complexes. J Med Chem, 56: 722–734.

192. Carcelli M, Tegoni M, Bartoli J, Marzano C, Pelosi G, Salvalaio M, Rogolino D, Gandin V (2020) In vitro and in vivo anticancer activity of tridentate thiosemicarbazone copper complexes: Unravelling an unexplored pharmacological target. Eur J Med Chem, 194: 112266.

193. Schimmer AD, Jitkova Y, Gronda M, Wang Z, Brandwein J, Chen C, Gupta V, Schuh A, Yee K, Chen J, Ackloo S, Booth T, Keays S, Minden MD (2012) A phase I study of the metal ionophore clioquinol in patients with advanced hematologic malignancies. Clin Lymphoma Myeloma Leuk, 12: 330–336.

194. Lainé A-L, Passirani C (2012) Novel metal-based anticancer drugs: a new challenge in drug delivery. Curr Opin Pharmacol, 12: 420–426.

195. Shi X, Chen Z, Wang Y, Guo Z, Wang X (2018) Hypotoxic copper complexes with potent anti-metastatic and anti-angiogenic activities against cancer cells. Dalton Trans, 47: 5049–5054.

196. Shobha Devi C, Thulasiram B, Aerva RR, Nagababu P (2018) Recent Advances in Copper Intercalators as Anticancer Agents. J Fluoresc, 28: 1195–1205.

197. Larrick JW, Cresswell P (1979) Modulation of cell surface iron transferrin receptors by cellular density and state of activation. J Supramol Struct, 11: 579–586.

198. Whitnall M, Howard J, Ponka P, Richardson DR (2006) A class of iron chelators with a wide spectrum of potent antitumor activity that overcomes resistance to chemotherapeutics. Proc Natl Acad Sci U S A, 103: 14901–14906.

199. Yuan J, Lovejoy DB, Richardson DR (2004) Novel di-2-pyridyl-derived iron chelators with marked and selective antitumor activity: in vitro and in vivo assessment. Blood, 104: 1450–1458.

200. Rao VA, Klein SR, Agama KK, Toyoda E, Adachi N, Pommier Y, Shacter EB (2009) The iron chelator Dp44mT causes DNA damage and selective inhibition of topoisomerase IIalpha in breast cancer cells. Cancer Res, 69: 948–957.

201. Jansson PJ, Sharpe PC, Bernhardt PV, Richardson DR (2010) Novel thiosemicarbazones of the ApT and DpT series and their copper complexes: identification of pronounced redox activity and characterization of their antitumor activity. J Med Chem, 53: 5759–5769.

202. Heffeter P, Pape VFS, Enyedy ÉA, Keppler BK, Szakacs G, Kowol CR (2018) Anticancer Thiosemicarbazones: Chemical Properties, Interaction with Iron Metabolism, and Resistance Development. Antioxid Redox Signal. 30: 1062-1082.

203. Chen S-H, Lin J-K, Liu S-H, Liang Y-C, Lin-Shiau S-Y (2008) Apoptosis of Cultured Astrocytes Induced by the Copper and Neocuproine Complex through Oxidative Stress and JNK Activation. Toxicol Sci, 102: 138–149.

204. Xiao Y, Chen D, Zhang X, Cui Q, Fan Y, Bi C, Dou QP (2010) Molecular study on copper-mediated tumor proteasome inhibition and cell death. Int J Oncol, 37: 81–87.

205. Zhu BZ, Chevion M (2000) Copper-mediated toxicity of 2,4,5-trichlorophenol: biphasic effect of the copper(I)-specific chelator neocuproine. Arch Biochem Biophys, 380: 267–273.

206. Zhu B-Z, Carr AC, Frei B (2002) Pyrrolidine dithiocarbamate is a potent antioxidant against hypochlorous acid-induced protein damage. FEBS Lett, 532: 80–84.

207. Chen D, Peng F, Cui QC, Daniel KG, Orlu S, Liu J, Dou QP (2005) Inhibition of prostate cancer cellular proteasome activity by a pyrrolidine dithiocarbamate-copper complex is associated with suppression of proliferation and induction of apoptosis. Front Biosci J Virtual Libr, 10: 2932–2939.

208. Jain S, Chandra V, Kumar Jain P, Pathak K, Pathak D, Vaidya A (2019) Comprehensive review on current developments of quinoline-based anticancer agents. Arab J Chem, 12: 4920–4946.

209. Solomon VR, Lee H (2011) Quinoline as a privileged scaffold in cancer drug discovery. Curr Med Chem, 18: 1488–1508.

210. Zwergel C, Fioravanti R, Stazi G, Sarno F, Battistelli C, Romanelli A, Nebbioso A, Mendes E, Paulo A, Strippoli R, Tripodi M, Pechalrieu D, Arimondo PB, De Luca T, Del Bufalo D, Trisciuoglio D, Altucci L, Valente S, Mai A (2020) Novel Quinoline Compounds Active in Cancer Cells through Coupled DNA Methyltransferase Inhibition and Degradation. Cancers, 12: 447.

211. Sgarlata C, Arena G, Bonomo RP, Giuffrida A, Tabbì G (2018) Simple and mixed complexes of copper(II) with 8-hydroxyquinoline derivatives and amino acids: Characterization in solution and potential biological implications. J Inorg Biochem, 180: 89–100.

212.   Xie F, Cai H, Peng F (2018) Anti-prostate cancer activity of 8-hydroxyquinoline-2-carboxaldehyde-thiosemicarbazide copper complexes in vivo by bioluminescence imaging. J Biol Inorg Chem JBIC Publ Soc Biol Inorg Chem, 23: 949–956.

213.   Jiang H, Taggart JE, Zhang X, Benbrook DM, Lind SE, Ding W-Q (2011) Nitroxoline (5-amino-8-hydroxyquinoline) is more a potent anti-cancer agent than clioquinol (5-chloro-7-iodo-8-quinoline). Cancer Lett, 312: 11–17.

214.   Schimmer AD (2011) Clioquinol - a novel copper-dependent and independent proteasome inhibitor. Curr Cancer Drug Targets, 11: 325–331.

215.   Daniel KG, Gupta P, Harbach RH, Guida WC, Dou QP (2004) Organic copper complexes as a new class of proteasome inhibitors and apoptosis inducers in human cancer cells. Biochem Pharmacol, 67: 1139–1151.

216.   Pape VFS, May NV, Gál GT, Szatmári I, Szeri F, Fülöp F, Szakács G, Enyedy ÉA (2018) Impact of copper and iron binding properties on the anticancer activity of 8-hydroxyquinoline derived Mannich bases. Dalton Trans Camb Engl 2003, 47: 17032–17045.

217. Schilt AA. Analytical Applications of 1,10-Phenanthroline and Related Compounds. In: International Series of Monographs in Analytical Chemistry. Pergamon Press, Oxford, 1969: 1-193.

218.   Starosta R, Brzuszkiewicz A, Bykowska A, Komarnicka UK, Bażanów B, Florek M, Gadzała Ł, Jackulak N, Król J, Marycz K (2013) A novel copper(I) complex, $[CuI(2,2'-biquinoline)P(CH_2N(CH_2CH_2)_2O)_3]$ – Synthesis, characterisation and comparative studies on biological activity. Polyhedron, 50: 481–489.

219.   Zhao Q, Yu M, Shi L, Liu S, Li C, Shi M, Zhou Z, Huang C, Li F (2010) Cationic Iridium(III) Complexes with Tunable Emission Color as Phosphorescent Dyes for Live Cell Imaging. Organometallics, 29: 1085–1091.

220.   Chan H, Ghrayche JB, Wei J, Renfrew AK (2017) Photolabile Ruthenium(II)–Purine Complexes: Phototoxicity, DNA Binding, and Light-Triggered Drug Release. Eur J Inorg Chem, 2017: 1679–1686.

221.   Zhang J, Li L, Ma L, Zhang F, Zhang Z, Wang S (2011) Synthesis, characterization and cytotoxicity of mixed-ligand complexes of palladium(II) with 2, 2′-biquinoline/1, 4-diaminobutane and 4-toluenesulfonyl-L-amino acid dianion. Eur J Med Chem, 46: 5711–5716.

222. Ntoi LLA, Buitendach BE, von Eschwege KG (2017) Seven Chromisms Associated with Dithizone. J Phys Chem A, 121: 9243–9251.

223. MCNARY WF (1954) ZINC-DITHIZONE REACTION OF PANCREATIC ISLETS. J Histochem Cytochem, 2: 185–195.

224. Ricordi C, Gray DW, Hering BJ, Kaufman DB, Warnock GL, Kneteman NM, Lake SP, London NJ, Socci C, Alejandro R (1990) Islet isolation assessment in man and large animals. Acta Diabetol Lat, 27: 185–195.

225. Khiatah B, Qi M, Wu Y, Chen K-T, Perez R, Valiente L, Omori K, Isenberg JS, Kandeel F, Yee J-K, Al-Abdullah IH (2019) Pancreatic human islets and insulin-producing cells derived from embryonic stem cells are rapidly identified by a newly developed Dithizone. Sci Rep, 9: 1–6.

226. Lo M-C (1960) Clinical Application of Diphenylthiocarbazone (Dithizone) in Carcinoma of the Prostate. Can Med Assoc J, 82: 1203–1216.

227. Mackenzie AR, Bhisitkul IP, Whitmore WF (1963) The treatment of metastatic prostatic cancer with dithizone (diphenylthiocarbazone). Invest Urol, 1:229-37.

228. Kohroki J, Muto N, Tanaka T, Itoh N, Inada A, Tanaka K (1998) Induction of differentiation and apoptosis by dithizone in human myeloid leukemia cell lines. Leuk Res, 22: 405–412.

229. Park K (2014) Controlled drug delivery systems: past forward and future back. J Control Release, 190: 3–8.

230. Li C, Wang J, Wang Y, Gao H, Wei G, Huang Y, Yu H, Gan Y, Wang Y, Mei L, Chen H, Hu H, Zhang Z, Jin Y (2019) Recent progress in drug delivery. Acta Pharm Sin B, 9: 1145–1162.

231. Menezes P dos P, Andrade T de A, Frank LA, de Souza EPBSS, Trindade G das GG, Trindade IAS, Serafini MR, Guterres SS, Araújo AA de S (2019) Advances of nanosystems containing cyclodextrins and their applications in pharmaceuticals. Int J Pharm, 559: 312–328.

232. Soppimath KS, Aminabhavi TM, Kulkarni AR, Rudzinski WE (2001) Biodegradable polymeric nanoparticles as drug delivery devices. J Control Release, 70: 1–20.

233. Haley RM, Gottardi R, Langer R, Mitchell MJ (2020) Cyclodextrins in drug delivery: applications in gene and combination therapy. Drug Deliv Transl Res. https://doi.org/10.1007/s13346-020-00724-5

234. Parmar V, Patel G, Abu-Thabit NY (2018) 20 - Responsive cyclodextrins as polymeric carriers for drug delivery applications. In: Makhlouf ASH, Abu-Thabit NY (eds) Stimuli Responsive Polymeric Nanocarriers for Drug Delivery Applications, Volume 1. Woodhead Publishing, pp 555–580

235. Daraee H, Etemadi A, Kouhi M, Alimirzalu S, Akbarzadeh A (2016) Application of liposomes in medicine and drug delivery. Artif Cells Nanomedicine Biotechnol, 44: 381–391.

236. Chen S, Hao X, Liang X, Zhang Q, Zhang C, Zhou G, Shen S, Jia G, Zhang J (2016) Inorganic Nanomaterials as Carriers for Drug Delivery. J Biomed Nanotechnol, 12: 1–27.

237. Zhao M-X, Zeng E-Z, Zhu B-J (2015) The Biological Applications of Inorganic Nanoparticle Drug Carriers. ChemNanoMat, 1: 82–91.

238. Liang R, Wei M, Evans DG, Duan X (2014) Inorganic nanomaterials for bioimaging, targeted drug delivery and therapeutics. Chem Commun, 50: 14071–14081.

239. Li Y, Maciel D, Rodrigues J, Shi X, Tomás H (2015) Biodegradable Polymer Nanogels for Drug/Nucleic Acid Delivery. Chem Rev, 115: 8564–8608.

240. Dreiss CA (2020) Hydrogel design strategies for drug delivery. Curr Opin Colloid Interface Sci, 48: 1–17.

241. Narayanaswamy R, Torchilin VP (2019) Hydrogels and Their Applications in Targeted Drug Delivery. Mol Basel Switz, 24:

242. Garg T, Singh O, Arora S, Murthy R (2012) Scaffold: a novel carrier for cell and drug delivery. Crit Rev Ther Drug Carrier Syst, 29: 1–63.

243. Kretlow JD, Klouda L, Mikos AG (2007) Injectable matrices and scaffolds for drug delivery in tissue engineering. Adv Drug Deliv Rev, 59: 263–273.

244. Zhang Y, Sun T, Jiang C (2018) Biomacromolecules as carriers in drug delivery and tissue engineering. Acta Pharm Sin B, 8: 34–50.

245. Hossen S, Hossain MK, Basher MK, Mia MNH, Rahman MT, Uddin MJ (2019) Smart nanocarrier-based drug delivery systems for cancer therapy and toxicity studies: A review. J Adv Res, 15: 1–18.

246. Senapati S, Mahanta AK, Kumar S, Maiti P (2018) Controlled drug delivery vehicles for cancer treatment and their performance. Signal Transduct Target Ther, 3: 7.

247. Matsumura Y, Maeda H (1986) A new concept for macromolecular therapeutics in cancer chemotherapy: mechanism of tumoritropic accumulation of proteins and the antitumor agent smancs. Cancer Res, 46: 6387–6392.

248. Rabanel JM, Aoun V, Elkin I, Mokhtar M, Hildgen P (2012) Drug-loaded nanocarriers: passive targeting and crossing of biological barriers. Curr Med Chem, 19: 3070–3102.

249. Tiwari G, Tiwari R, Sriwastawa B, Bhati L, Pandey S, Pandey P, Bannerjee SK (2012) Drug delivery systems: An updated review. Int J Pharm Investig, 2: 2–11.

250. Lee Y, Thompson DH (2017) Stimuli-Responsive Liposomes for Drug Delivery. Wiley Interdiscip Rev Nanomed Nanobiotechnol, 9: 10.

251. Kalaydina R-V, Bajwa K, Qorri B, Decarlo A, Szewczuk MR (2018) Recent advances in "smart" delivery systems for extended drug release in cancer therapy. Int J Nanomedicine, 13: 4727–4745.

252. Iwamoto T (2013) Clinical application of drug delivery systems in cancer chemotherapy: review of the efficacy and side effects of approved drugs. Biol Pharm Bull, 36: 715–718.

253. Kim MW, Kwon S-H, Choi JH, Lee A (2018) A Promising Biocompatible Platform: Lipid-Based and Bio-Inspired Smart Drug Delivery Systems for Cancer Therapy. Int J Mol Sci, 19: 3859.

254. Yingchoncharoen P, Kalinowski DS, Richardson DR (2016) Lipid-Based Drug Delivery Systems in Cancer Therapy: What Is Available and What Is Yet to Come. Pharmacol Rev, 68: 701–787.

255. Shrestha H, Bala R, Arora S (2014) Lipid-Based Drug Delivery Systems. In: J. Pharm. https://www.hindawi.com/journals/jphar/2014/801820/. Accessed 2 Apr 2020

256. Beltrán-Gracia E, López-Camacho A, Higuera-Ciapara I, Velázquez-Fernández JB, Vallejo-Cardona AA (2019) Nanomedicine review: clinical developments in liposomal applications. Cancer Nanotechnol, 10: 11.

257. Shah MK, Khatri P, Vora N, Patel NK, Jain S, Lin S (2019) Chapter 5 - Lipid nanocarriers: Preparation, characterization and absorption mechanism and applications to improve oral bioavailability of poorly water-soluble drugs. In: Grumezescu AM (ed) Biomedical Applications of Nanoparticles. William Andrew Publishing, pp 117–147

258. Home - ClinicalTrials.gov. https://clinicaltrials.gov/. Accessed 1 Apr 2020

259. EU Clinical Trials Register - Update. https://www.clinicaltrialsregister.eu/. Accessed 1 Apr 2020

260. Juliano RL, Stamp D (1975) The effect of particle size and charge on the clearance rates of liposomes and liposome encapsulated drugs. Biochem Biophys Res Commun, 63: 651–658.

261. Bourquin J, Milosevic A, Hauser D, Lehner R, Blank F, Petri-Fink A, Rothen-Rutishauser B (2018) Biodistribution, Clearance, and Long-Term Fate of Clinically Relevant Nanomaterials. Adv Mater Deerfield Beach Fla, 30: e1704307.

262. Kraft JC, Freeling JP, Wang Z, Ho RJY (2014) Emerging research and clinical development trends of liposome and lipid nanoparticle drug delivery systems. J Pharm Sci, 103: 29–52.

263. Maranhão RC, Vital CG, Tavoni TM, Graziani SR (2017) Clinical experience with drug delivery systems as tools to decrease the toxicity of anticancer chemotherapeutic agents. Expert Opin Drug Deliv, 14: 1217–1226.

264. Li W, Zhan P, De Clercq E, Lou H, Liu X (2013) Current drug research on PEGylation with small molecular agents. Prog Polym Sci, 38: 421–444.

265. Allen TM, Hansen C, Martin F, Redemann C, Yau-Young A (1991) Liposomes containing synthetic lipid derivatives of poly(ethylene glycol) show prolonged circulation half-lives in vivo. Biochim Biophys Acta BBA - Biomembr, 1066: 29–36.

266. Allen C, Dos Santos N, Gallagher R, Chiu GNC, Shu Y, Li WM, Johnstone SA, Janoff AS, Mayer LD, Webb MS, Bally MB (2002) Controlling the physical behavior and biological performance of liposome formulations through use of surface grafted poly(ethylene glycol). Biosci Rep, 22: 225–250.

267. Newman MS, Colbern GT, Working PK, Engbers C, Amantea MA (1999) Comparative pharmacokinetics, tissue distribution, and therapeutic effectiveness of cisplatin encapsulated in long-circulating, pegylated liposomes (SPI-077) in tumor-bearing mice. Cancer Chemother Pharmacol, 43: 1–7.

268. Deshpande PP, Biswas S, Torchilin VP (2013) Current trends in the use of liposomes for tumor targeting. Nanomed, 8: 1509-1528.

269. Suzuki T, Ichihara M, Hyodo K, Yamamoto E, Ishida T, Kiwada H, Ishihara H, Kikuchi H (2012) Accelerated blood clearance of PEGylated liposomes containing doxorubicin upon repeated administration to dogs. Int J Pharm, 436: 636–643.

270. Yang Q, Ma Y, Zhao Y, She Z, Wang L, Li J, Wang C, Deng Y (2013) Accelerated drug release and clearance of PEGylated epirubicin liposomes following repeated injections: a new challenge for sequential low-dose chemotherapy. Int J Nanomedicine, 8: 1257–1268.

271. Mishra P, Nayak B, Dey RK (2016) PEGylation in anti-cancer therapy: An overview. Asian J Pharm Sci, 11: 337–348.

272. Duggan ST, Keating GM (2011) Pegylated Liposomal Doxorubicin. Drugs, 71: 2531–2558.

273. Anselmo AC, Mitragotri S (2019) Nanoparticles in the clinic: An update. Bioeng Transl Med, 4: e10143.

274. Olusanya TOB, Haj Ahmad RR, Ibegbu DM, Smith JR, Elkordy AA (2018) Liposomal Drug Delivery Systems and Anticancer Drugs. Mol J Synth Chem Nat Prod Chem, 23:

275. Briuglia M-L, Rotella C, McFarlane A, Lamprou DA (2015) Influence of cholesterol on liposome stability and on in vitro drug release. Drug Deliv Transl Res, 5: 231–242.

276. Zununi Vahed S, Salehi R, Davaran S, Sharifi S (2017) Liposome-based drug co-delivery systems in cancer cells. Mater Sci Eng C, 71: 1327–1341.

277. Chiu GNC, Abraham SA, Ickenstein LM, Ng R, Karlsson G, Edwards K, Wasan EK, Bally MB (2005) Encapsulation of doxorubicin into thermosensitive liposomes via complexation with the transition metal manganese. J Control Release, 104: 271–288.

278. Schwendener RA, Wüthrich R, Duewell S, Wehrli E, von Schulthess GK (1990) A pharmacokinetic and MRI study of unilamellar gadolinium-, manganese-, and iron-DTPA-stearate liposomes as organ-specific contrast agents. Invest Radiol, 25: 922–932.

279. Pan D, Schmieder AH, Wickline SA, Lanza GM (2011) Manganese-based MRI contrast agents: past, present and future. Tetrahedron, 67: 8431–8444.

280. Allen TM, Cullis PR (2013) Liposomal drug delivery systems: From concept to clinical applications. Adv Drug Deliv Rev, 65: 36–48.

281. Bozzuto G, Molinari A (2015) Liposomes as nanomedical devices. Int J Nanomedicine, 10: 975–999.

282. Gangadaran P, Hong CM, Ahn B-C (2018) An Update on in Vivo Imaging of Extracellular Vesicles as Drug Delivery Vehicles. Front Pharmacol, 9: 169.

283. Xu R, Rai A, Chen M, Suwakulsiri W, Greening DW, Simpson RJ (2018) Extracellular vesicles in cancer - implications for future improvements in cancer care. Nat Rev Clin Oncol, 15: 617–638.

284. Monson CF, Cong X, Robison AD, Pace HP, Liu C, Poyton MF, Cremer PS (2012) Phosphatidylserine reversibly binds Cu2+ with extremely high affinity. J Am Chem Soc, 134: 7773–7779.

285. Mlakar M, Cuculić V, Frka S, Gašparović B (2018) Copper-phospholipid interaction at cell membrane model hydrophobic surfaces. Bioelectrochemistry, 120: 10–17.

286. Varga Z. PhD thesis: Structural perturbations in phospholipid model membrane systems: the effect of dihalogenated phenol compounds and metal ions. Budapest University of Technology and Economics, Budapest, 2009: 75-77.

287. Wang Y, Zeng S, Lin T-M, Krugner-Higby L, Lyman D, Steffen D, Xiong MP (2014) Evaluating the Anticancer Properties of Liposomal Copper in a Nude Mouse Xenograft Model of Human Prostate Cancer: Formulation, In Vitro, In Vivo, Histology and Tissue Distribution Studies. Pharm Res, 31: 3106–3119.

288. Wang Y, Zeng S, Lin T-M, Krugner-Higby L, Lyman D, Steffen D, Xiong MP (2014) Evaluating the Anticancer Properties of Liposomal Copper in a Nude Mouse Xenograft Model of Human Prostate Cancer: Formulation, In Vitro, In Vivo, Histology and Tissue Distribution Studies. Pharm Res, 31: 3106–3119.

289. Wehbe M, Anantha M, Shi M, Leung AW-Y, Dragowska WH, Sanche L, Bally MB (2017) Development and optimization of an injectable formulation of copper diethyldithiocarbamate, an active anticancer agent. Int J Nanomedicine, 12: 4129–4146.

290. Wehbe M, Malhotra AK, Anantha M, Lo C, Dragowska WH, Dos Santos N, Bally MB (2018) Development of a copper-clioquinol formulation suitable for intravenous use. Drug Deliv Transl Res, 8: 239–251.

291. Leung AWY, Anantha M, Dragowska WH, Wehbe M, Bally MB (2018) Copper-CX-5461: A novel liposomal formulation for a small molecule rRNA synthesis inhibitor. J Control Release, 286: 1–9.

292. Chen KTJ, Anantha M, Leung AWY, Kulkarni JA, Militao GGC, Wehbe M, Sutherland B, Cullis PR, Bally MB (2020) Characterization of a liposomal copper(II)-quercetin formulation suitable for parenteral use. Drug Deliv Transl Res, 10: 202–215.

293. Kheirolomoom A, Mahakian LM, Lai C-Y, Lindfors HA, Seo JW, Paoli EE, Watson KD, Haynam EM, Ingham ES, Xing L, Cheng RH, Borowsky AD, Cardiff RD, Ferrara KW (2010) Copper−Doxorubicin as a Nanoparticle Cargo Retains Efficacy with Minimal Toxicity. Mol Pharm, 7: 1948–1958.

294. Kheirolomoom A, Lai C-Y, Tam SM, Mahakian LM, Ingham ES, Watson KD, Ferrara KW (2013) Complete regression of local cancer using temperature-sensitive liposomes combined with ultrasound-mediated hyperthermia. J Control Release, 172: 266–273.

295. Al Sabbagh C, Tsapis N, Novell A, Calleja-Gonzalez P, Escoffre J-M, Bouakaz A, Chacun H, Denis S, Vergnaud J, Gueutin C, Fattal E (2015) Formulation and pharmacokinetics of thermosensitive stealth® liposomes encapsulating 5-Fluorouracil. Pharm Res, 32: 1585–1603.

296. Luo D, Goel S, Liu H-J, Carter KA, Jiang D, Geng J, Kutyreff CJ, Engle JW, Huang W-C, Shao S, Fang C, Cai W, Lovell JF (2017) Intrabilayer ^{64}Cu Labeling of Photoactivatable, Doxorubicin-Loaded Stealth Liposomes. ACS Nano, 11: 12482–12491.

297. Tardi P, Johnstone S, Harasym N, Xie S, Harasym T, Zisman N, Harvie P, Bermudes D, Mayer L (2009) In vivo maintenance of synergistic cytarabine:daunorubicin ratios greatly enhances therapeutic efficacy. Leuk Res, 33: 129–139.

298. Nave M, Castro RE, Rodrigues CM, Casini A, Soveral G, Gaspar MM (2016) Nanoformulations of a potent copper-based aquaporin inhibitor with cytotoxic effect against cancer cells. Nanomed, 11: 1817–1830.

299. Patankar NA, Waterhouse D, Strutt D, Anantha M, Bally MB (2013) Topophore C: a liposomal nanoparticle formulation of topotecan for treatment of ovarian cancer. Invest New Drugs, 31: 46–58.

300. Ramsay E, Alnajim J, Anantha M, Taggar A, Thomas A, Edwards K, Karlsson G, Webb M, Bally M (2006) Transition metal-mediated liposomal encapsulation of irinotecan (CPT-11) stabilizes the drug in the therapeutically active lactone conformation. Pharm Res, 23: 2799–2808.

301.   Ramsay E, Alnajim J, Anantha M, Zastre J, Yan H, Webb M, Waterhouse D, Bally M (2008) A novel liposomal irinotecan formulation with significant anti-tumour activity: Use of the divalent cation ionophore A23187 and copper-containing liposomes to improve drug retention. Eur J Pharm Biopharm, 68: 607–617.

302.   Dromi S, Frenkel V, Luk A, Traughber B, Angstadt M, Bur M, Poff J, Xie J, Libutti SK, Li KCP, Wood BJ (2007) Pulsed-high intensity focused ultrasound and low temperature-sensitive liposomes for enhanced targeted drug delivery and antitumor effect. Clin Cancer Res, 13: 2722–2727.

303. Grüll H, Langereis S (2012) Hyperthermia-triggered drug delivery from temperature-sensitive liposomes using MRI-guided high intensity focused ultrasound. J Control Release, 161: 317–327.

304.   Rossmann C, McCrackin MA, Armeson KE, Haemmerich D (2017) Temperature sensitive liposomes combined with thermal ablation: Effects of duration and timing of heating in mathematical models and in vivo. PLoS ONE, 12: e0179131.

305.   Catala A. Thermosensitive Liposomes. In: Catala A. (ed) Liposomes. BoD – Books on Demand, Norderstedt, Germany, 2017: 187-213.

306.   Karino T, Koga S, Maeta M (1988) Experimental studies of the effects of local hyperthermia on blood flow, oxygen pressure and pH in tumors. Jpn J Surg, 18: 276–283.

307. Can Mild Hyperthermia Improve Tumour Oxygenation? - PubMed. https://pubmed.ncbi.nlm.nih.gov/9147141/. Accessed 2 Apr 2020

308.   Cope DA, Dewhirst MW, Friedman HS, Bigner DD, Zalutsky MR (1990) Enhanced delivery of a monoclonal antibody F(ab')2 fragment to subcutaneous human glioma xenografts using local hyperthermia. Cancer Res, 50: 1803–1809.

309.   Hosono MN, Hosono M, Endo K, Ueda R, Onoyama Y (1994) Effect of hyperthermia on tumor uptake of radiolabeled anti-neural cell adhesion molecule antibody in small-cell lung cancer xenografts. J Nucl Med, 35: 504–509.

310.   Schuster JM, Zalutsky MR, Noska MA, Dodge R, Friedman HS, Bigner DD, Dewhirst MW (1995) Hyperthermic modulation of radiolabelled antibody uptake in a human glioma xenograft and normal tissues. Int J Hyperthermia, 11: 59–72.

311. Hauck ML, Coffin DO, Dodge RK, Dewhirst MW, Mitchell JB, Zalutsky MR (1997) A local hyperthermia treatment which enhances antibody uptake in a glioma xenograft model does not affect tumour interstitial fluid pressure. Int J Hyperth, 13: 307–316.

312. Fujiwara K, Watanabe T (1990) Effects of hyperthermia, radiotherapy and thermoradiotherapy on tumor microvascular permeability. Acta Pathol Jpn, 40: 79–84.

313. Lefor AT, Makohon S, Ackerman NB (1985) The effects of hyperthermia on vascular permeability in experimental liver metastasis. J Surg Oncol, 28: 297–300.

314. Gaber MH, Wu NZ, Hong K, Huang SK, Dewhirst MW, Papahadjopoulos D (1996) Thermosensitive liposomes: extravasation and release of contents in tumor microvascular networks. Int J Radiat Oncol Biol Phys, 36: 1177–1187.

315. Lee AG (1977) Lipid phase transitions and phase diagrams I. Lipid phase transitions. Biochim Biophys Acta BBA - Rev Biomembr, 472: 237–281.

316. Needham D, Anyarambhatla G, Kong G, Dewhirst MW (2000) A new temperature-sensitive liposome for use with mild hyperthermia: characterization and testing in a human tumor xenograft model. Cancer Res, 60: 1197–1201.

317. May JP, Li S-D (2013) Hyperthermia-induced drug targeting. Expert Opin Drug Deliv, 10: 511–527.

318. Kong G, Anyarambhatla G, Petros WP, Braun RD, Colvin OM, Needham D, Dewhirst MW (2000) Efficacy of liposomes and hyperthermia in a human tumor xenograft model: importance of triggered drug release. Cancer Res, 60: 6950–6957.

319. Kneidl B, Peller M, Winter G, Lindner LH, Hossann M (2014) Thermosensitive liposomal drug delivery systems: state of the art review. Int J Nanomedicine, 9: 4387–4398.

320. Pratt KW, Buck RP, Rondinini S, Covington AK, Baucke FG, Brett CM, Camoes MF, Milton MJ, Mussini T, Naumann R, Spitzer P, Wilson GS (2002) Measurement of pH: Definition, Standards, and Procedures (IUPAC Recommendations 2002). 74: 2169–2200.

321. Szakács Z, Noszál B (2006) Determination of dissociation constants of folic acid, methotrexate, and other photolabile pteridines by pressure-assisted capillary electrophoresis. Electrophoresis, 27: 3399–3409.

322. Solution Equilibria Analysis with the OPIUM Computer Program. https://web.natur.cuni.cz/~kyvala/opium.html. Accessed 23 Mar 2020

323. Hwang TL, Shaka AJ (1995) Water Suppression That Works. Excitation Sculpting Using Arbitrary Wave-Forms and Pulsed-Field Gradients. J Magn Reson A, 112: 275–279.

324.   Takács-Novák K, Avdeel A (1996) Interlaboratory study of log P determination by shake-flask and potentiometric methods. J Pharm Biomed Anal, 14: 1405–1413.

325.   ATCC: The Global Bioresource Center. https://www.lgcstandards-atcc.org/?geo_country=hu. Accessed 24 Mar 2020

326.   Liu Y, Peterson DA, Kimura H, Schubert D (1997) Mechanism of cellular 3-(4,5-dimethylthiazol-2-yl)-2,5-diphenyltetrazolium bromide (MTT) reduction. J Neurochem, 69: 581–593.

327.   Twentyman PR, Luscombe M (1987) A study of some variables in a tetrazolium dye (MTT) based assay for cell growth and chemosensitivity. Br J Cancer, 56: 279–285.

328.   Mueller H, Kassack MU, Wiese M (2004) Comparison of the usefulness of the MTT, ATP, and calcein assays to predict the potency of cytotoxic agents in various human cancer cell lines. J Biomol Screen, 9: 506–515.

329.   Skehan P, Storeng R, Scudiero D, Monks A, McMahon J, Vistica D, Warren JT, Bokesch H, Kenney S, Boyd MR (1990) New colorimetric cytotoxicity assay for anticancer-drug screening. J Natl Cancer Inst, 82: 1107–1112.

330.   Vichai V, Kirtikara K (2006) Sulforhodamine B colorimetric assay for cytotoxicity screening. Nat Protoc, 1: 1112–1116.

331.   Rittler D, Baranyi M, Molnár E, Garay T, Jalsovszky I, Varga IK, Hegedűs L, Aigner C, Tóvári J, Tímár J, Hegedűs B (2019) The Antitumor Effect of Lipophilic Bisphosphonate BPH1222 in Melanoma Models: The Role of the PI3K/Akt Pathway and the Small G Protein Rheb. Int J Mol Sci, 20: 4917.

332.   Xu M, McCanna DJ, Sivak JG (2015) Use of the viability reagent PrestoBlue in comparison with alamarBlue and MTT to assess the viability of human corneal epithelial cells. J Pharmacol Toxicol Methods, 71: 1–7.

333.   Moon EJ, Sonveaux P, Porporato PE, Danhier P, Gallez B, Batinic-Haberle I, Nien Y-C, Schroeder T, Dewhirst MW (2010) NADPH oxidase-mediated reactive oxygen species production activates hypoxia-inducible factor-1 (HIF-1) via the ERK pathway after hyperthermia treatment. Proc Natl Acad Sci U S A, 107: 20477–20482.

334.   ImageJ open source software (NIH). https://imagej.nih.gov/ij/download.html. Accessed 23 Mar 2020

335.   Cai Z, Chattopadhyay N, Liu WJ, Chan C, Pignol J-P, Reilly RM (2011) Optimized digital counting colonies of clonogenic assays using ImageJ software and customized macros: comparison with manual counting. Int J Radiat Biol, 87: 1135–1146.

336.   Ivanov DP, Parker TL, Walker DA, Alexander C, Ashford MB, Gellert PR, Garnett MC (2014) Multiplexing spheroid volume, resazurin and acid phosphatase viability assays for high-throughput screening of tumour spheroids and stem cell neurospheres. PloS One, 9: e103817.

337. Szabó I, Bősze S, Orbán E, Sipos É, Halmos G, Kovács M, Mező G (2015) Comparative in vitro biological evaluation of daunorubicin containing GnRH-I and GnRH-II conjugates developed for tumor targeting. J Pept Sci, 21: 426–435.

338. Chang H-Y, Huang H-C, Huang T-C, Yang P-C, Wang Y-C, Juan H-F (2012) Ectopic ATP Synthase Blockade Suppresses Lung Adenocarcinoma Growth by Activating the Unfolded Protein Response. Cancer Res, 72: 4696–4706.

339. Polgári Z, Ajtony Z, Kregsamer P, Streli C, Mihucz VG, Réti A, Budai B, Kralovánszky J, Szoboszlai N, Záray G (2011) Microanalytical method development for Fe, Cu and Zn determination in colorectal cancer cells. Talanta, 85: 1959–1965.

340. Szoboszlai N, Polgári Z, Mihucz VG, Záray G (2009) Recent trends in total reflection X-ray fluorescence spectrometry for biological applications. Anal Chim Acta, 633: 1–18.

341. Szoboszlai N, Réti A, Budai B, Szabó Z, Kralovánszky J, Záray G (2008) Direct elemental analysis of cancer cell lines by total reflection X-ray fluorescence. Spectrochim Acta Part B At Spectrosc, 63: 1480–1484.

342. Sawhney KJS, Dolbnya IP, Tiwari MK, Alianelli L, Scott SM, Preece GM, Pedersen UK, Walton RD (2010) A Test Beamline on Diamond Light Source. AIP Conf Proc, 1234: 387–390.

343. Mihucz VG, Meirer F, Polgári Z, Réti A, Pepponi G, Ingerle D, Szoboszlai N, Streli C (2016) Iron overload of human colon adenocarcinoma cells studied by synchrotron-based X-ray techniques. JBIC J Biol Inorg Chem, 21: 241–249.

344. PyMca Home. http://pymca.sourceforge.net/. Accessed 23 May 2020

345. Varga Z, van der Pol E, Pálmai M, Garcia-Diez R, Gollwitzer C, Krumrey M, Fraikin J-L, Gasecka A, Hajji N, van Leeuwen TG, Nieuwland R (2018) Hollow organosilica beads as reference particles for optical detection of extracellular vesicles. J Thromb Haemost, 16: 1646–1655.

346. Fraikin J-L, Teesalu T, McKenney CM, Ruoslahti E, Cleland AN (2011) A high-throughput label-free nanoparticle analyser. Nat Nanotechnol, 6: 308–313.

347. Grabarek AD, Weinbuch D, Jiskoot W, Hawe A (2019) Critical Evaluation of Microfluidic Resistive Pulse Sensing for Quantification and Sizing of Nanometer- and Micrometer-Sized Particles in Biopharmaceutical Products. J Pharm Sci, 108: 563–573.

348. Barnett GV, Perhacs JM, Das TK, Kar SR (2018) Submicron Protein Particle Characterization using Resistive Pulse Sensing and Conventional Light Scattering Based Approaches. Pharm Res, 35: 58.

349. Tomayko MM, Reynolds CP (1989) Determination of subcutaneous tumor size in athymic (nude) mice. Cancer Chemother Pharmacol, 24: 148–154.

350. OriginLab - Origin and OriginPro - Data Analysis and Graphing Software. https://www.originlab.com/. Accessed 24 Mar 2020

351. Prism - GraphPad. https://www.graphpad.com/scientific-software/prism/. Accessed 24 Mar 2020

352. Gaál A, Orgován G, Polgári Z, Réti A, Mihucz VG, Bősze, S, Szoboszlai N, Streli C (2014) Complex forming competition and in-vitro toxicity studies on the applicability of di-2-pyridylketone-4, 4,-dimethyl-3-thiosemicarbazone (Dp44mT) as a metal chelator. J Inorg Biochem, 130: 52–58.

353. González M, Tapia L, Alvarado M, Tornero JD, Fernández R (1999) Intracellular determination of elements in mammalian cultured cells by total reflection X-ray fluorescence spectrometry. J Anal At Spectrom, 14: 885–888.

354. Jeney A, Hujber Z, Szoboszlai N, Fullár A, Oláh J, Pap É, Márk Á, Kriston C, Kralovánszky J, Kovalszky I, Vékey K, Sebestyén A (2016) Characterisation of bioenergetic pathways and related regulators by multiple assays in human tumour cells. Cancer Cell Int, 16: 4.

355. NCI-60 Human Tumor Cell Lines Screen | Discovery & Development Services | Developmental Therapeutics Program (DTP). https://dtp.cancer.gov/discovery_development/nci-60/default.htm. Accessed 24 May 2020

356. Gaál A, Orgován G, Mihucz VG, Pape I, Ingerle D, Streli C, Szoboszlai N (2018) Metal transport capabilities of anticancer copper chelators. J Trace Elem Med Biol Organ Soc Miner Trace Elem GMS, 47: 79–88.

357. Zhai S, Yang L, Cui QC, Sun Y, Dou QP, Yan B (2010) Tumor cellular proteasome inhibition and growth suppression by 8-hydroxyquinoline and clioquinol requires their capabilities to bind copper and transport copper into cells. J Biol Inorg Chem JBIC Publ Soc Biol Inorg Chem, 15: 259–269.

358. Gaál A, Mihucz VG, Bősze S, Szabó I, Baranyi M, Horváth P, Streli C, Szoboszlai N (2016) Comparative in vitro investigation of anticancer copper chelating agents. Microchem J. https://doi.org/10.1016/j.microc.2016.12.007

359. Finney L, Vogt S, Fukai T, Glesne D (2009) Copper and angiogenesis: unravelling a relationship key to cancer progression. Clin Exp Pharmacol Physiol, 36: 88–94.

360. Rana U, Kothinti R, Meeusen J, Tabatabai NM, Krezoski S, Petering DH (2008) Zinc binding ligands and cellular zinc trafficking: Apo-metallothionein, glutathione, TPEN, proteomic zinc, and Zn-Sp1. J Inorg Biochem, 102: 489–499.

361. Chandler P, Kochupurakkal BS, Alam S, Richardson AL, Soybel DI, Kelleher SL (2016) Subtype-specific accumulation of intracellular zinc pools is associated with the malignant phenotype in breast cancer. Mol Cancer, 15: 2.

362. Kagara N, Tanaka N, Noguchi S, Hirano T (2007) Zinc and its transporter ZIP10 are involved in invasive behavior of breast cancer cells. Cancer Sci, 98: 692–697.

363. Microscopic X-Ray Fluorescence Analysis - Wiley 2000 Ed: Koen H. A. Janssens, Freddy C. V. Adams, Anders Rindby

364. Wang F, Sayre LM (1989) Oxidation of tertiary amine buffers by copper(II). Inorg Chem, 28: 169–170.

365. Caffrey M (1993) Lipid thermotropic phase transition database (LIPIDAT). user's guide Version 1.0 Version 1.0. U.S. Dept. of Commerce, National Institute of Standards and Technology, Standard Reference Data Program, Gaithersburg, MD

366. Silvius JR (1982) Thermotropic Phase Transitions of Pure Lipids in Model Membranes and Their Modifications by Membrane Proteins. In: Jost PC, Griffith OH, editors. Lipid-Protein Interactions, John Wiley & Sons, Inc., New York, pp. 239–281. - Open Access Library. http://www.oalib.com/references/8155109. Accessed 8 Mar 2020

367. Varga Z, Fehér B, Kitka D, Wacha A, Bóta A, Berényi S, Pipich V, Fraikin J-L (2020) Size Measurement of Extracellular Vesicles and Synthetic Liposomes: The Impact of the Hydration Shell and the Protein Corona. Colloids Surf B Biointerfaces, 192: 111053.

368. Lewis RN, McElhaney RN, Pohle W, Mantsch HH (1994) Components of the carbonyl stretching band in the infrared spectra of hydrated 1,2-diacylglycerolipid bilayers: a reevaluation. Biophys J, 67: 2367–2375.

369. Berényi S, Mihály J, Wacha A, Tőke O, Bóta A (2014) A mechanistic view of lipid membrane disrupting effect of PAMAM dendrimers. Colloids Surf B Biointerfaces, 118: 164–171.

370. Gaál A, Mihucz VG, Bősze S, Szabó I, Baranyi M, Horváth P, Streli C, Szoboszlai N (2018) Comparative in vitro investigation of anticancer copper chelating agents. Microchem J, 136: 227–235.

371. Petersen AL, Henriksen JR, Binderup T, Elema DR, Rasmussen PH, Hag AM, Kjær A, Andresen TL (2016) In vivo evaluation of PEGylated ^{64}Cu-liposomes with theranostic and radiotherapeutic potential using micro PET/CT. Eur J Nucl Med Mol Imaging, 43: 941–952.

372. Man F, Gawne PJ, T.M. de Rosales R (2019) Nuclear imaging of liposomal drug delivery systems: A critical review of radiolabelling methods and applications in nanomedicine. Adv Drug Deliv Rev, 143: 134–160.

373. Bar-David S, Larush L, Goder N, Aizic A, Zigmond E, Varol C, Klausner J, Magdassi S, Nizri E (2019) Size and lipid modification determine liposomal Indocyanine green performance for tumor imaging in a model of rectal cancer. Sci Rep, 9: 1–8.

374.   Caracciolo G, Pozzi D, Capriotti AL, Cavaliere C, Piovesana S, Amenitsch H, Laganà A (2014) Lipid composition: a "key factor" for the rational manipulation of the liposome–protein corona by liposome design. RSC Adv, 5: 5967–5975.

375.   Chakravarty R, Chakraborty S, Dash A (2016) 64Cu2+ Ions as PET Probe: An Emerging Paradigm in Molecular Imaging of Cancer. Mol Pharm, 13: 3601–3612.

376.   Peng F, Lu X, Janisse J, Muzik O, Shields AF (2006) PET of human prostate cancer xenografts in mice with increased uptake of 64CuCl2. J Nucl Med, 47: 1649–1652.

377.   Phillips null (1999) Delivery of gamma-imaging agents by liposomes. Adv Drug Deliv Rev, 37: 13–32.

378.   Pape VFS, May NV, Gál GT, Szatmári I, Szeri F, Fülöp F, Szakács G, Enyedy ÉA (2018) Impact of copper and iron binding properties on the anticancer activity of 8-hydroxyquinoline derived Mannich bases. Dalton Trans, 47: 17032–17045.

379.   Ruiz-Azuara L, Bravo-Gómez ME (2010) Copper compounds in cancer chemotherapy. Curr Med Chem, 17: 3606–3615.

380.   Bernhardt PV, Sharpe PC, Islam M, Lovejoy DB, Kalinowski DS, Richardson DR (2009) Iron chelators of the dipyridylketone thiosemicarbazone class: precomplexation and transmetalation effects on anticancer activity. J Med Chem, 52: 407–415.

381.   Enyedy ÉA, Nagy NV, Zsigó É, Kowol CR, Arion VB, Keppler BK, Kiss T (2010) Comparative Solution Equilibrium Study of the Interactions of Copper(II), Iron(II) and Zinc(II) with Triapine (3-Aminopyridine-2-carbaldehyde Thiosemicarbazone) and Related Ligands. Eur J Inorg Chem, 2010: 1717–1728.

382.   Richardson DR, Sharpe PC, Lovejoy DB, Senaratne D, Kalinowski DS, Islam M, Bernhardt PV (2006) Dipyridyl thiosemicarbazone chelators with potent and selective antitumor activity form iron complexes with redox activity. J Med Chem, 49: 6510–6521.

383.   Gundelach JH, Madhavan AA, Wettstein PJ, Bram RJ (2013) The anticancer drug Dp44mT inhibits T-cell activation and CD25 through a copper-dependent mechanism. FASEB J, 27: 782–792.

384.   Cen D, Brayton D, Shahandeh B, Meyskens FL, Farmer PJ (2004) Disulfiram facilitates intracellular Cu uptake and induces apoptosis in human melanoma cells. J Med Chem, 47: 6914–6920.

385.   Safi R, Nelson ER, Chitneni SK, Franz KJ, George DJ, Zalutsky MR, McDonnell DP (2014) Copper signaling axis as a target for prostate cancer therapeutics. Cancer Res, 74: 5819–5831.

386.   Daniel KG, Chen D, Orlu S, Cui QC, Miller FR, Dou QP (2005) Clioquinol and pyrrolidine dithiocarbamate complex with copper to form proteasome inhibitors and apoptosis inducers in human breast cancer cells. Breast Cancer Res, 7: R897.

387. Chen S-H, Lin J-K, Liu S-H, Liang Y-C, Lin-Shiau S-Y (2008) Apoptosis of cultured astrocytes induced by the copper and neocuproine complex through oxidative stress and JNK activation. Toxicol Sci, 102: 138–149.

388. Tardito S, Barilli A, Bassanetti I, Tegoni M, Bussolati O, Franchi-Gazzola R, Mucchino C, Marchiò L (2012) Copper-dependent cytotoxicity of 8-hydroxyquinoline derivatives correlates with their hydrophobicity and does not require caspase activation. J Med Chem, 55: 10448–10459.

389. Ishiguro K, Lin ZP, Penketh PG, Shyam K, Zhu R, Baumann RP, Zhu Y-L, Sartorelli AC, Rutherford TJ, Ratner ES (2014) Distinct mechanisms of cell-kill by triapine and its terminally dimethylated derivative Dp44mT due to a loss or gain of activity of their copper(II) complexes. Biochem Pharmacol, 91: 312–322.

390. Gaur K, Vázquez-Salgado AM, Duran-Camacho G, Dominguez-Martinez I, Benjamín-Rivera JA, Fernández-Vega L, Carmona Sarabia L, Cruz García A, Pérez-Deliz F, Méndez Román JA, Vega-Cartagena M, Loza-Rosas SA, Rodriguez Acevedo X, Tinoco AD (2018) Iron and Copper Intracellular Chelation as an Anticancer Drug Strategy. Inorganics, 6: 126.

391. Zhao C, Liu B, Bi X, Liu D, Pan C, Wang L, Pang Y (2016) A novel flavonoid-based bioprobe for intracellular recognition of Cu2+ and its complex with Cu2+ for secondary sensing of pyrophosphate. Sens Actuators B Chem, 229: 131–137.

392. Barilli A, Atzeri C, Bassanetti I, Ingoglia F, Dall'Asta V, Bussolati O, Maffini M, Mucchino C, Marchiò L (2014) Oxidative stress induced by copper and iron complexes with 8-hydroxyquinoline derivatives causes paraptotic death of HeLa cancer cells. Mol Pharm, 11: 1151–1163.

393. Kasibhatla S, Tseng B (2003) Why Target Apoptosis in Cancer Treatment? Mol Cancer Ther, 2: 573–580.

394. Bold RJ, Termuhlen PM, McConkey DJ (1997) Apoptosis, cancer and cancer therapy. Surg Oncol, 6: 133–142.

395. Amaravadi RK, Thompson CB (2007) The Roles of Therapy-Induced Autophagy and Necrosis in Cancer Treatment. Clin Cancer Res, 13: 7271–7279.

396. Basu S, Binder RJ, Suto R, Anderson KM, Srivastava PK (2000) Necrotic but not apoptotic cell death releases heat shock proteins, which deliver a partial maturation signal to dendritic cells and activate the NF-kappa B pathway. Int Immunol, 12: 1539–1546.

397. Sauter B, Albert ML, Francisco L, Larsson M, Somersan S, Bhardwaj N (2000) Consequences of cell death: exposure to necrotic tumor cells, but not primary tissue cells or apoptotic cells, induces the maturation of immunostimulatory dendritic cells. J Exp Med, 191: 423–434.

398. Kiaris H, Schally AV (1999) Apoptosis Versus Necrosis: Which Should Be the Aim of Cancer Therapy? Proc Soc Exp Biol Med, 221: 87–88.

399. Srivastava PK (2003) Hypothesis: Controlled necrosis as a tool for immunotherapy of human cancer. Cancer Immun Arch, 3: 4.

400. Guerriero JL, Ditsworth D, Fan Y, Zhao F, Crawford HC, Zong W-X (2008) Chemotherapy Induces Tumor Clearance Independent of Apoptosis. Cancer Res, 68: 9595–9600.

401. Tardito S, Marchiò L (2009) Copper compounds in anticancer strategies. Curr Med Chem, 16: 1325–1348.

402. Foo JB, Ng LS, Lim JH, Tan PX, Lor YZ, Loo JSE, Low ML, Chan LC, Beh CY, Leong SW, Yazan LS, Tor YS, How CW (2019) Induction of cell cycle arrest and apoptosis by copper complex Cu(SBCM)$_2$ towards oestrogen-receptor positive MCF-7 breast cancer cells. RSC Adv, 9: 18359–18370.

403. Rezaei A, Falahati-Pour SK, Mohammadizadeh F, Hajizadeh MR, Mirzaei MR, Khoshdel A, Fahmidehkar MA, Mahmoodi M (2018) Effect of a Copper (II) Complex on The Induction of Apoptosis in Human Hepatocellular Carcinoma Cells. Asian Pac J Cancer Prev APJCP, 19: 2877–2884.

404. Hussain A, AlAjmi MF, Rehman MT, Amir S, Husain FM, Alsalme A, Siddiqui MA, AlKhedhairy AA, Khan RA (2019) Copper(II) complexes as potential anticancer and Nonsteroidal anti-inflammatory agents: In vitro and in vivo studies. Sci Rep, 9: 1–17.

405. ZHANG X, BI C, FAN Y, CUI Q, CHEN D, XIAO Y, DOU QP (2008) Induction of tumor cell apoptosis by taurine Schiff base copper complex is associated the with inhibition of proteasomal activity. Int J Mol Med, 22: 677–682.

406. Hu J, Liao C, Guo Y, Yang F, Sang W, Zhao J (2017) Copper(II) complexes inducing apoptosis in cancer cells, and demonstrating DNA and HSA interactions. Polyhedron, 132: 28–38.

407. Bulatov E, Sayarova R, Mingaleeva R, Miftakhova R, Gomzikova M, Ignatyev Y, Petukhov A, Davidovich P, Rizvanov A, Barlev NA (2018) Isatin-Schiff base-copper (II) complex induces cell death in p53-positive tumors. Cell Death Discov, 4: 1–9.

408. Jungwirth U, Kowol CR, Keppler BK, Hartinger CG, Berger W, Heffeter P (2011) Anticancer activity of metal complexes: involvement of redox processes. Antioxid Redox Signal, 15: 1085–1127.

409. Guo W, Ye S, Cao N, Huang J, Gao J, Chen Q (2010) ROS-mediated autophagy was involved in cancer cell death induced by novel copper(II) complex. Exp Toxicol Pathol, 62: 577–582.

410. Recio Despaigne AA, Da Silva JG, Da Costa PR, Dos Santos RG, Beraldo H (2014) ROS-Mediated Cytotoxic Effect of Copper(II) Hydrazone Complexes against Human Glioma Cells. Molecules, 19: 17202–17220.

411. Hosseini M-J, Shaki F, Ghazi-Khansari M, Pourahmad J (2014) Toxicity of Copper on Isolated Liver Mitochondria: Impairment at Complexes I, II, and IV Leads to Increased ROS Production. Cell Biochem Biophys, 70: 367–381.

412. Ng CH, Kong SM, Tiong YL, Maah MJ, Sukram N, Ahmad M, Khoo ASB (2014) Selective anticancer copper(II)-mixed ligand complexes: targeting of ROS and proteasomes. Met Integr Biometal Sci, 6: 892–906.

413. Prosser KE, Chang SW, Saraci F, Le PH, Walsby CJ (2017) Anticancer copper pyridine benzimidazole complexes: ROS generation, biomolecule interactions, and cytotoxicity. J Inorg Biochem, 167: 89–99.

414. Gandin V, Tisato F, Dolmella A, Pellei M, Santini C, Giorgetti M, Marzano C, Porchia M (2014) In Vitro and in Vivo Anticancer Activity of Copper(I) Complexes with Homoscorpionate Tridentate Tris(pyrazolyl)borate and Auxiliary Monodentate Phosphine Ligands. J Med Chem, 57: 4745–4760.

415. Gandin V, Ceresa C, Esposito G, Indraccolo S, Porchia M, Tisato F, Santini C, Pellei M, Marzano C (2017) Therapeutic potential of the phosphino Cu(I) complex (HydroCuP) in the treatment of solid tumors. Sci Rep, 7: 13936.

416. Xu Y, Zhou Q, Feng X, Dai Y, Jiang Y, Jiang W, Liu X, Xing X, Wang Y, Ni Y, Zheng C (2020) Disulfiram/copper markedly induced myeloma cell apoptosis through activation of JNK and intrinsic and extrinsic apoptosis pathways. Biomed Pharmacother Biomedecine Pharmacother, 126: 110048.

417. Clinical Trial: Vinorelbine, Cisplatin, Disulfiram and Copper in CTC_EMT Positive Refractory Metastatic Breast Cancer. - ClinicalTrials.gov. https://clinicaltrials.gov/ct2/show/NCT04265274. Accessed 14 Apr 2020

418. Phase II Trial of Disulfiram With Copper in Metastatic Breast Cancer - Full Text View - ClinicalTrials.gov. https://clinicaltrials.gov/ct2/show/NCT03323346. Accessed 14 Apr 2020

419. A Phase Ib Study of Intravenous Copper Loading With Oral Disulfiram in Metastatic, Castration Resistant Prostate Cancer - Full Text View - ClinicalTrials.gov. https://clinicaltrials.gov/ct2/show/NCT02963051. Accessed 14 Apr 2020

420. Phase I Study of Disulfiram and Copper Gluconate for the Treatment of Refractory Solid Tumors Involving the Liver - Full Text View - ClinicalTrials.gov. https://clinicaltrials.gov/ct2/show/NCT00742911. Accessed 14 Apr 2020

421.   Dalecki AG, Haeili M, Shah S, Speer A, Niederweis M, Kutsch O, Wolschendorf F (2015) Disulfiram and Copper Ions Kill Mycobacterium tuberculosis in a Synergistic Manner. Antimicrob Agents Chemother, 59: 4835–4844.

422.   Keen CL, Saltman P, Hurley LS (1980) Copper nitrilotriacetate: a potent therapeutic agent in the treatment of a genetic disorder of copper metabolism. Am J Clin Nutr, 33: 1789–1800.

423.   Mohindru A, Fisher JM, Rabinovitz M (1983) 2,9-Dimethyl-1,10-phenanthroline (neocuproine): a potent, copper-dependent cytotoxin with anti-tumor activity. Biochem Pharmacol, 32: 3627–3632.

424.   Copper and Its Chelates in cytotoxicity and Chemotherapy. National Cancer Institute (U.S.). Annual Report 1982 - National Cancer Institute, Division of Cancer Treatment. Department of Health, Education, and Welfare, Public Health Service, National Institutes of Health] National Cancer Institute, Division of Cancer Treatment, 1892: 566-570.

425.   Lainé A-L, Passirani C (2012) Novel metal-based anticancer drugs: a new challenge in drug delivery. Curr Opin Pharmacol, 12: 420–426.

426.   Mayer LD, Tardi P, Louie AC (2019) CPX-351: a nanoscale liposomal co-formulation of daunorubicin and cytarabine with unique biodistribution and tumor cell uptake properties. Int J Nanomedicine, 14: 3819–3830.

427.   Güçlü K, Sözgen K, Tütem E, Ozyürek M, Apak R (2005) Spectrophotometric determination of ascorbic acid using copper(II)-neocuproine reagent in beverages and pharmaceuticals. Talanta, 65: 1226–1232.

428.   Cuculić V, Mlakar M, Branica M (1998) Influence of the HEPES Buffer on Electrochemical Reaction of the Copper(II)-Salicylaldoxime Complex. Electroanalysis, 10: 852–856.

429.   Lichtenberg D, Pinchuk I (2017) P 212 - The second order mechanism of copper induced lipid peroxidation. Free Radic Biol Med, 108: S90.

430.   Kowol CR, Heffeter P, Miklos W, Gille L, Trondl R, Cappellacci L, Berger W, Keppler BK (2012) Mechanisms underlying reductant-induced reactive oxygen species formation by anticancer copper(II) compounds. J Biol Inorg Chem JBIC Publ Soc Biol Inorg Chem, 17: 409–423.

431.   Li J, Wang X, Zhang T, Wang C, Huang Z, Luo X, Deng Y (2015) A review on phospholipids and their main applications in drug delivery systems. Asian J Pharm Sci, 10: 81–98.

432.   Najlah M, Said Suliman A, Tolaymat I, Kurusamy S, Kannappan V, Elhissi AMA, Wang W (2019) Development of Injectable PEGylated Liposome Encapsulating Disulfiram for Colorectal Cancer Treatment. Pharmaceutics, 11: 610.

433.   Wehbe M, Anantha M, Backstrom I, Leung A, Chen K, Malhotra A, Edwards K, Bally MB (2016) Nanoscale Reaction Vessels Designed for Synthesis of Copper-Drug Complexes Suitable for Preclinical Development. PLOS ONE, 11: e0153416.

434.   Li L, ten Hagen TLM, Haeri A, Soullié T, Scholten C, Seynhaeve ALB, Eggermont AMM, Koning GA (2014) A novel two-step mild hyperthermia for advanced liposomal chemotherapy. J Control Release, 174: 202–208.

435.   Tucci ST, Kheirolomoom A, Ingham ES, Mahakian LM, Tam SM, Foiret J, Hubbard NE, Borowsky AD, Baikoghli M, Cheng RH, Ferrara KW (2019) Tumor-specific delivery of gemcitabine with activatable liposomes. J Control Release, 309: 277–288.

436.   Jabłońska-Trypuć A, Świderski G, Krętowski R, Lewandowski W (2017) Newly Synthesized Doxorubicin Complexes with Selected Metals—Synthesis, Structure and Anti-Breast Cancer Activity. Molecules, 22: 1106.

437.   Bonetto A, Rupert JE, Barreto R, Zimmers TA (2016) The Colon-26 Carcinoma Tumor-bearing Mouse as a Model for the Study of Cancer Cachexia. J Vis Exp JoVE. 30: 54893.

10. Publication list

10.1. Publications related to the thesis

Gaál A, Orgován G, Polgári Z, Réti A, Mihucz VG, Bősze, S, Szoboszlai N, Streli C (2014) Complex forming competition and *in-vitro* toxicity studies on the applicability of di-2-pyridylketone-4, 4,-dimethyl-3-thiosemicarbazone (Dp44mT) as a metal chelator. Journal of Inorganic Biochemistry, 130: 52–58.

Gaál A, Mihucz VG, Bősze S, Szabó I, Baranyi M, Horváth P, Streli C, Szoboszlai N (2018) Comparative *in vitro* investigation of anticancer copper chelating agents. Microchemical Journal, 136: 227–235.

Gaál A, Orgován G, Mihucz VG, Pape I, Ingerle D, Streli C, Szoboszlai N (2018) Metal transport capabilities of anticancer copper chelators. Journal of Trace Elements in Medicine and Biology, 47: 79–88.

Gaál A, Garay TM, Horváth I, Máthé D, Szöllősi D, Veres DS, Mbuotidem J, Kovács T, Tóvári J, Bergmann R, Streli C, Szakács G, Mihály J, Varga Z, Szoboszlai N (2020) Development and *in vivo* application of a water-soluble anticancer copper ionophore system using a temperature-sensitive liposome formulation. Pharmaceutics, 12: 466.

10.2. Further publications in peer-review journals not related to the thesis

Majer Z, Bősze S, Szabó I, Mihucz VG, **Gaál A**, Szilvágyi G, Pepponi G, Meirer F, Wobrauschek P, Szoboszlai N, Ingerle D, Streli C (2015) Study of dinuclear Rh(II) complexes of phenylalanine derivatives as potential anticancer agents by using X-ray fluorescence and X-ray absorption. Microchemical Journal, 120: 51–57.

Cserepes M, Türk D, Tóth S, Pape VFS, **Gaál A**, Gera M, Szabó JE, Kucsma N, Várady G, Vértessy BG, Streli C, Szabó PT, Tovari J, Szoboszlai N, Szakács G (2020) Unshielding Multidrug Resistant Cancer through Selective Iron Depletion of P-Glycoprotein-Expressing Cells. Cancer Research, 80: 663–674.

11. Acknowledgement